



TEZ ŞABLONU ONAY FORMU  
THESIS TEMPLATE CONFIRMATION FORM

1. Şablonda verilen yerleşim ve boşluklar değiştirilmemelidir.
2. **Jüri tarihi** Başlık Sayfası, İmza Sayfası, Abstract ve Öz'de ilgili yerlere yazılmalıdır.
3. İmza sayfasında jüri üyelerinin unvanları doğru olarak yazılmalıdır. Tüm imzalar **mavi pilot kalemle** atılmalıdır.
4. **Disiplinlerarası** programlarda görevlendirilen öğretim üyeleri için jüri üyeleri kısmında tam zamanlı olarak çalıştıkları anabilim dalı başkanlığının ismi yazılmalıdır. Örneğin: bir öğretim üyesi Biyoteknoloji programında görev yapıyor ve biyoloji bölümünde tam zamanlı çalışıyorsa, İmza sayfasına biyoloji bölümü yazılmalıdır. İstisnai olarak, disiplinler arası program başkanı ve tez danışmanı için disiplinlerarası program adı yazılmalıdır.
5. Tezin **son sayfasının sayfa** numarası Abstract ve Öz'de ilgili yerlere yazılmalıdır.
6. Bütün chapterlar, referanslar, ekler ve CV sağ sayfada başlamalıdır. Bunun için **kesmeler** kullanılmıştır. **Kesmelerin kayması** fazladan boş sayfaların oluşmasına sebep olabilir. Bu gibi durumlarda paragraf (¶) işaretine tıklayarak kesmeleri görünür hale getirin ve yerlerini **kontrol edin**.
7. Figürler ve tablolar kenar boşluklarına taşmamalıdır.
8. Şablonda yorum olarak eklenen uyarılar dikkatle okunmalı ve uygulanmalıdır.
9. Tez yazdırılmadan önce PDF olarak kaydedilmelidir. Şablonda yorum olarak eklenen uyarılar PDF dokümanında yer almamalıdır.
10. Tez taslaklarının kontrol işlemleri tamamlandığında, bu durum öğrencilere METU uzantılı öğrenci e-posta adresleri aracılığıyla duyurulacaktır.
11. Tez yazım süreci ile ilgili herhangi bir sıkıntı yaşarsanız, [Sıkça Sorulan Sorular \(SSS\)](#) sayfamızı ziyaret ederek yaşadığınız sıkıntıyla ilgili bir çözüm bulabilirsiniz.

1. Do not change the spacing and placement in the template.
2. Write **defense date** to the related places given on Title page, Approval page, Abstract and Öz.
3. Write the titles of the examining committee members correctly on Approval Page. **Blue ink** must be used for all signatures.
4. For faculty members working in **interdisciplinary programs**, the name of the department that they work full-time should be written on the Approval page. For example, if a faculty member staffs in the biotechnology program and works full-time in the biology department, the department of biology should be written on the approval page. Exceptionally, for the interdisciplinary program chair and your thesis supervisor, the interdisciplinary program name should be written.
5. Write **the page number of the last page** in the related places given on Abstract and Öz pages.
6. All chapters, references, appendices and CV must be started on the right page. **Section Breaks** were used for this. **Change in the placement** of section breaks can result in extra blank pages. In such cases, make the section breaks visible by clicking paragraph (¶) mark and **check their position**.
7. All figures and tables must be given inside the page. Nothing must appear in the margins.
8. All the warnings given on the comments section through the thesis template must be read and applied.
9. Save your thesis as pdf and Disable all the comments before taking the printout.
10. This will be announced to the students via their METU students e-mail addresses when the control of the thesis drafts has been completed.
11. If you have any problems with the thesis writing process, you may visit our [Frequently Asked Questions \(FAQ\)](#) page and find a solution to your problem.

Yukarıda bulunan tüm maddeleri okudum, anladım ve kabul ediyorum. / I have read, understand and accept all of the items above.

Name : Merve  
Surname : Canyurt  
E-Mail : merve.canyurt@metu.edu.tr  
Date : 21.01.2022  
Signature : \_\_\_\_\_



EFFORTS TOWARDS SYNTHESIS OF HYDROGEN SULFIDE ACTIVATED  
BODIPY BASED PDT AGENTS

A THESIS SUBMITTED TO  
THE GRADUATE SCHOOL OF NATURAL AND APPLIED SCIENCES  
OF  
MIDDLE EAST TECHNICAL UNIVERSITY

BY

MERVE CANYURT

IN PARTIAL FULFILLMENT OF THE REQUIREMENTS  
FOR  
THE DEGREE OF MASTER OF SCIENCE  
IN  
CHEMISTRY

MAY 2022



Approval of the thesis:

**EFFORTS TOWARDS SYNTHESIS OF HYDROGEN SULFIDE  
ACTIVATED BODIPY BASED PDT AGENTS**

submitted by **MERVE CANYURT** in partial fulfillment of the requirements for the degree of **Master of Science in Chemistry, Middle East Technical University** by,

Prof. Dr. Halil Kalıpçılar  
Dean, Graduate School of **Natural and Applied Sciences**

\_\_\_\_\_

Prof. Dr. Özdemir Doğan  
Head of the Department, **Chemistry**

\_\_\_\_\_

Assoc. Prof. Dr. Görkem Günbaş  
Supervisor, **Chemistry, METU**

\_\_\_\_\_

**Examining Committee Members:**

Prof. Dr. Özdemir Doğan  
Chemistry, METU

\_\_\_\_\_

Assoc. Prof. Dr. Görkem Günbaş  
Chemistry, METU

\_\_\_\_\_

Assoc. Prof. Dr. Özgül Persil Çetinkol  
Chemistry, METU

\_\_\_\_\_

Assoc. Prof. Dr. Salih Özçubukçu  
Chemistry, METU

\_\_\_\_\_

Assist. Prof. Dr. Safacan Kölemen  
Chemistry, Koç University

\_\_\_\_\_

Date: 13.05.2022

**I hereby declare that all information in this document has been obtained and presented in accordance with academic rules and ethical conduct. I also declare that, as required by these rules and conduct, I have fully cited and referenced all material and results that are not original to this work.**

Name Last name : Merve Canyurt

Signature :

## ABSTRACT

### EFFORTS TOWARDS SYNTHESIS OF HYDROGEN SULFIDE ACTIVATED BODIPY BASED PDT AGENTS

Canyurt, Merve  
Master of Science, Chemistry  
Supervisor : Assoc. Prof. Dr. Gökem Günbaş

May 2022, 117 pages

Photodynamic Therapy (PDT) is an effective and minimally invasive method that has recently gained widespread acceptance as a new medical treatment for a variety of conditions. PDT uses photosensitizers in combination with a specific light source and molecular oxygen to form cytotoxic species that can damage organelles and cell membranes directly. The photodynamic reactions start with light absorption by the PS in the target tissue, which sets off a chain of photochemical events. In comparison to existing sensitizers, BODIPY (4,4-difluoro-4-bora-3a,4a-diaza-*s*-indacene) allows for the creation of next-generation photosensitizers due to their high fluorescence and triplet quantum yields, ease of functionalization, and tunable photophysical properties. The aim of this project is to synthesize two different water-soluble, mitochondria-targeted and activatable photosensitizers. For this purpose, brominated BODIPY core is modified at different positions with pyridinium unit and azido-benzyl masking unit which is activated with H<sub>2</sub>S, an over-expressed tumor metabolite. In the first sensitizer (S-BODMe), two consecutive Knoevenagel condensation processes were attempted to introduce pyridinium unit to the 5-position and the corresponding protected aldehyde to the 3-position which would have been deprotected and modified with the masking unit for H<sub>2</sub>S activation. Unfortunately, the target molecule could not be attained. In the second approach (S2-BODMe), the

pyridine unit was incorporated to the bromo-BODIPY core and the aldehyde incorporation was introduced with a double Knoevenagel condensation reaction successfully, but insertion of the azido-based masking unit could not be accomplished. Later on, azido-based masking group was successfully attached to the corresponding aldehyde. As a future work, this new aldehyde containing masking unit will be used to modify the bromo-BODIPY core, followed by methylation of the pyridine unit to attain the target molecule.

**Keywords:** Photodynamic Therapy, BODIPY, Photosensitizer, Singlet Oxygen



## ÖZ

### HİDROJEN SÜLFÜR İLE AKTİVE OLAN BODIPY TABANLI PDT AJANLARININ SENTEZİ DOĞRULTUSUNDA ÇALIŞMALAR

Canyurt, Merve  
Yüksek Lisans, Kimya  
Tez Yöneticisi: Doç. Dr. Görkem Günbaş

Mayıs 2022, 117 sayfa

Fotodinamik Terapi (PDT), son zamanlarda çeşitli hastalıklar için yeni bir tıbbi tedavi olarak yaygın bir şekilde kabul görmüş, etkili ve minimal invaziv bir yöntemdir. PDT, organeller ve hücre zarlarına doğrudan zarar verebilecek sitotoksik türü oluşturmak için ışığa duyarlaştırıcılarla birlikte belli bir ışık kaynağı ve moleküler oksijen kullanır. Fotodinamik tepkimeler hedef dokuda bu duyarlaştırıcıların ışığı soğurmasıyla başlar, bu durum ise fotokimyasal olaylar zincirini oluşturur. Mevcut duyarlaştırıcılara kıyasla, BODIPY (4,4-difloro-4-bora-3a,4a-diaza-s-indacene), yüksek floresan ve üçlü kuantum verimi, işlevselleştirme kolaylığı ve ayarlanabilir foto fiziksel özellikleri sayesinde yeni nesil ışığa duyarlaştırıcıların oluşturulmasını sağlar. Bu çalışmanın amacı, suda çözünebilir, mitokondri hedefli ve aktive edilebilir, iki farklı ışığa duyarlılaştırıcı sentezlemektir. Bu amaçla, bromlu BODIPY çekirdeği, piridinyum ünitesi ve aşırı eksprese edilmiş bir tümör metaboliti olan H<sub>2</sub>S ile aktive edilen azido-benzil maskeleme ünitesi ile farklı pozisyonlarda modifiye edilir. İlk duyarlılaştırıcıda (S-BODMe), ardışık iki Knoevenagel kondenzasyon işlemi denenerek Piridinyum ünitesi 5-pozisyonuna ve karşılık gelen korunmuş aldehit 3-pozisyonuna takılmaya çalışıldı. Bu aldehit koruma grubundan ayrılarak H<sub>2</sub>S aktivasyonunu sağlayan maskeleme birimi ile modifiye edilmeye çalışıldı. Maalesef ki hedef molekül elde edilemedi.

İkinci yaklaşımda (S2-BODMe), piridin birimi bromo-BODIPY çekirdeğine dahil edildi ve bir çift Knoevenagel kondenzasyon reaksiyonu ile aldehit birleşmesi başarılı bir şekilde uygulandı, ancak azido bazlı maskeleme ünitesinin yerleştirilmesi gerçekleştirilemedi. Daha sonra, azido bazlı maskeleme grubu, belirtilen aldehite başarılı bir şekilde bağlandı. Gelecekteki bir çalışma olarak, bu yeni aldehit içeren maskeleme ünitesi, bromlanmış BODIPY çekirdeğini modifiye etmek için kullanılacak, ardından hedef moleküle ulaşmak için piridin ünitesinin metilasyonu yapılacaktır.

Anahtar Kelimeler: Fotodinamik Terapi, BODIPY, Işığa Duyarlılaştırıcı, Singlet Oksijen

**To my beloved family...**

## ACKNOWLEDGMENTS

First, I would like to express my sincere gratitude to my supervisor Assoc. Prof. Dr. Grkem Gnbař for his dedicated support, enthusiastic encouragement, and useful critiques of this research work. His valuable suggestions and fruitful discussions have encouraged me in my academic research and helped me grow in my career.

I would like to express my deepest appreciation to my committee members, Prof. zdemir Doęan, Assoc. Prof. Dr. Salih zubuku, Assoc. Prof. Dr. zgl Persil etinkol and Assist. Prof. Dr. Safacan Klemen for investing their time and effort to evaluate my thesis.

I would like to express my special thanks to Osman Karaman whose support which helped me to solve the scientific and technical problems and to conduct this thesis. I want to also thank to Sena Tarım for her continuous support and help during the completion of this work. Their contributions have been invaluable throughout this study.

I am also thankful to all technicians of the Chemistry Department for all their technical help and support.

I am grateful to my friends, Emine Ayře Turhan, Merve Tutundzic, Saliha Grgl, Kbra zsoy, Ayře Bařsoy and Gizem iędem Demir, who were always encouraging, motivating, and cheering me on through hard times.

I would like to thank all Gnbař Research Group members for their support and friendship during my journey.

I would like to express my special thanks to Volkan Demir, for his priceless support in different forms and unconditional love. You believed in me more than I do and without you, this adventure could be so hard for me. I am so lucky to have you in my life.

And my deepest gratitude to my family for the unconditional love and support they have shown me during my research process and all my life. I deeply thank my parents, Zehra Canyon and Kadir Canyon for unfailing emotional support and trust and I am grateful to my brother, Emircan Canyon for always being there for me. I owe this thesis to my family members who always stood by me and provided the strength in pursuing this research.

## TABLE OF CONTENTS

ABSTRACT .....	v
ÖZ.....	vii
ACKNOWLEDGMENTS .....	x
TABLE OF CONTENTS .....	xii
LIST OF TABLES .....	xv
LIST OF FIGURES .....	xvi
LIST OF SCHEMES .....	xvii
LIST OF ABBREVIATIONS .....	xix
LIST OF SYMBOLS.....	xxi
CHAPTERS	
1 INTRODUCTION.....	1
1.1 Photodynamic Therapy.....	2
1.2 Development of Photodynamic Therapy .....	4
1.3 Photodynamic Reaction .....	11
1.4 Cell Death and Tumor Destruction Imposed by PDT.....	14
1.4.1 Apoptosis, Necrosis, and Autophagy .....	15
1.4.2 Vascular Mechanisms.....	16
1.4.3 Immunological Mechanisms .....	17
1.5 Subcellular Uptake and Localization of Photosensitizers.....	18
1.6 Major Components of PDT.....	19
1.6.1 Light in PDT.....	19
1.6.2 Oxygen .....	24

1.6.3	Photosensitizers.....	25
1.7	BODIPY .....	30
1.7.1	Functionalization.....	33
2	RESULTS AND DISCUSSIONS .....	36
2.1	Aim of the Study and Design of Target Photosensitizers .....	36
2.1.1	Efforts Towards Synthesis of S-BODMe .....	37
2.1.2	Efforts Towards Synthesis of S2-BODMe .....	46
3	CONCLUSION.....	50
4	EXPERIMENTAL.....	53
4.1	Materials and Methods .....	53
4.2	Equipments.....	53
4.3	Experiments Towards Synthesis of S-BODMe.....	54
4.3.1	Synthesis of Compound 1 .....	54
4.3.2	Synthesis of Compound 2 .....	55
4.3.3	Synthesis of Compound 4 .....	56
4.3.4	Synthesis of PMB-Cl .....	57
4.3.5	Synthesis of Compound 7 .....	58
4.3.6	Synthesis of Compound 6 .....	59
4.3.7	Synthesis of Compound 8 .....	60
4.3.8	Synthesis of Compound 9 .....	61
4.3.9	Synthesis of Compound 11 .....	62
4.3.10	Synthesis of Compound 12 .....	63
4.3.11	Deprotection of TBDMS Protection Group.....	64
4.3.12	Synthesis of Compound 13 .....	65

4.3.13	Synthesis of Compound 13.....	66
4.4	Experiments Towards Synthesis of S2-BODMe .....	67
4.4.1	Synthesis of Compound 15.....	67
4.4.2	Synthesis of Compound 16.....	68
4.4.3	Synthesis of Compound 17.....	69
4.4.4	Synthesis of Compound 19.....	70
REFERENCES	.....	71
APPENDICES	.....	92
A.	NMR Spectra .....	93



## LIST OF TABLES

<b>Table 1.1.</b> Timeline of PDT. The timeline shows selected applications of PDT for cancer .....	11
<b>Table 1.2.</b> Advantages and disadvantages of laser, LED, and lamp sources .....	22
<b>Table 1.3.</b> Types of light sources available for use in PDT .....	23

## LIST OF FIGURES

<b>Figure 1.1.</b> Clinical course of PDT using intravenous photosensitizer .....	3
<b>Figure 1.2.</b> (a) Structure of porphyrin ring, (b)Structure of hematoporphyrin .....	5
<b>Figure 1.3.</b> Structure of Acridine orange and Eosin .....	6
<b>Figure 1.4.</b> Synthesis of hematoporphyrin derivative (HpD) from heme.....	8
<b>Figure 1.5.</b> (a) Structure of ALA, (b) Structure of PpIX .....	9
<b>Figure 1.6.</b> Structure of Porfimer Sodium (Photofrin) .....	10
<b>Figure 1.7.</b> Schematic illustration of PDT including Jablonski Diagram.....	13
<b>Figure 1.8.</b> Schematic illustration of PDT mechanisms for tumor destruction .....	15
<b>Figure 1.9.</b> Penetration depth of different wavelength range to the skin.....	20
<b>Figure 1.10.</b> Optical window in tissue .....	21
<b>Figure 1.11.</b> Presentation of the electronic configuration of ground, singlet and triplet excited states of the molecular oxygen .....	25
<b>Figure 1.12.</b> Examples of Tetrapyrrole structures .....	26
<b>Figure 1.13.</b> Examples of First & Second Generation of photosensitizer .....	29
<b>Figure 1.14.</b> The main application fields of BODIPYs .....	31
<b>Figure 1.15.</b> Schematic view of the structural modifications and chemical reactions tested herein.....	32
<b>Figure 1.16.</b> Example of sulfonation or halogenation of BODIPY derivatives at 2-, 6- positions .....	33
<b>Figure 1.17.</b> Example of the heteroaryl-fused BODIPY based photosensitizer synthesized by Suzuki coupling reaction .....	34
<b>Figure 1.18.</b> Schematic representation of created tetra-styryl BODIPY derivatives .....	35
<b>Figure 1.19.</b> Schematic representation of tetra-styryl BODIPY derivatives .....	35
<b>Figure 2.1.</b> S-BODMe & S2-BODMe molecular systems which are BODIPY-based and activable with physiologically active species (H <sub>2</sub> S).....	36

## LIST OF SCHEMES

<b>Scheme 2.1.</b> Synthetic pathway of compounds 1 & 2 .....	38
<b>Scheme 2.2.</b> Attempted synthetic pathway of compound 3 .....	38
<b>Scheme 2.3.</b> Synthetic pathways for compound 4.....	39
<b>Scheme 2.4.</b> Attempted synthetic pathways for compound 5 .....	40
<b>Scheme 2.5.</b> Attempted synthetic pathway of compound 6 .....	40
<b>Scheme 2.6.</b> Synthetic pathway for compound 7 .....	41
<b>Scheme 2.7.</b> Synthetic pathway for compound 6 .....	41
<b>Scheme 2.8.</b> Synthetic pathway for compound 8 .....	41
<b>Scheme 2.9.</b> Synthetic pathway for compound 9 .....	42
<b>Scheme 2.10.</b> Attempted synthetic pathways for compound 10 .....	43
<b>Scheme 2.11.</b> Synthetic pathway for compound 11 .....	43
<b>Scheme 2.12.</b> Synthetic pathway for compound 12 .....	44
<b>Scheme 2.13.</b> Synthetic pathway for compound 10 .....	44
<b>Scheme 2.14.</b> Synthetic pathway for compound 13 .....	45
<b>Scheme 2.15.</b> Synthetic pathway for compound 13. ....	45
<b>Scheme 2.16.</b> Attempted synthetic pathway for compound 14 .....	46
<b>Scheme 2.17.</b> Synthesis of compounds 15 and 16.....	47
<b>Scheme 2.18.</b> Attempted synthetic pathway for compound 17 .....	47
<b>Scheme 2.19.</b> Synthetic pathway for compound 17 .....	48
<b>Scheme 2.20.</b> Attempted synthetic pathway for compound 18 .....	48
<b>Scheme 2.21.</b> Synthetic pathway for compound 19. ....	49
<b>Scheme 2.22.</b> Schematic representation of the final steps towards realizing S2- BODMe .....	49
<b>Scheme 4.1.</b> Synthetic route of compound 1 .....	54
<b>Scheme 4.2.</b> Synthetic route of compound 2 .....	55
<b>Scheme 4.3.</b> Synthetic route of compound 4 .....	56
<b>Scheme 4.4.</b> Synthetic route of PMB-Cl .....	57

<b>Scheme 4.5.</b> Synthetic route of Compound 7.....	58
<b>Scheme 4.6.</b> Synthetic route of Compound 6 .....	59
<b>Scheme 4.7.</b> Synthetic route of Compound 8.....	60
<b>Scheme 4.8.</b> Synthetic route of Compound 9.....	61
<b>Scheme 4.9.</b> Synthetic route of Compound 11.....	62
<b>Scheme 4.10.</b> Synthetic route of Compound 12.....	63
<b>Scheme 4.11.</b> Synthetic route of Deprotection of the TBDMS Group .....	64
<b>Scheme 4.12.</b> Synthetic route of Compound 13.....	65
<b>Scheme 4.13.</b> Synthetic route of Compound 13.....	66
<b>Scheme 4.14.</b> Synthetic route of compound 15 .....	67
<b>Scheme 4.15.</b> Synthetic route of compound 16 .....	68
<b>Scheme 4.16.</b> Synthetic route of compound 17 .....	69
<b>Scheme 4.17.</b> Synthetic route of Azide containing masking unit .....	70

## LIST OF ABBREVIATIONS

AcOH	Acetic Acid
ALA	5-aminolevulinic Acid
BODIPY	4,4-difluoro-4-bora-3a, 4a-diaza-s-indacene
DCM	Dichloromethane
DDQ	2,3-Dichloro-5,6-Dicyanobenzoquinone
DLI	Drug–Light Interval
DMF	Dimethylformamide
FDA	Food and Drug Administration
HpD	Hematoporphyrin Derivative
LED	Laser-Emitting Diode
MeOH	Methanol
MP	Methyl Pyridinium
NBS	N-bromosuccinimide
NIR	Near Infrared
NMR	Nuclear Magnetic Resonance
PDT	Photodynamic Therapy
PMB-Cl	4-Methoxybenzyl chloride
PS	Photosensitizer
PS <sub>0</sub>	Ground State of PS
PS <sub>1</sub>	Singlet Excited State of PS
p-TsOH	p-Toluensulfonic Acid

ROS	Reactive Oxygen Species
RT	Room Temperature
T <sub>1</sub>	Triplet-State of PS
TBAF	Tetra-n-butylammonium Fluoride
TBDMS-Cl	Tert-Butyldimethylsilyl Chloride
TEA	Triethylamine
TLC	Thin-Layer Chromatography
UV	Ultraviolet

## LIST OF SYMBOLS

$\mu\text{s}$	Microsecond
$\text{ns}$	Nanosecond
$\Phi\Delta$	Quantum Yield of PS
$\Phi\text{T}$	Quantum Yield of PS's Triplet Excited State
$\tau\text{T}$	Lifespan of PS's Triplet Excited State
${}^3\Sigma_{\text{g}}^{-}$	Triplet Ground State of Molecular Oxygen
${}^1\Delta_{\text{g}}$	Low-lying Excited State of Molecular Oxygen ( ${}^1\text{O}_2$ )
${}^1\Sigma_{\text{g}}^{+}$	Triplet Excited State of Oxygen





## CHAPTER 1

### INTRODUCTION

Development of novel cancer treatment modalities has gained widespread interest in from scientific community since it is responsible for the deaths of more than 15% of the earth's population (Ismaiel, 2017). A typical body has trillions of cells that grow, reproduce, and die every second. The growth and proliferation of cells in an abnormal body, on the other hand, is uncontrolled. Instead of dying, these cells continue to expand as abnormal and cells invade adjacent tissues (Stone et al., 2003). Furthermore, DNA damage occurs occasionally, and normal cells have mechanisms to either fix the damage or trigger cell death. Cancer cells lack these abilities hence the damage spreads in a random and accelerating manner. As a result, cancer is perhaps one of the world's most dangerous and difficult diseases to treat. In coming years, the number of people living with cancer is foreseen to rise sharply unless new effective treatment modalities emerge (Korbelik, 2010).

Several treatment approaches, such as chemotherapy and radiotherapy, are commonly used worldwide (Triesscheijn et al., 2006). Other techniques include stem cell transplantation, surgery, immunotherapy, and hormone therapy (Rother & Harlan, 2004). The most challenging aspect of these techniques, in addition their general effectiveness, is the significant side effects and the potential for severe discomfort in patients. Hence, interest in developing innovative, safer, and non-invasive approaches became one of the leading research areas. Photodynamic Therapy has emerged as one of the most prominent and promising approaches towards accomplishing this aim. The role of organic chemists and biochemists are crucial in development of this technology as it requires synthesis of chemical agents specific to cancer cells inducing cell death (Drucker, 2005; Klonisch et al., 2008).

## 1.1 Photodynamic Therapy

Photodynamic Therapy (PDT) is a minimally invasive therapy that has recently gained widespread recognition as a potentially new treatment for several conditions, including various types of cancer, age-related macular degeneration and actinic keratosis (Gler et al., 2012; Triesscheijn et al., 2006). PDT uses a light activatable compound called a photosensitizer (PS), light of a certain wavelength, and molecular oxygen ( $^3\text{O}_2$ ). These three components are innocuous separately but, when combined, produce cytotoxic species (Dolmans et al., 2003) that can directly damage organelles and cell membranes (Bacellar et al., 2015).

PDT is a two-step approach involves administering a PS intravenously, intraperitoneally, or topically, which ideally, accumulates in tumor tissue (during a drug–light interval) in a selective manner, and then exposing the cells to light (Bacellar et al., 2015). Photosensitizers are designed in a way that they are taken up preferentially by tumor and macrophage cells. After that, when exposed to light, these photosensitizers undergo electron/energy transfer through their triplet excited state, which reacts with molecular oxygen ( $^3\text{O}_2$ ) to form reactive oxygen species (ROS), primarily singlet oxygen ( $^1\text{O}_2$ ) (Ochsner, 1997). These cytotoxic chemicals cause a cascade of biological processes that result in cell death or tissue damage locally (Josefsen & Boyle, 2008). As a result of the short half-life of singlet oxygen ( $0.6 \times 10^{-6}$  s) (Moan & Berg, 1991), this is a highly confined effect. In cancer treatment, PDT can harm the vasculature around tumor cells and trigger immune responses against them as well (Juarranz et al., 2008). The capacity to accomplish dual selectivity, which implies that the photosensitizer accumulates preferentially in diseased – rather than normal – tissues, and the ability to focus light on limiting damage to the specified location, is PDT's key feature (Castano et al., 2004). Because of several advantages, such as tumor targeting, minimal invasiveness, reduced systemic cytotoxicity, low cost, and spatiotemporal control of light exposed to tumors, PDT is increasingly recognized as a potential clinical tool in cancer therapy in addition to other therapies (such as surgery and radiation therapy) (Dang et al., 2017).

For PDT to be effective, several points must be taken into account. The location of the photosensitizer accumulation in the tumor cells influences PDT performance (Dolmans, Kadambi, Hill, Waters, et al., 2002). Another critical aspect in determining PDT efficacy is the time gap between sensitizer delivery and light exposure. The most successful technique to target both tumor blood arteries and cells is to administer photosensitizers at different time intervals before light activation (fractionated drug-dose PDT). Compared to single-dose regimens like anti-vascular PDT or antitumor-cell PDT, fractional drug-dose PDT regimens are found to have a higher therapeutic impact and promote long-term tumor growth suppression (Dolmans, Kadambi, Hill, Flores, et al., 2002). This is just another example of how targeting several areas is the most efficient method to treat a tumor. Using particular targeting carriers, such as conjugated antibodies aimed at tumor-associated antigens or vascular antigens, is another technique to route the photosensitizer to a specific cell type or compartment (Ruoslahti, 2002). Photosensitizers that can localize to mitochondria, plasma membrane, lysosomes, and nuclei have been produced since the mid-1990s (Peng et al., 1996). Efficiency of PDT is further influenced by the action location inside a cell (Bachor et al., 1991). These aspects are critical when combining PDT with other therapy methods, such as medicines that target different subcellular areas or cell activities (Duska et al., 1999).

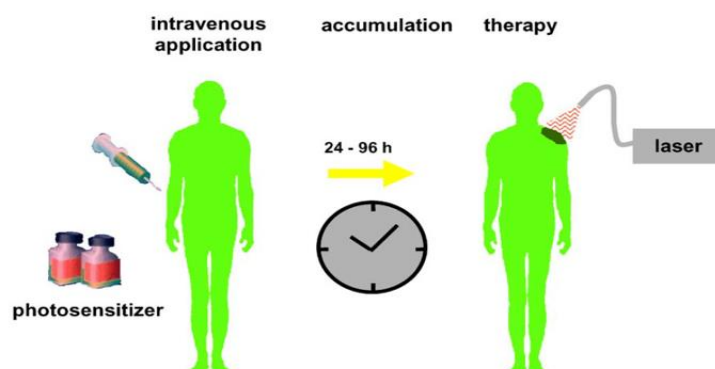


**Figure 1.1.** Clinical course of PDT using intravenous photosensitizer (Kübler, 2005)

## 1.2 Development of Photodynamic Therapy

Since the beginning of time, the light given by our sun has fostered the growth of life on Earth, and it continues to do so. In many early cultures and beliefs, the sun was linked to magical forces that were considered to provide humans with therapeutic effects. In ancient Egyptian, Indian, and Chinese civilizations, several skin illnesses such as psoriasis, vitiligo, skin cancer, rickets, and even psychosis were all treated with sunshine. Thousands of years have passed since light has been used as a medicinal agent (Epstein, 1990; Spikes, 1985).

The ancient Greeks used heliotherapy, or whole-body sunlight exposure, to cure diseases, and reclining naked in the sun was a common pastime. Herodotus, the father of heliotherapy, was a Greek physician who highlighted the value of sunlight exposure for health improvement. Sunlight was also used to treat a range of ailments in France during the 18<sup>th</sup> and 19<sup>th</sup> centuries, including tuberculosis, rickets, scurvy, rheumatism, paralysis, edema, and muscular weakness (Ackroyd et al., 2001).

Niels Finsen, a Danish physician, developed 'phototherapy', or 'light therapy' to treat ailments in the late 19<sup>th</sup> century. He discovered that exposure to red light reduces the production and release of smallpox pustules and can be utilized to cure the condition (Finsen, 1901). He also discovered carbon arc phototherapy and used UV radiation from the sun to treat cutaneous TB. Finsen was awarded the Nobel Prize for his discoveries in 1903, marking the birth of modern light treatment.

Phototherapy is the use of light to treat various diseases. In contrast, photochemotherapy is the delivery of a photosensitizing chemical followed by light on the tissues in which the agent is localized. Psoralens from natural plants were used by the Indians in the treatment of vitiligo over 3000 years ago. In contrast, the Egyptians used distinct psoralens to heal leukoderma in the 12<sup>th</sup> century (Fitzpatrick & Pathak, 1959).

Scientists have known for nearly a century that cell death is induced by the interaction of light and chemicals, which is referred to as photosensitizers. H. Scherer discovered hematoporphyrin (Hp) in 1841 while examining the structure of blood.

The extraction of hematoporphyrin from dried blood was a defining moment in the realm of photosensitizers (PSs) (Scherer, 1841). Although its luminous qualities were identified in 1867 (Thudichum, 1867), it wasn't until 1871 that it was given the name hematoporphyrin (Hoppe-Seyler, 1871).

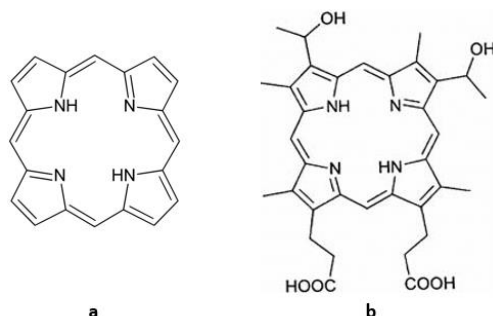


**Figure 1.2.** (a) Structure of porphyrin ring, (b) Structure of hematoporphyrin

Photodynamic therapy (PDT) has a long history in medicine, dating back to the early 20<sup>th</sup> century. In 1900, Oskar Raab, a German medical student working with Professor Herman von Tappeiner in Munich, reported for the first time that paramecia cells (*Paramecium caudatum*) were unaffected when exposed to either acridine orange or a light source but perished within 2 hours if exposed to both. In this study, the photosensitizer acridine orange was employed to sensitize paramecia cells to the effects of the light source (Raab, 1900). Raab identified the optical property of fluorescence and concluded that in vitro toxicity was caused by a component of fluorescence rather than by light. He theorized that the energy transferred from light to the chemical was responsible for this effect (von Tappeiner, 1900).

In 1900, eosin was the first recorded instance of a photosensitizing medication delivered intraperitoneally to humans. J. Prime, a French neurologist, was the first to use eosin orally to treat epilepsy. According to Prime, dermatitis appeared on parts of the body exposed to light (Prime, 1900). As a result of this discovery, H. von Tappeiner and dermatologist A. Jesionek employed a combination of topical eosin and white light to treat skin cancers in the first medical application of a fluorescent chemical with light (von Tappeiner & Jesionek, 1903). H. von Tappeiner and A.

Jodlbauer revealed in 1904 that photosensitization reactions require oxygen. These studies were compiled into a book in 1907, in which H. von Tappeiner created the phrase 'photodynamic action' to define oxygen-dependent photosensitization (von Tappeiner & Jodlbauer, 1907).

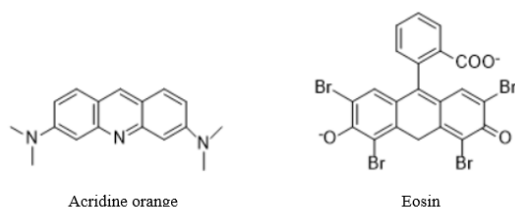


**Figure 1.3.** Structure of Acridine orange and Eosin

Hematoporphyrin (Hp) is formed when iron is paired with a porphyrin structure. W. Hausmann was the first to study the biological features of these compounds in 1908. He used hematoporphyrin and light to kill paramecium and red blood cells, and observed that the combination killed the cells. In addition, he described skin reactions in mice exposed to light after receiving hematoporphyrin (Hausmann, 1911).

When German scientist Friedrich Meyer-Betz injected himself with 200 mg of hematoporphyrin in 1913, he became the first person to show that porphyrins may work as photosensitizing substances in humans. He felt acute discomfort and swelling localized to the light-exposed areas shortly after exposure to the light (Meyer-Betz, 1913).

Policard, a Frenchman, detected the distinctive red fluorescence of hematoporphyrin in an experimental rat sarcoma irradiated with UV light from a Woods lamp in 1924, which was the first report of fluorescent porphyrin localization in a malignant tumor (Policard, 1924). Although the fluorescence was accurately attributed to porphyrin localization within the tumor, it was originally assumed to result from secondary infection because comparable fluorescence had been detected in bacterial cultures.

Auler and Banzer explored hematoporphyrin intake into tumors in 1942, firmly demonstrating its selective uptake and retention, with more significant levels in the tumor than in the normal surrounding tissues. During their study, they found that the fluorescing tumors were generally more necrotic, and identified photodynamic action of hematoporphyrin on tumors for the first time (Auler & Banzer, 1942). This discovery led Figge and Weiland to look into the tumor-localizing capabilities of porphyrins in order to develop its use for tumor detection and treatment (Figge et al., 1948).

Schwartz revealed in 1955 that the hematoporphyrin utilized in earlier studies was a combination of porphyrins with varying characteristics (Schwartz et al., 1955). He treated crude hematoporphyrin with acetic and sulfuric acids filtered and neutralized the precipitate with sodium acetate. He then redissolved the precipitate in saline to generate a hematoporphyrin derivative (HpD), among other things. This compound was discovered to be up to twice as phototoxic as crude hematoporphyrin, causing death in mice exposed to light. The drug dose, the duration of light exposure, and the length between medication and light exposure all influenced the intensity of the reaction.

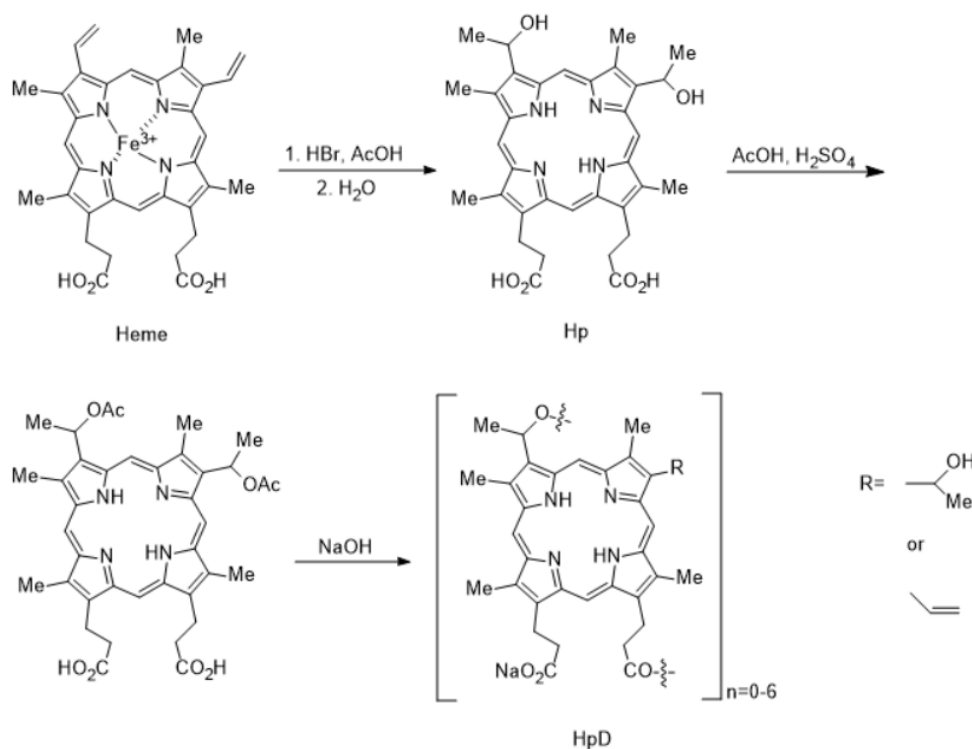


**Figure 1.4.** Synthesis of hematoporphyrin derivative (HpD) from heme (Ormond & Freeman, 2013)

Lipson of the Mayo Clinic, along with Baldes, showed the property of tumor localization (Lipson & Baldes, 1960), and they became intrigued by the applicability of HpD in tumor identification in the early 1960s. They went on to show that HpD was more efficient in tumor localization and distinction from normal tissues than crude hematoporphyrin and that they could do it with considerably lower concentrations (Lipson et al., 1961a). This was the first research to show that tumor localization and fluorescence may be used clinically to detect human tumors (Lipson et al., 1961b).

I. Diamond and fellow researchers in 1972 suggested that porphyrins could be used to destroy cancer cells by combining their tumor-localizing and tumor-phototoxic capabilities. PDT was found to slow the growth of gliomas injected in rats in vivo research. Tumor growth was slowed for 10–20 days, but after that, surviving areas in the tumor's deeper sections began to grow once more (Diamond et al., 1972).



In 1975, Thomas Dougherty and fellow researchers suggested that administering HpD and activating it with red light entirely abolished mammary tumor growth in mice (Dougherty et al., 1975). A significant discovery in PDT happened in 1975 when Thomas Dougherty and collaborators revealed that administering HpD and activating it with red light eliminated breast tumor growth in mice (Dougherty et al., 1975). J.F.Kelly and collaborators found in the same year that light stimulation of HpD also eradicated bladder carcinoma in mice (Kelly et al., 1975). Another significant milestone in the evolution of PDT occurred in 1976 when the first human trials of PDT with HpD began. J. F. Kelly and M. E. Snell needed thus in patients with bladder cancer, and HpD was used to diagnose cancer in five cases (Kelly & Snell, 1976)

Moan and Wold evolved different electron spin resonance in 1979 to monitor the extremely reactive singlet oxygen radical ( $^1\text{O}_2$ ) generation when HpD was exposed to light (Moan & Wold, 1979). J. S. McCaughan was the first to employ this approach in treating gastrointestinal disorders in 1984 when he used PDT to treat patients with esophageal cancer. Y. Hayata employed PDT to treat patients with gastric carcinoma the following year (Ackroyd et al., 2001; Dolmans et al., 2003). When Kennedy published the first topical porphyrin derivative, aminolevulinic acid (ALA), in 1990, they forever transformed the nature of PDT. This photosensitizer is a prodrug that is converted to its active form in the skin (Kennedy et al., 1990).

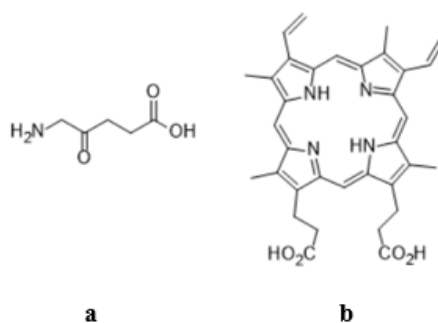


**Figure 1.5.** (a) Structure of ALA, (b) Structure of PpIX

PDT generates an apoptotic response in cells (Agarwal et al., 1991) , which was discovered in 1991, and this presented an explanation for PDT's overall effectiveness.

T. Dougherty and fellow researchers also purified HpD and developed porfimer sodium, also known as Photofrin, the first photosensitizer (PS) molecule to be approved by the US Food and Drug Administration (FDA) for cancer treatment in 1995 (C.N. Lee et al., 2020).

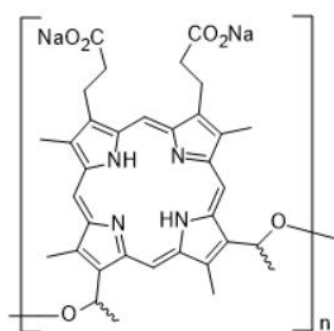
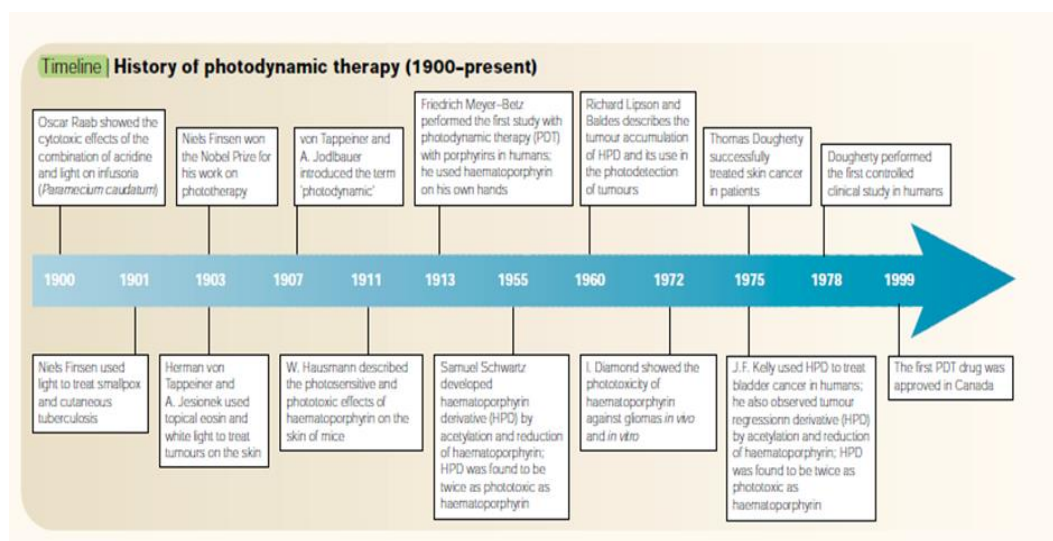


**Figure 1.6.** Structure of Porfimer Sodium (Photofrin)

Since then, PDT has progressed, and its therapeutic potential has broadened outside tumor treatment.

**Table 1.1.** Timeline of PDT. The timeline shows selected applications of PDT for cancer (Gunaydin et al., 2021)



### 1.3 Photodynamic Reaction

Photodynamic therapy is a medical treatment method that uses photosensitizers in combination with a specific light source to cause tumor cells to die (Dougherty et al., 1998). The photodynamic reaction (PDR) starts with light absorption by the PS in the target tissue, which sets off a chain of photochemical events that produce reactive oxygen species (ROS) (Huang et al., 2008).

The photosensitizer formulation is administered systemically via intravenous injection in the PDT process. After injection, the affected tissue is irradiated with light of the proper wavelength and energy dose that corresponds to the most significant photosensitizer accumulation in the target tissue. PDT is based on the mechanisms of light absorption and energy transfer (Nelius et al., 2004).

Photosensitizers have a persistent electronic structure in which two electrons with opposite spins are in a singlet state in their lowest or ground energy level ( $PS_0$ ) (Konan et al., 2002), indicating that there are no unpaired electron spins (Kalyanasundaram, 1992). The activation of these electrons into a higher-energy

orbital is caused by the absorption of a photon of light with the right wavelength. This singlet excited-state PS ( $PS_1$ ) is a volatile short-lived species that loses its surplus energy as light (fluorescence) or generates heat (internal conversion) (Foote, 1968). Because most PSs are fluorescent, sensitive techniques for quantifying PS in cells or tissues have been designed, as well as in vivo fluorescence imaging in living animals or patients to assess PS pharmacokinetics and allocation (Castano et al., 2004).

The excited singlet PS ( $PS_1$ ) may undergo 'intersystem crossing,' which results in the formation of a more stable excited triplet state ( $T_1$ ) with parallel spins (Foote, 1968), which has a longer survival time and lower energy than  $PS_1$  (Ochsner, 1997).

The triplet-state PS molecule ( $T_1$ ) can deteriorate back to its ground by losing energy through light emission (phosphorescence), but this is a 'forbidden process' according to quantum selection theory. Hence, the triplet state is much more stable than the singlet state, with a life span of microseconds ( $10^{-6}$ ,  $\mu s$ ) compared to only nanoseconds ( $10^{-9}$ , ns) for the excited singlet (Foote, 1968). Moreover, the photosensitizer is not always eliminated; it can return to its initial state via phosphorescence without undergoing any chemical changes. It may be likely to repeat the energy transfer process multiple times (Ochsner, 1997). This triplet state ( $T_1$ ) is the photoactive state, capable of generating cytotoxic species through two major reactions known as Type-I and Type-II.

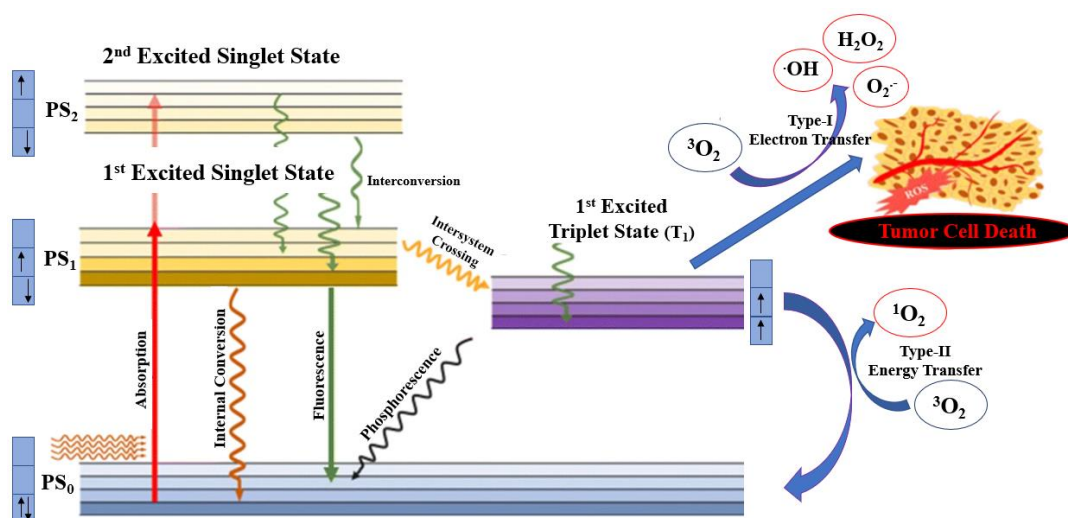


**Figure 1.7.** Schematic illustration of PDT including Jablonski Diagram (Baskaran et al., 2018)

The excited triplet state of photosensitizer ( $T_1$ ) can carry electrons to biomolecules from its surroundings in the Type-I mechanism.  $T_1$ -PS combines directly with malignant tissue (substrate) and performs hydrogen atom abstraction or electron transfer processes, resulting in free radicals and anionic radicals (Luksiene, 2003; Nowak-Stepniowska et al., 2013). These radicals interact with molecular oxygen ( $^3O_2$ ) to generate reactive oxygen species (ROS), such as superoxide ( $O_2^{\cdot-}$ ) and peroxide ( $H_2O_2$ ), which cause oxidative damage in the body (Fitzgerald, 2017). Because the triplet state has such a long life, it has enough time for energy transition by combining with molecular oxygen ( $^3O_2$ ), which is conceivable because their spins are the same. The reaction is known as a Type-II photochemical process (Foote, 1968), because it results in the creation of singlet oxygen ( $^1O_2$ ), which has powerful oxidizing capabilities, as well as ground-state PS ( $PS_0$ ).

The Type-II reaction is preferred over the Type-I response since it has a shorter mechanism and is generally thermodynamically preferable for red-absorbing PS. This helps to explain why  $^1O_2$  is thought to be the primary cause of PDT phototoxicity. One of the essential properties of a PS is its quantum yield ( $\Phi\Delta$ ),

which is defined by the quantum yield ( $\Phi_T$ ) and lifespan ( $\tau_T$ ) of its triplet-excited state (Calzavara-Pinton et al., 2007).

Only molecules and structures proximal to the area of its production (areas of PS localization) are directly affected by PDT because of the high reactivity and short half-life of singlet oxygen and hydroxyl radicals. Because singlet oxygen has a half-life of 40 nanoseconds in biological systems, its radius of action is on the order of 20 nanometers (Moan & Berg, 1991).

The amount of damage and cytotoxicity caused by PDT varies due to the type of PS, its extracellular and intracellular location, the total dose injected, the light dose (light fluence) and the light fluence rate, oxygen availability, and the time between PS administration and light exposure (Dolmans et al., 2003).

#### **1.4 Cell Death and Tumor Destruction Imposed by PDT**

Surgery is not a drastic treatment for some types or extents of cancer when it comes to treatment. Radiation and chemotherapy can be ineffective and have several adverse effects. As a result, new cancer therapy options are required. Direct phototoxicity to tumor cells, which results in apoptosis, necrosis, or autophagy cell death, is one of the three processes involving photochemical reactions. The breakdown of the tumor vascular system and immune-mediated inflammatory damage to tumor cells are the other two options (Buytaert et al., 2007).

Photochemical processes produce reactive oxygen species (ROS), which have a direct phototoxic effect on tumor cells and cause irreversible photodamage to specific targets at the molecular level, such as membranes and organelles. Other cell death pathways, such as tumor-associated vasculature destruction and immune response against tumor cells, are commonly thought to be useful targets for inducing and thus increasing photo-killing in tumor cells with apoptotic pathway defects, which is a crucial step in carcinogenesis and therapy resistance (Buytaert et al., 2007; Henderson & Dougherty, 1992; Moan & Berg, 1992). Improving the efficacy of PDT

against cancer cells by focusing on the fundamental distinctions of cell death processes generated by PDT would undoubtedly provide helpful hints for the development of new treatment modalities and medication selectivity.

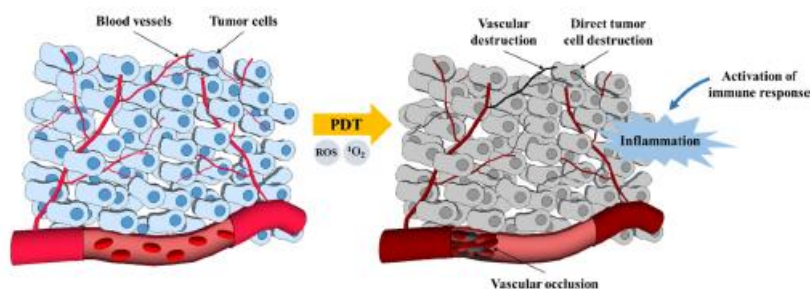


**Figure 1.8.** Schematic illustration of PDT mechanisms for tumor destruction (Correia et al., 2021)

#### 1.4.1 Apoptosis, Necrosis, and Autophagy

PS is required for intracellular action, and it has a profound impact on the cell's fate. Depending on its properties, a PS will often localize to organelles such as the plasma membrane, lysosomes, mitochondria, golgi apparatus, or endoplasmic reticulum (ER) (Castano et al., 2004). PDT can cause tumor death by both planned (apoptotic) and non-programmed (necrosis) pathways (Boyle & Dolphin, 1996; Igney & Krammer, 2002). Apoptosis is defined as a genetically encoded and energy-dependent mechanism of planned cell death. Apoptosis is more likely to be induced by PSs that localizes to mitochondria (Kessel & Reiners, 2007). Apoptotic death can also be triggered by PDT, primarily when low light dosages are used (Agarwal et al., 1991).

Components of the apoptotic cascade may be disrupted due to significant cell damage, and apoptosis may not be correctly implemented. This process is favored by more severe PDT techniques, which include high dose of PS and light, resulting in increased cell damage and necrosis (Lavie et al., 1999; Luo & Kessel, 1997; Nagata et al., 2003). Necrosis, in contrast to the apoptotic pathway, is thought to be less controlled and is more common when the PS site of action is the plasma

membrane. Photodamage to the plasma membrane causes intracellular substances to flow into the immediate environment, causing inflammation (Castano et al., 2006).

Autophagy is the ability of a cell to recycle damaged organelles and cytoplasmic components. The damaged particles are swallowed by an autophagosome, a double-membrane structure that merges with lysosomes to destroy the contents (Levine & Klionsky, 2004). Autophagy has been observed as a cell death mechanism in response to PDT (Buytaert et al., 2006; Kessel et al., 2006) despite being thought to be a cytoprotective mechanism. Autophagy appears to be the main step responsible for cell death when apoptosis is compromised (Kessel & Oleinick, 2009; Xue et al., 2007).

#### **1.4.2 Vascular Mechanisms**

Vascular mechanism of PDT therapy appears to be promising, notably in cancer treatment. Compared to traditional cell-targeting techniques, this approach is more efficient, easier to access tumor cells, and has a lower risk of developing drug resistance (Chen et al., 2006).

The amount of nutrients and oxygen delivered by tumor-related blood arteries determines tumor growth. Blood vessel formation and maintenance are dependent on growth factors supplied by tumor or host cells. The disruption of the vascular walls causes the tumor's nutrition (i.e., oxygen and nutrients) to be interrupted, resulting in tumor cell death (Rocha, 2015). When the PS is largely localized in the vasculature, a brief drug–light interval (the time between systemic PS injection and light illumination) can considerably boost the vascular effect of PDT (Hamblin & Huang, 2017).



### **1.4.3 Immunological Mechanisms**

For many years, PDT was thought to be a limited treatment that only affected tumor cells and microvasculature. PDT has recently been shown to have a major impact on immune system of patients, either through stimulation or repression of the immunological response. In areas outside of the irradiation field, the PDT-induced immune response can contribute considerably to the effectiveness of therapy and may even influence the development of disseminated tumors (Chen et al., 1999; Gollnick & Brackett, 2010; Kabingu et al., 2007; Mroz et al., 2010).

Long-term tumor control is most likely a combination of direct PDT effects on the lesion and its vasculature, as well as immune system upregulation. PDT causes immunosuppression under specific circumstances, which has been linked to reactions to topical treatments with high fluence rates and broad regions of irradiation (Rocha, 2015).

An immune cascade is triggered when PDT causes necrosis of tumors and associated vasculature (Gollnick et al., 1997). Inflammatory mediators, including as cytokines, growth factors, and proteins, are released from the treated site. This release causes numerous white blood cells, such as neutrophils and macrophages, to become activated, causing them to converge on the treatment area. When macrophages arrive, they phagocytize PDT-damaged cancer cells and deliver proteins from the tumors to CD4 helper T lymphocytes, which activate CD8 cytotoxic T lymphocytes. These cytotoxic T cells can detect and destroy tumor cells and also circulate throughout the body for lengthy periods, enabling a systemic antitumor immune response (Coutier et al., 1999; Gollnick et al., 2003).

## 1.5 Subcellular Uptake and Localization of Photosensitizers

For efficient PDT, PS absorption by cancer or other cells is critical. Due to its short half-life duration (0.04 s), singlet oxygen has a limited action radius. As a result, exact localization of PS is critical to its therapeutic impact. Understanding and managing PS localization is thus vital for effective selection (Castano et al., 2004; van Straten et. al., 2017). The better the selectivity, the more PS accumulates in cancer cells, increasing PDT's potential and reducing adverse effects compared to other therapeutic techniques (Rancan et al., 2005).

After the photosensitizer enters the cells, they are primarily found in the plasma membrane, lysosomes, endoplasmic reticulum, golgi apparatus, and mitochondria (Castano et al., 2004). The monitoring of activity and damage following illumination can be done using fluorescence resonance energy transfer (FRET) or introducing particular probes with different fluorescence (Kessel et al., 1997).

The cellular localization of a variety of photosensitizers with vastly varying structures has been determined. The net ionic charge, which can range from -4 anionic to +4 cationic, the degree of hydrophobicity and the degree of asymmetry contained in the PS molecule are all key structural properties (Castano et al., 2004).

According to studies, changing the lipophilicity of a PS influences its plasma distribution and, as a result, its uptake and localization. The photosensitizer's selectivity is directly proportionate to its lipophilic nature. Hydrophobic sensitizers with two or fewer negative charges connect to lipoproteins and are delivered to tumor tissues (Castano et al., 2005), but hydrophobic sensitizers with more than two negative charges become too polar to move across the cellular membrane. As a result, they lose their chance to transmit through and are taken into cells via endocytosis, resulting in localization to lysosomes, which harms the cells mostly through direct contacts (Robertson et al., 2009).

Lipophilicity can substitute low negative charges (Castano et al., 2004). Cationic PSs, on the other hand, circulate freely across the plasma membrane and

predominantly localize to mitochondrial membranes in the cell (Dummin et al., 1997; Woodburn et al., 1991). Higher lipophilicity contributes to enhanced absorption at the tissue level. With greater amphiphilicity, lipophilicity altered subcellular localization as it moved away from lysosomes and toward mitochondria. Higher affinity of more lipophilic substances for membrane contacts improves their localization to mitochondria (Pavani et al., 2009).

In comparison to hydrophilic PSs, hydrophobic PSs usually stay in the person's body for longer. Hydrophilic PSs, on the other hand, have the advantage of decomposing or disappearing from the body quickly, resulting in fewer adverse effects. As a result, water solubility can boost bioavailability and in vivo distribution (Sakamoto et al., 2002).

## **1.6 Major Components of PDT**

The molecular mechanism of photodynamic therapy comprises three non-toxic components that mutually interact to create the desired effects within problematic tissues: the photosensitizer (PS), proper wavelength of light, and oxygen dissolved in the cells (Allison & Moghissi, 2013).

### **1.6.1 Light in PDT**

Photodynamic interactions begin with the photosensitizer being activated by treatment light of the proper photosensitizer wavelength.

To perform PDT effectively, the light must reach all of the affected tissue. The depth of penetration of light in tissues is proportional to the amount of light utilized (Castano et al., 2004).

Depending on the composition of the tissue and the wavelength of light, the spatial distribution of light inside the target tissue is primarily dispersed or absorbed.

Still, it can also be reflected or transmitted (Juzeniene & Moan, 2007; Tong & Kohane, 2012).

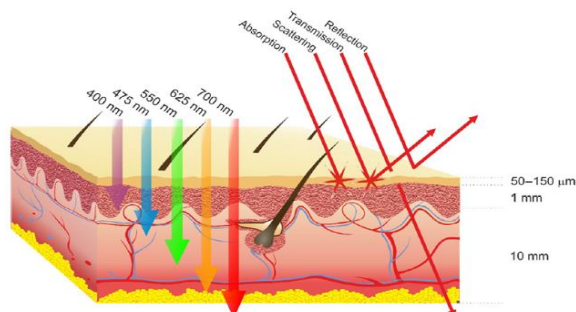


**Figure 1.9.** Penetration depth of different wavelength range to the skin (Dąbrowski, 2017)

The structure of the tissues is not uniform because of the existence of macromolecules, cellular organelles, and specific other forms, which contribute significantly to light scattering due to their turbidity, particularly at shorter wavelengths (Tong & Kohane, 2012).

Light absorption by endogenous chromophores, including hemoglobin or melanin, occurs below 600 nm, but tissue water light absorption goes up exponentially above 1300 nm. The range of wavelengths that can best enter tissue is thus limited, which is referred to as the optical window of tissue (Agostinis et al., 2011; Castano et al., 2006). Because light absorption by tissues reduces as wavelength increases, longer wavelengths of light (red or infrared light) reach tissue more efficiently (Agostinis et al., 2011). Shorter wavelengths (< 600 nm) penetrate the skin less and are absorbed more, resulting in greater skin photosensitivity. However, longer wavelengths (>850 nm) do not bear sufficient energy to excite oxygen in its singlet form and create enough reactive oxygen species. As a result, tissue penetration is greatest between 600 and 850 nm. This range is referred to as the "therapeutic window" in PDT (Agostinis et al., 2011; Kwiatkowski et al., 2018; Rocha, 2015; Simões et al., 2020).

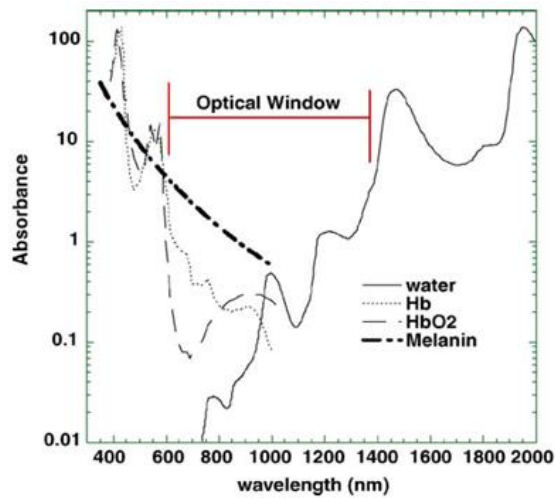


**Figure 1.10.** Optical window in tissue (Dąbrowski, 2017)

It is unlikely that a single light source could encompass all types of PDT employed with different light sources, such as lasers, incandescent light, and laser-emitting diodes (LEDs) (Yanovsky et al., 2019). The light source should be tailored to the photophysical characteristics (absorption spectrum) of the photosensitizers, the kind of disease (location, tumor size, tissue type), and usability (cost, size, handling) (Brancaleon & Moseley, 2002).

Lasers are commonly employed in clinical PDT because they are strong and can be connected to optical fibers to illuminate deeply placed lesions using diffusing tips (Brancaleon & Moseley, 2002). Creating monochromatic light with a highly narrow bandwidth is a distinctive attribute of lasers. Lasers have good optical power and can be tuned to match the wavelength of a given photosensitizer (Saleh & Teich, 2007). However, laser light sources are typically costly and necessitate the employment of an optical system to widen the light beam for irradiation of a greater tissue region (Chen et al., 2012).

Lamps are better for superficial tumors, such as those on the skin or in the mouth. Because the light generated by lamps has a broad spectrum (wavelengths of 300–1200 nm), adequate optical filtering is required to match the photoactivating

wavelength to the absorption band of photosensitizer. Optical filtering is also necessary to guarantee that the output light is free of unwanted ultraviolet and infrared wavelengths. Lamps have several advantages, including a simple design, lower cost, and a large illuminating field (Morton et. al., 2008). On the other hand, traditional lights may have heat effects that must be eliminated in PDT (Chen et. al., 2012).

Numerous studies are exploring alternative ways to optimize light sources. The use of Light Emitting Diodes (LEDs) in PDT, for example, is being examined (van Straten et al., 2017). LEDs are inexpensive, simple to produce, less dangerous, offer a high-power output, are thermally non-destructive, and are easily accessible in flexible arrays. On the other hand, they are limited in their application for larger tumors requiring an interstitial approach (Cantisani et al., 2015; Lacour et al., 2015).

As shown in Table 1.2, the advantages and disadvantages of various light sources are compared.

**Table 1.2.** Advantages and disadvantages of laser, LED, and lamp sources (Gunaydin et al., 2021a; M. M. Kim & Darafsheh, 2020)

Light Source	Advantages	Disadvantages
Laser	<ul style="list-style-type: none"> <li>• Capable of high powers</li> <li>• Highly monochromatic</li> <li>• Adaptable to various source fibers</li> </ul>	<ul style="list-style-type: none"> <li>• Expensive</li> <li>• Can be large</li> <li>• Requires high maintenance</li> </ul>
LED	<ul style="list-style-type: none"> <li>• Small, adaptable</li> <li>• Low cost</li> <li>• Can be used directly for endoscopic/interstitial applications</li> </ul>	<ul style="list-style-type: none"> <li>• Thermal effects</li> <li>• Low power</li> <li>• Broad spectral width</li> <li>• Large beam divergence</li> </ul>
Lamp	<ul style="list-style-type: none"> <li>• Simple design</li> <li>• Low cost</li> <li>• Broad field irradiation</li> </ul>	<ul style="list-style-type: none"> <li>• Can suffer from coupling losses with light guides</li> <li>• Very broad spectrum</li> <li>• Large beam divergence</li> <li>• Needs optical filtering</li> </ul>

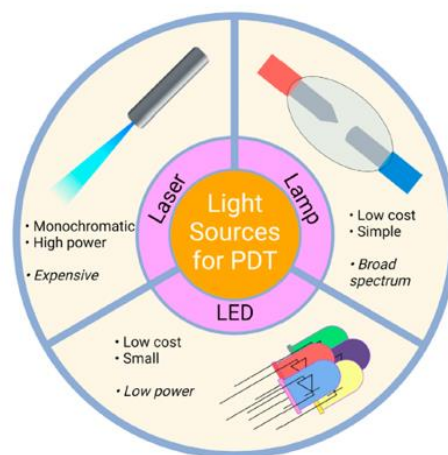


Table 1.3. summarizes the types of light sources (lamps, lasers, and new prospective sources) and their attributes features.

**Table 1.3.** Types of light sources available for use in PDT (Brancaleon & Moseley, 2002)

Type	Wavelength(s)	Bandwidth	Light Delivery
<b>Lasers</b>			
Argon laser	488 and 514.5 nm	Monochrome	Direct or optical fiber
Dye laser pumped by argon laser	500–750 nm (depending on the dye)	5–10 nm	Direct or optical fiber
Metal vapor laser	UV or visible (depending on metal)	Monochrome	Direct or optical fiber
Dye laser pumped by metal vapor laser	500–750 nm (depending on the dye)	5–10 nm	Direct or optical fiber
Solid state	For a Nd:Yag 1064, 532, 355, 266 nm	Monochrome	Direct or optical fiber
Dye laser pumped by solid state laser	400–750 nm (depending on dye)	5–10 nm	Direct or optical fiber
Solid state optical parametric oscillator	250–2000 nm	Monochrome	Direct or optical fiber
Semiconductor diode lasers	600–950 nm	Monochrome	Optical fiber
<b>Lamps</b>			
Tungsten filament	400–1100 nm	10–100 nm (depending on filters used)	Direct or via liquid light guide
Xenon arc	300–1200 nm	10–100 nm (depending on filters used)	Normally liquid light guide
Metal halide	Depending on the metal, lines between 250–730 nm	10–100 nm (depending on filters used)	Direct or liquid light guide
Sodium (phosphor coated)	590–670 nm	10–80 nm (depending on filters)	Direct illumination
Fluorescent	400–450 nm	Approximately 30 nm	Direct illumination
<b>Potential New Sources</b>			
Solid state lasers for two photon PDT	Near infrared	Monochrome	Direct, scanned over the lesion
LED	Visible and infrared	5–10 nm	Direct

## 1.6.2 Oxygen

Molecular oxygen ( $^3\text{O}_2$ ) is a significant component in the PDT mechanism since it is required for the generation of ROS, particularly singlet oxygen, during PDT (Woodhams et al., 2007).

The success of photodynamic therapy using photosensitizers that localize in tumor tissue is largely determined by the yield of singlet oxygen ( $^1\text{O}_2$ ), which is dependent on the oxygen content in the tumor tissue (Weishaupt et al., 1976).

The amount of free oxygen present in a tissue is determined by blood supply and oxygen consumption (Tromberg et al., 1990). In tumors, hypoxic regions (loss of oxygen) constitute a significant therapy stumbling block (Vaupel et al., 2001). The creation of reactive oxygen species (ROS), which kill tumors, happens in the existence of molecular oxygen during cancer therapy.

A stable triplet ground state ( $^3\Sigma^-_g$ ) occurs for an oxygen molecule. When oxygen is excited, it forms one of two excited states: the low-lying excited singlet ( $^1\Delta_g$ , also known as  $^1\text{O}_2$ ) and the triplet state ( $^1\Sigma^+_g$ ), which have energies of 95 kJ/mol (22.5 kcal/mol) and 158 kJ/mol (31.5 kcal/mol) above the ground, respectively (Jovanović et al., 2017).

In Figure 1.11, the electrical configurations of both excited states are shown.



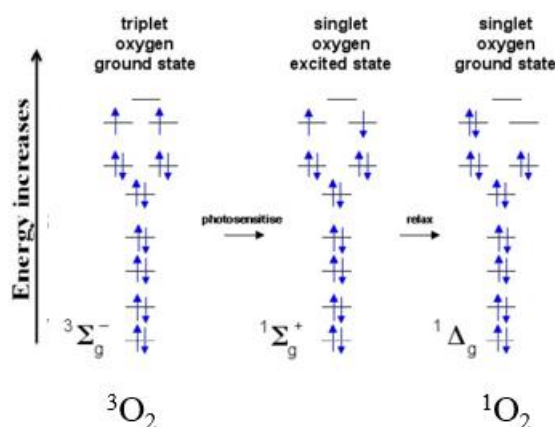


**Figure 1.11.** Presentation of the electronic configuration of ground, singlet and triplet excited states of the molecular oxygen. (The Chemogenesis Web Book - Collecting It All Together: The Five Reaction Chemistries [https://www.meta-synthesis.com/webbook/11\\_five/five.php](https://www.meta-synthesis.com/webbook/11_five/five.php). (n.d.)).

The orbital occupancy and spin orientation are significant variations between ground, singlet, and triplet excited states. Electrons in the triplet ground state are random and transmitted in the highest occupied orbital. In contrast, they are paired in a single orbital in the first excited state ( $^1\Delta_g$ ). Electrons in the triplet excited states ( $^1\Sigma_g^+$ ) have the same distribution as in the ground state, except their spin orientation is antiparallel. Spin is restricted in the transition from ( $^1\Delta_g$ ) to ( $^1\Sigma_g^+$ ), yet allowed in the opposite transition (Jovanović et al., 2017).

### 1.6.3 Photosensitizers

The presence of photosensitizers, along with light and oxygen, is one of the three critical elements of PDT. These dyes are substances that can absorb light of a specific wavelength, causing photochemical or photophysical reactions (Agostinis et al., 2011).

Most of the PSs that are used to treat cancer depend on the tetrapyrrole backbone which, in a sense, resembles the structure contained in the protoporphyrin prosthetic group which is also be found in hemoglobin. The structures of tetrapyrrole form the largest group of PSs which are benefited in applications such as naturally appearing anti-cancer and tetrapyrrole structures are used with many significant biomolecules, including chlorophyll and bacteriochlorophyll, which are called ‘pigments of life’ (Battersby, 2000).

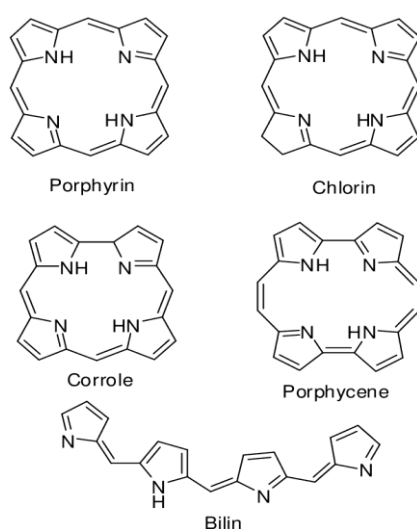


**Figure 1.12.** Examples of Teyrapyrrole structures

The perfect photosensitizer is a single pure composition that eventually will help to produce good manufacturing practice (GMP) and essentials with low manufacturing cost and quality control which paves the way for better storage stability (Allison & Sibata, 2010). PS must be soluble in water or a mixture that is harmless and water-soluble. It should not accumulate too much in a biological environment because it may decrease its photochemical efficiency (Allison et al., 2004; Detty et al., 2004). Single-photon absorption of a wavelength of more than 800 nm does not provide sufficient energy to excite oxygen to its singlet state and for the production of other reactive oxygen species but with a strong absorption rise from the red to the near-infrared spectral region (between 650 and 800 nm) will provide enough energy

(Allison & Sibata, 2010). The tissue penetration will be less likely to cause skin light sensitivity if the absorption band has a short wavelength. In addition, the larger absorption band might reduce the amount of PS required to get the desired effect (Allison et al., 2004; Detty et al., 2004). PSs should have a high triplet quantum yield resulting in good ROS generation when exposed to light. It should have no dark toxicity and clear relatively quickly from normal tissues that will reduce negative effects of phototoxicity (Allison & Sibata, 2010). Although it used to be thought that the time between drug administration and irradiation (drug–light interval, DLI) is sufficient (up to 4 days), and allows the PS to clear from normal tissues while remaining condensed in tumors, many studies currently indicate that the tumor response may be significantly better when light is delivered at a much shorter DLI (minutes or hours). At the same time, the majority of the PS is still visible in the blood vessels, which is cost-efficient and in favor of patients, resulting in significant vascular damage (B. Chen et al., 2002). Although it was previously assumed that light-mediated elimination of the PS (photobleaching) was unfavorable, recent studies suggest that this process may lead light dosimetry to be less crucial during PDT, because over-treatment is prevented when the residual PS is removed during illumination (Ascencio et al., 2008).

### **1.6.3.1 Photosensitizers Based on Other Dyes**

#### **1.6.3.1.1 First Generation Photosensitizers**

Hematoporphyrins (Hp), which first appeared in the 19<sup>th</sup> century and were generated from dried blood, are the first generation PSs. It was originally utilized as a fluorescent diagnostic tool for tumors and was made up of multiple porphyrins, but due to its heterotypical structure, huge doses were required to obtain desired results (O'Connor et al., 2009).

Purification and chemical alteration of the first porphyrin used as PS which was hematoporphyrin (Hp) resulted in the formation of hematoporphyrin derivative

(HpD). When compared to Hp, HpD demonstrated better tumor tissue selectivity and less photosensitizing potential on the skin (Abrahamse & Hamblin, 2016).

Porfimer sodium (Photofrin) was produced after a further purification process, and it was recognized for use in the clinic by the US Food and Drug Administration (FDA) and the European Medicine Agency (EMA) to treat cancers and pre-cancers (O'Connor et al., 2009).

Given the different uses of PDT, its clinical application is limited by the following conditions: low chemical pureness (it consists of more than 60 molecules) or weak tissue infiltration due to maximum absorption at a relatively short wavelength (630 nm). Furthermore, because of the extended half-life of PS and its significant concentration in the skin, skin hypersensitivity to light exists for some weeks after PDT. Due to the drawbacks of first-generation photosensitizers, the search for novel compounds necessitated which led to the invention and advancement of second-generation photosensitizers (Chatterjee et al., 2008; Zhang et al., 2018).

#### **1.6.3.1.2 Second Generation Photosensitizers**

Despite being the most commonly used PS for cancer treatment, Photofrin is a complex mixture of molecules with minimal tissue selectivity, low light absorbance, and poor light penetration into tissues. The therapeutic success of PDT necessitates a high dosage of Photofrin, which causes patients to have chronic skin sensitivity after treatment (O'Connor et al., 2009).

The second generation photosensitizers presently involve hematoporphyrin derivatives and synthetic photosensitizers such as 5-aminolevulinic acid (ALA), benzoporphyrin derivatives, texaphyrins, thiopurine derivatives, chlorin, bacteriochlorin analogues, and phthalocyanines (Moriwaki et al., 2018; Yoon et al., 2013). The usage of 5-aminolevulinic acid (ALA), which is the precursor of protoporphyrin IX, proved to be a significant finding (PpIX). Therefore, ALA is a type of prodrug that only becomes an active PS after being converted into

protoporphyrin. As a result, ALA or its esters could be utilized topically or orally in a wide range of clinical practices (de Rosa & Bentley, 2000; C. Morton, 2002).

The second generation photosensitizers have increased chemical pureness and reproducibility, allowing for better control of production and drug behavior, as well as a higher yield of singlet oxygen creation and improved penetration into deep-lying tissues. They also show fewer side effects, such as skin photosensitivity, because of a stronger selectivity for cancerous tissues and faster clearance of the photosensitizer from the body, which has been lowered from weeks to days or even hours as a result of the impact of lower PS dosages. The major drawback of the second generation PS is their low water solubility, which is a serious limiting factor in intravenous administration and necessitates the development of novel drug delivery systems (Nowak-Stepniowska et al., 2013; O'Connor et al., 2009).

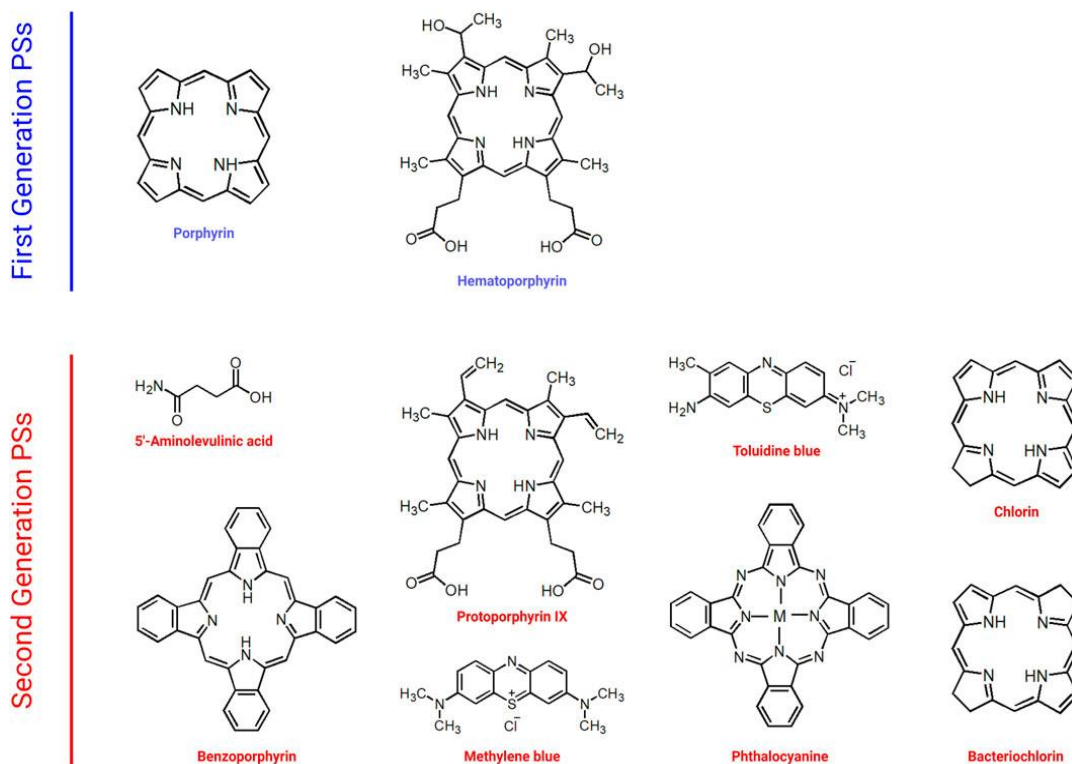


**Figure 1.13.** Examples of First & Second Generation of photosensitizer

### **1.6.3.1.3 Third Generation Photosensitizers**

The invention of third generation photosensitizers is based on the production of chemicals that have a stronger affinity for tumor tissue, resulting in less harm to healthy tissues in the surrounding area (Josefsen & Boyle, 2008). As a result, the second generation PSs are adjusted with biologic conjugates such as carriers, antibodies, or liposomes to enhance their physical, chemical and therapeutic qualities. These chemicals are frequently actively targeted towards the tumor, leading to greater selectivity, lower dose, and fewer undesired side effects. These PSs have also been developed to absorb light of the best wavelength feasible for optimal tissue penetration (Yoon et al., 2013).

## **1.7 BODIPY**

It is stated that there is a comprehensive list of commonly produced fluorophores that cover the whole ultraviolet-visible area of the electromagnetic spectrum, and perhaps, even touch the near infrared (NIR). Nonetheless, finding molecular structures with enhanced photophysical characteristics and photostability remains an active challenge in the design of novel organic fluorophores. It is highlighted that all of those are critical qualities for any real implementation, including the aforesaid bio-imaging, as they govern the sensitivity and efficiency of the recognition process, as well as the operating lifespan. Those chromophores classified as borondipyrrromethene (BODIPY) are unquestionably at the top of the list.

The dyes of 4,4-difluoro-4-bora-3a, 4a-diaza-s-indacene (hereinafter abbreviated as BODIPY) are among the most prominent photosensitizers in the world. Treibs and Kreuzer discovered BODIPY dyes in 1968, and they are now quite popular due to their vast range of applications. The chemical, photochemical, and thermal stability of their boron-dipyrrone core, which gives high absorption and fluorescence spectrum bands, is the basis for their success (Bañuelos, 2016; Benstead et al., 2011; Loudet & Burgess, 2007).

BODIPY dyes are used as photoactive media in a variety of bio-technical applications. For instance, they can be employed in organic dye lasers, fluorescence probes and sensors for bioimaging identification, photosensitizers in imaging guided chemotherapeutic agents, photovoltaic performance artificial antennas, and photovoltaic systems (Sola-Llano & Bañuelos, 2019).

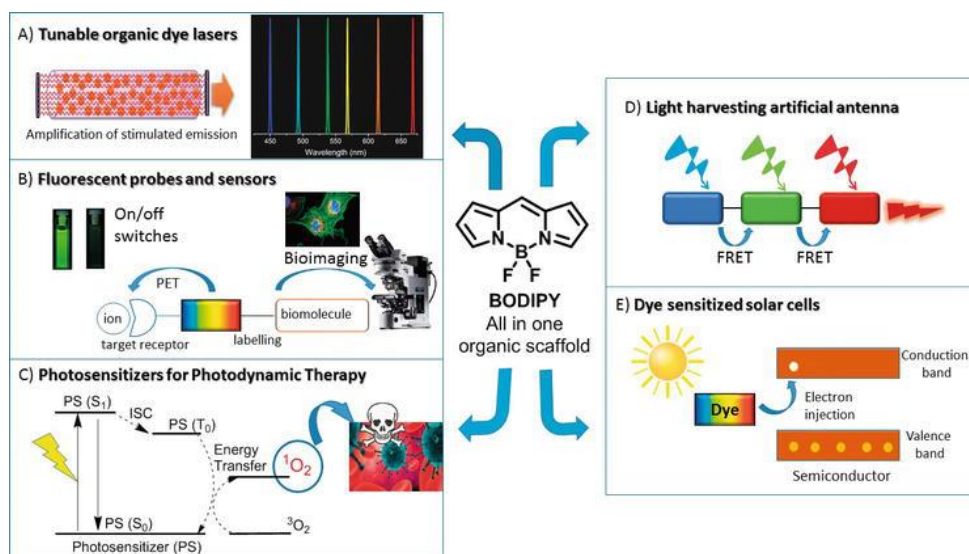
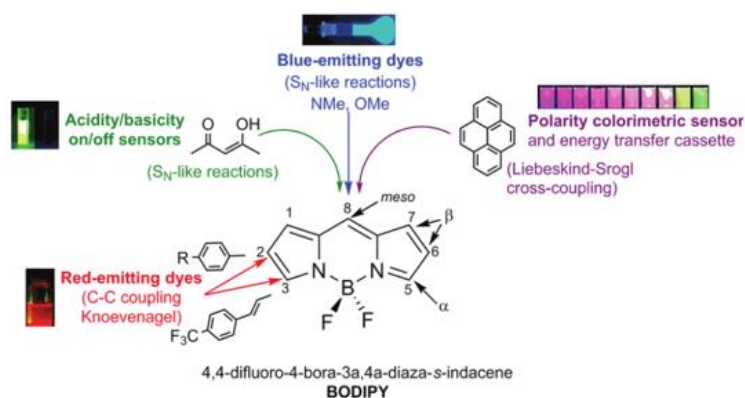
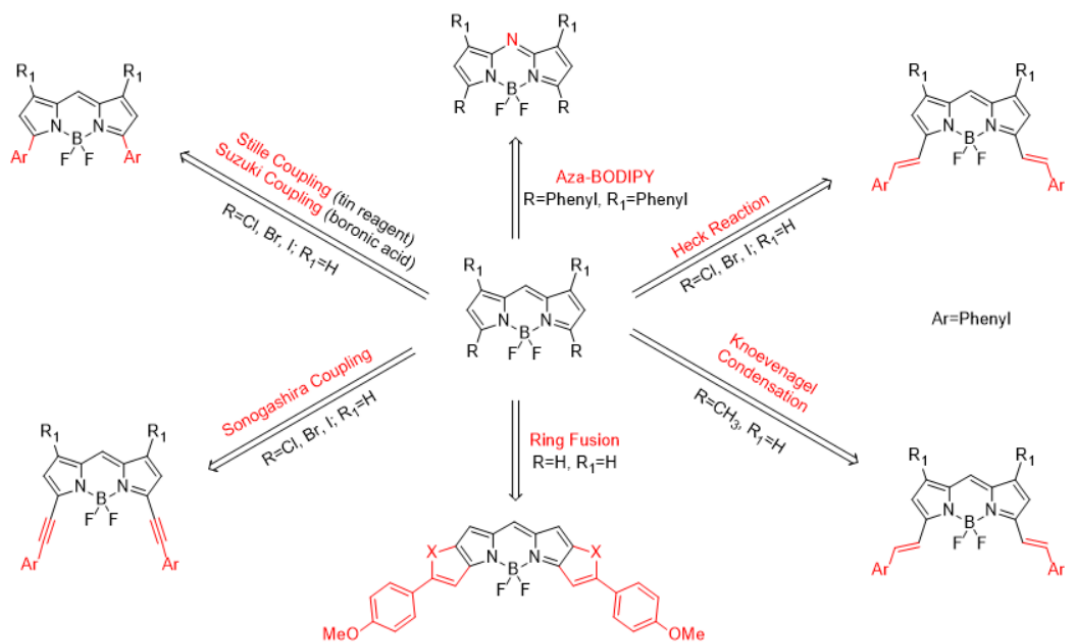


**Figure 1.14.** The main application fields of BODIPYs (Sola-Llano & Bañuelos, 2019).

Compared to other sensitizers, BODIPYs are advantageous due to their high molar extinction coefficients, high fluorescence quantum yields, and the fact that most of them have high triplet quantum yields. On the other hand, they are interesting for investigation and conducting study because they are in just the correct therapeutic window, and as they have the correct physiological pH, and can maintain acceptable solvent polarity. Lastly, the luminescence property of the BODIPY dye is fine-tuned thanks to synthetic modifications made using various organic techniques (Loudet & Burgess, 2007; Rihn et al., 2012; Yogo et al., 2005).



**a**



**b**

**Figure 1.15.** Schematic view of the structural modifications and chemical reactions tested herein (**a**:Sola-Llano & Bañuelos, 2019; **b**:Awuah & You, 2012)



### 1.7.1 Functionalization

The core of the 4,4-difluoro-4-bora-3a,4a-diaza-s-indacene (BODIPY) is appropriate for alterations in order to increase the effect of PDT. The modified BODIPY should be designed to have long wavelength absorption and enhance intersystem crossing capability. Because this activity occurs at the triplet excited state, absorption at longer wavelengths allows for the therapeutic window to be reached (650 nm – 850 nm), and intersystem crossing allows for the generation of singlet oxygen from molecular oxygen (Hinkeldey et al., 2008). Additionally, targeted and/or cancer cell specific activated agents are highly sought after due to their potential diminished side effects during treatment.

An electrophilic process, such as sulfonation or halogenation, is required to functionalize the 2-, 6- positions. This is due to the fact that the 2- and 6-positions have less positive charge. The insertion of a heavy atom, Br or I, into the 2- and 6-positions produces a considerable red shift in the absorption and emission maxima. Because of the low brightness generated by electron transport, this kind of functionalization is preferred by PDT application.

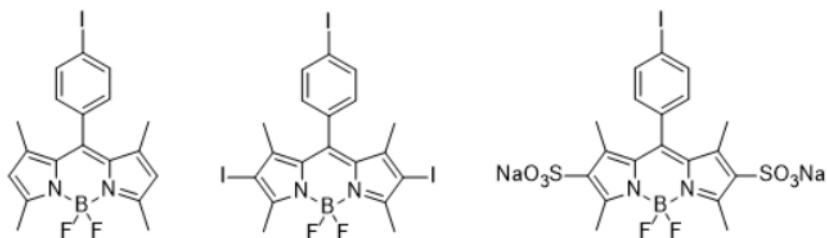


**Figure 1.16.** Example of sulfonation or halogenation of BODIPY derivatives at 2-, 6- positions (Awuah & You, 2012)

In terms of the influence of crosslinking positioning on absorption and emission bands, aryl group substitution on the meso position has a small effect. Substitution on 1-, 7- locations, on the other hand, boosts the quantum yield compared to

unsubstituted places (Loudet & Burgess, 2007). It is due to the fact that 1-, 7-substitution prevents rotational movement of the phenyl ring on the meso position.

Functionalization on 1-, 3-, 5-, and 7-positions involving various types of interactions, such as transition metal catalyzed processes (Suzuki, Sonagashira, Stille and Heck couplings), could be used to create BODIPY dyes with prolonged conjugation and distributed emission maxima. Bathochromic shift occurs when thioalkoxides or amino groups are substituted on the 3- and 5-positions, resulting in BODIPY derivatives with altered emission and absorption maxima. Knoevenagel reactions generate a high yield due to the acidic nature of the methyl groups on these locations (Rurack et al., 2001).

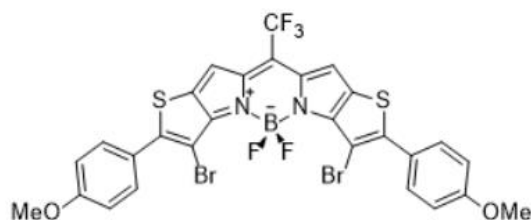


**Figure 1.17.** Example of the heteroaryl-fused BODIPY based photosensitizer synthesized by Suzuki coupling reaction (Kamkaew et al., 2013)

A nucleophilic addition of active hydrogen to a carbonyl molecule is known as the Knoevenagel condensation process. The reaction medium necessitates a basic atmosphere as well as the removal of water, which is achieved using the Dean-Stark apparatus. With substitution on the 1-, 3-, 5-, and 7-positions, this strategy produces excellent results. As a consequence, mono-, di-, tri-, and tetra-styryl-Bodipy derivatives can all be produced in one Knoevenagel process (Guliyev et al., 2009; H. Y. Lee et al., 2009; Qi et al., 2008).

The first tetra-styryl derivative of BODIPY dye was created in 2009 by Akkaya et al. According to the findings of this study, the 1,7-position of the BODIPY core is as acidic as the methyls at the 3- and 5-positions. Mulliken-charge study on the core carbon atoms of tetramethyl-BODIPY reveals the acidic character of various places.

Bromine atoms in 2- and 6-positions, as well as pyridine groups in tetrasteryl substitution, were utilized in this investigation (Buyukcakil et al., 2009).

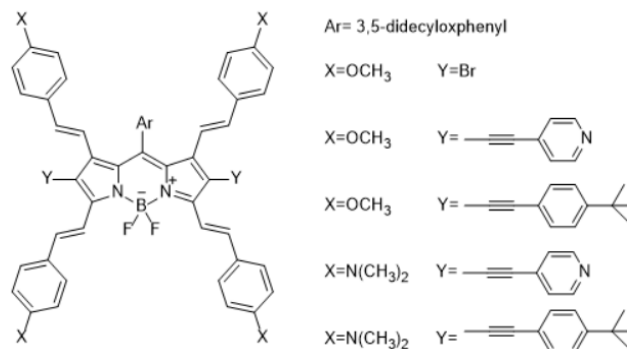


**Figure 1.18.** Schematic representation of created tetra-styryl BODIPY derivatives (Buyukcakil et al., 2009)

Following the tetrasteryl substitution article, Ziessel et al. produced many BODIPY derivatives containing the same and different aldehydes. The absorption maxima of the novel tetrasteryl substituted BODIPY derivatives are 720 nm while the emission maxima are 800 nm. As according Ziessel et al., methyls at 3-, 5- positions on the BODIPY core are more reactive than methyls at 1-, 7- positions in Knoevenagel condensation (Bura et al., 2011).

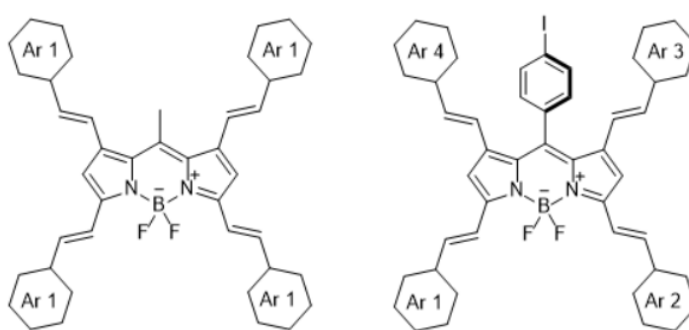


**Figure 1.19.** Schematic representation of tetra-styryl BODIPY derivatives (Bura et al., 2011)

## CHAPTER 2

### RESULTS AND DISCUSSIONS

#### 2.1 Aim of the Study and Design of the Target Photosensitizers

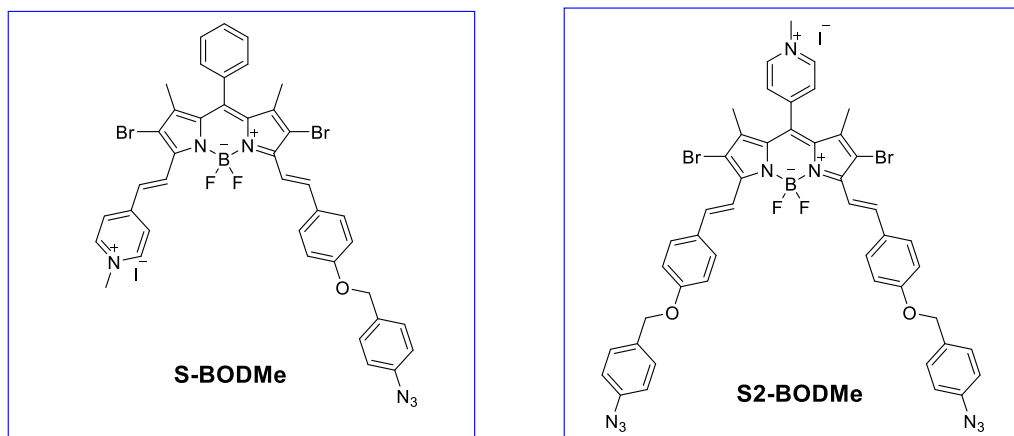


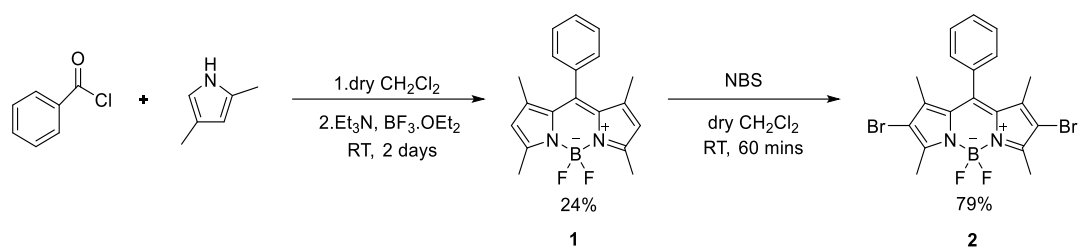
**Figure 2.1.** S-BODMe & S2-BODMe molecular systems which are BODIPY-based and activable with physiologically active species ( $\text{H}_2\text{S}$ )

The BODIPY dyes are among the most widely used photosensitizers worldwide. Their success is based on the chemical, photochemical, and thermal stability of their boron-dipyrone core, which produces high absorption and fluorescence spectrum bands. But, the core needs be changed to improve PDT performance (Bañuelos, 2016). High fluorescence quantum yields, high molar extinction coefficients and high triplet quantum yields are essential for sensitization that the minimal dosage of photosensitizer may abstain from disrupting the natural distribution of physiologically active species (Loudet & Burgess, 2007; Yu et al., 2014). BODIPY-based photosensitizers are great candidates specifically if they can be decorated in a way that they show their activity upon reaction with a tumor metabolite. In this project, two essential alterations on the BODIPY core were pursued. Firstly, methyl pyridinium (MP) substituents are incorporated to the hydrophobic bromine-containing BODIPY core to realize a water-soluble agent (Hammerer et al., 2018).

This insertion not only increases the solubility of photosensitizer in water, but also permits it to be localized in the mitochondria, where the oxygen-rich nature of this organelle enhances the PDT efficiency (Wang et al., 2013). In addition, this adjustment also causes a considerable red shift in the photosensitizer's absorption maxima (Wallace, 2012) will be achieved through increase in extend of conjugation. Secondly, by utilizing an azide containing masking unit that is activated by a cancer cell metabolite, H<sub>2</sub>S, significant activation difference between healthy and cancerous cells is aimed. In this context, the reduction of an azide to an amine by hydrogen sulfide was utilized as a practical technique for targeted phototherapy (Yu et al., 2014). Hence, azido-benzene containing masking units are attempted to be introduced to the photosensitizer core. On our previous work from our group, we have already demonstrated that the methyl pyridinium incorporation through a Knoevenagel condensation resulted in both the NIR shift and water solubility. However, this agent lacked selective activation in cancer cells and only moderate differentiation was achieved between healthy and cancerous cells. With the activatable design proposed here we are attempting the first example of a BODIPY based agent utilizing NIR absorption, significant water solubility, mitochondria targeting with activatable nature.

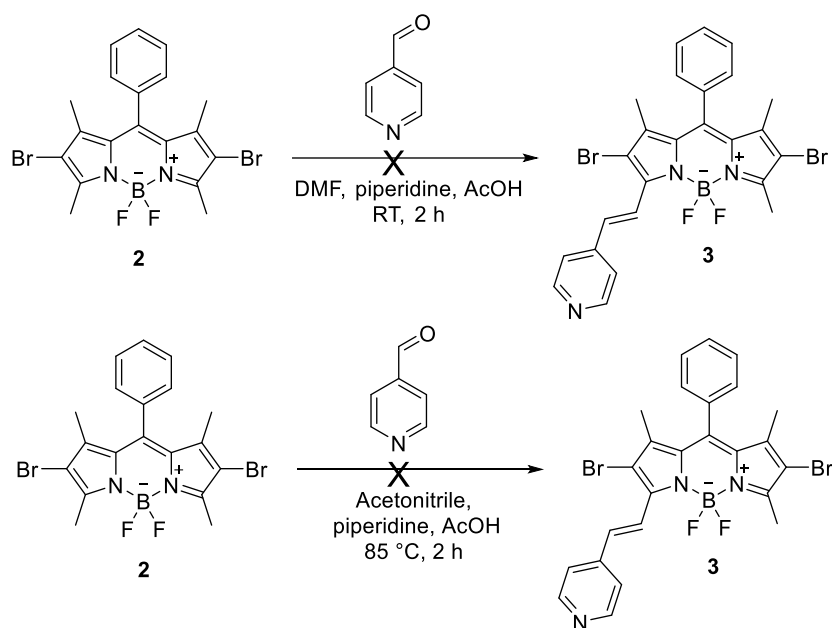
### **2.1.1 Efforts Towards Synthesis of S-BODMe**

First step towards obtaining the final product was the synthesis of phenyl BODIPY core (**1**) from benzaldehyde and 2,4-dimethyl pyrrole as starting materials. Secondly, the BODIPY core (**1**) was brominated (**2**) from 2 and 6 position via NBS in DCM. The reactions were performed according to the established procedures.



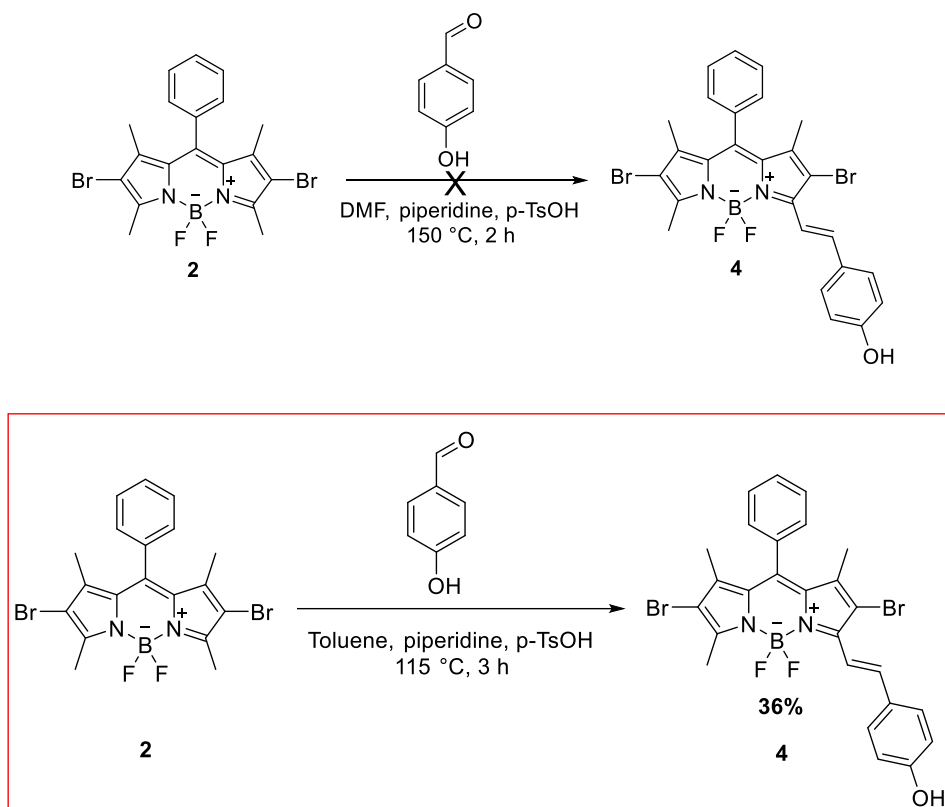
**Scheme 2.1.** Synthetic pathway of compounds **1** and **2**

Thirdly, mono Knoevenagel condensation was attempted on brominated-BODIPY core (**2**) with 4-pyridinecarboxaldehyde as the aldehyde component. A variety of temperature/solvent couples has been reported in the literature for similar reactions however the attempted condensation could not be achieved. Then, we decided to investigate if 4-pyridinecarboxaldehyde was the reason for difficulties in the mono condensation. Hence, we pursued mono condensation with the other aldehyde counterpart, 4-hydroxybenzaldehyde.



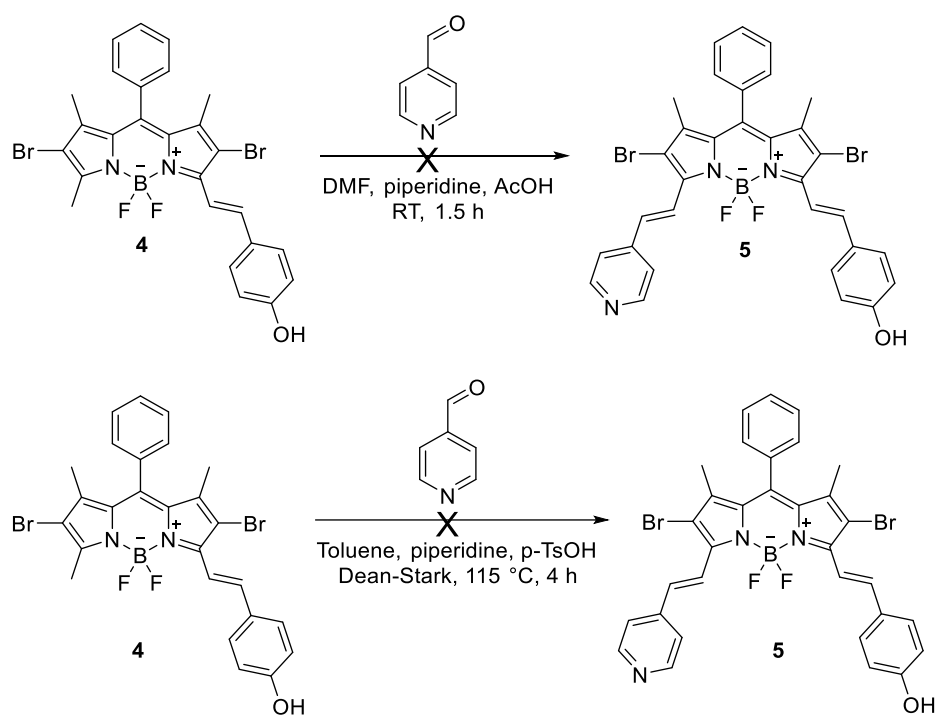
**Scheme 2.2.** Attempted synthetic pathway of compound **3**

While Knoevenagel reaction in DMF with piperidine/TsOH couple was not successful, changing of the solvent to toluene under Dean-Stark conditions gave the desired compound **4** in moderate yield.



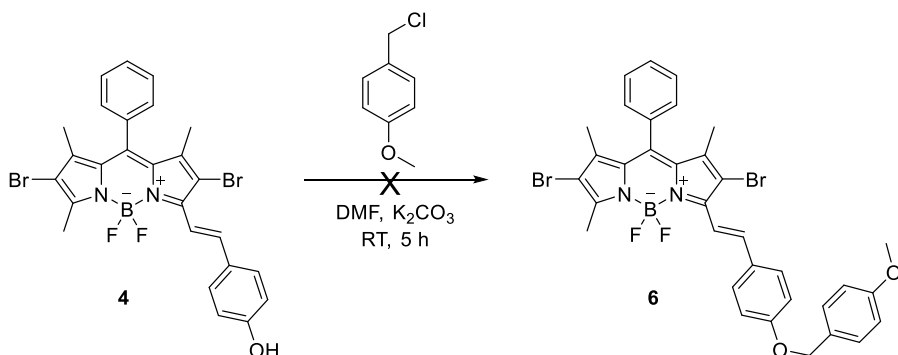
**Scheme 2.3.** Synthetic pathways for compound **4**

With mono condensation product **4** in hand, we attempted to introduce pyridine unit via a second Knoevenagel under different conditions. Although a new spot with absorption in the longer wavelength region forms, the reaction was plagued with number of side reactions and due to difficulties in purification attempt, the desired product **5** could not be attained.



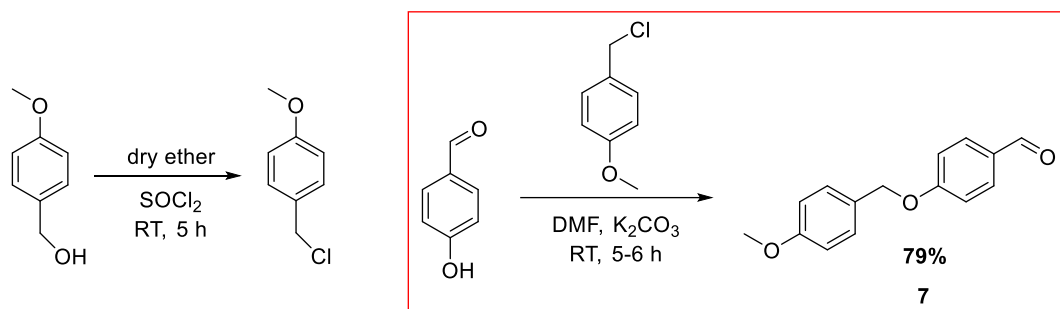
**Scheme 2.4.** Attempted synthetic pathways for compound **5**

Next, we wanted to investigate if the unprotected phenol present in compound **4** was the reason for unsuccessful second condensation. Hence, we decided to protect the phenol with PMB. Alkylation efforts with PMB-Cl under the effect of  $\text{K}_2\text{CO}_3$  in DMF was proved ineffective. Thus, we decided to protect the 4-hydroxybenzaldehyde first followed by the condensation reaction. This sequence of reactions was proved fruitful and protected BODIPY **6** was attained successfully.

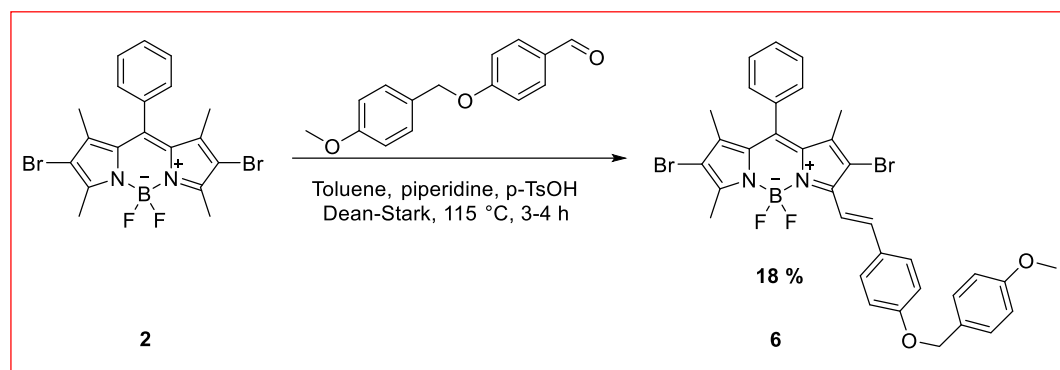


**Scheme 2.5.** Attempted synthetic pathway of compound **6**



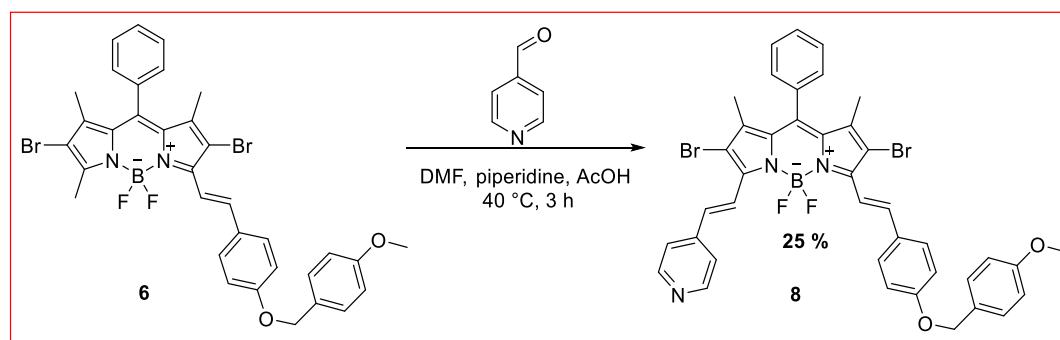


**Scheme 2.6.** Synthetic pathway for compound **7**



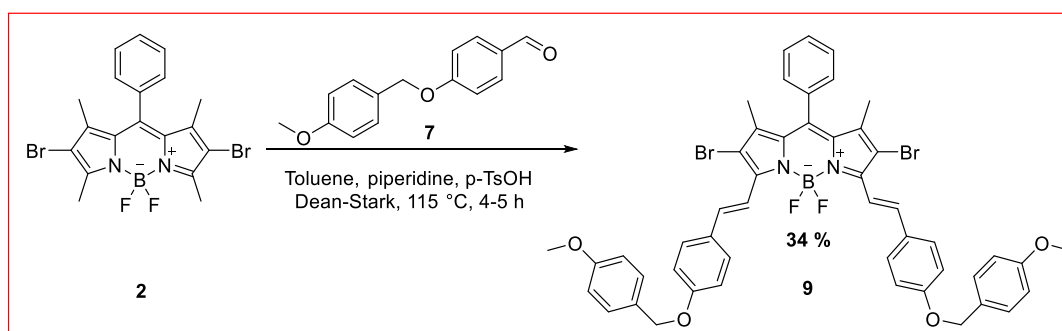
**Scheme 2.7.** Synthetic pathway for compound **6**

With compound **6** in hand, Knoevenagel reaction was performed with 4-pyridinecarboxaldehyde once more, and to our delight, target material **8** was attained successfully.

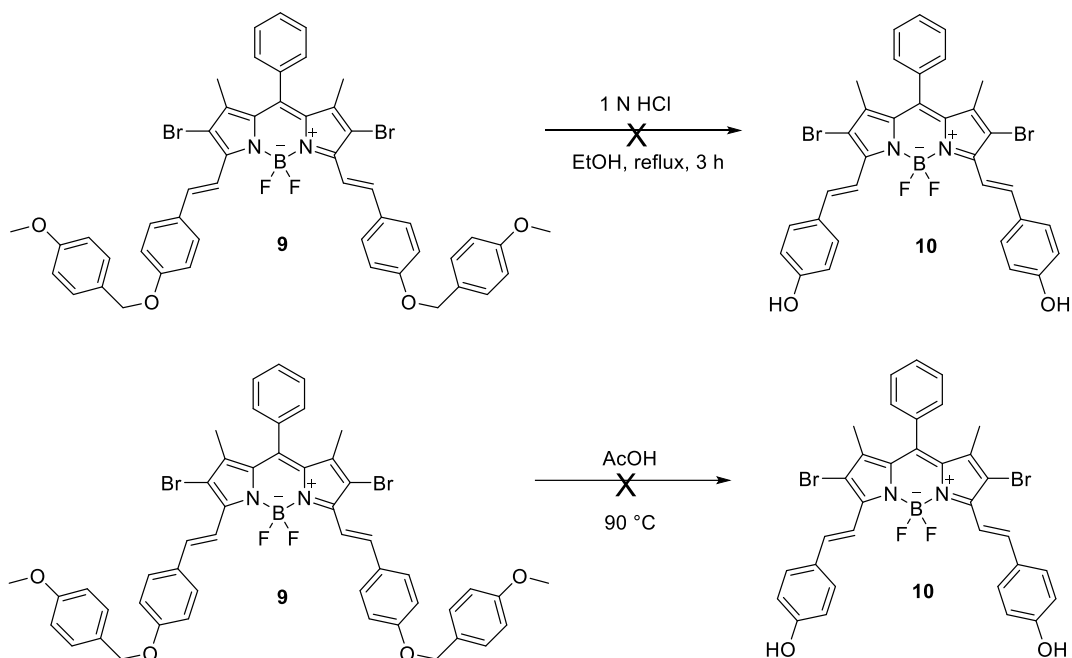


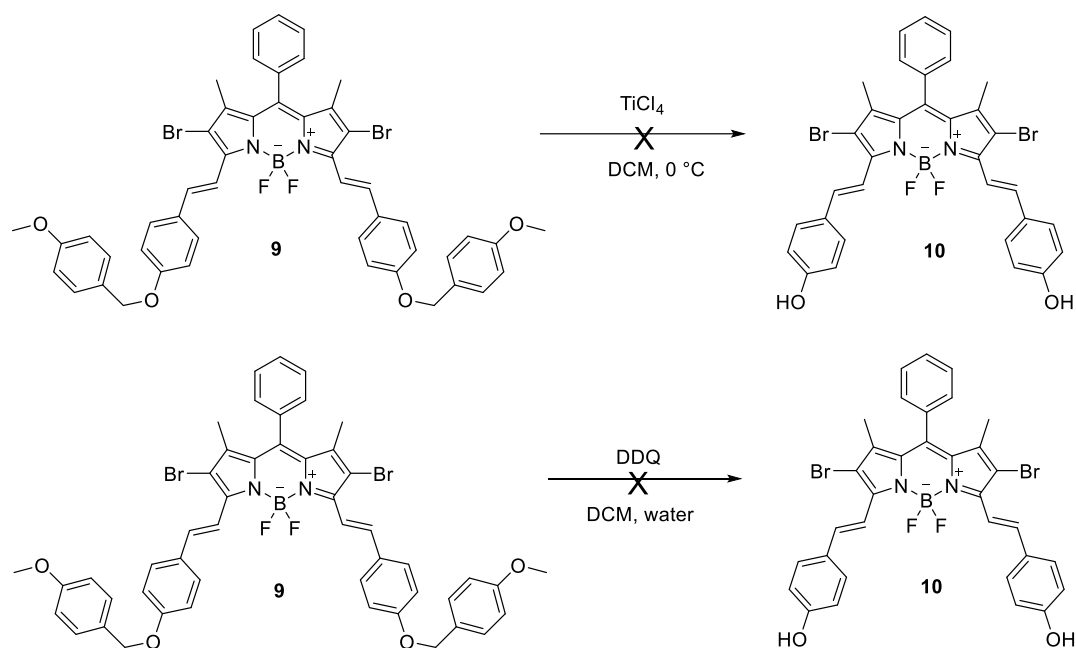
**Scheme 2.8.** Synthetic pathway for compound **8**

Due to low yields, which are quite common in Knoevenagel reactions of the BODIPY core, attaining compound **8** was proved difficult. To be able to determine the optimal conditions for the deprotection reaction, model compound **9** was prepared by the double condensation of the BODIPY **2** with the protected aldehyde **7** successfully. Next, we attempted to cleanly deprotect the PMB group with commonly applied methods in literature. Unfortunately, none of the acidic or oxidative cleavage approaches gave the target deprotected compound **10** and starting material was recovered in most cases.



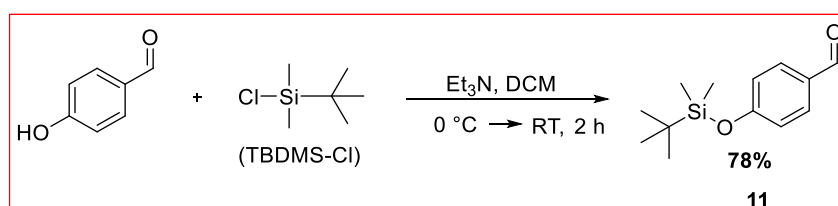
**Scheme 2.9.** Synthetic pathway for compound **9**



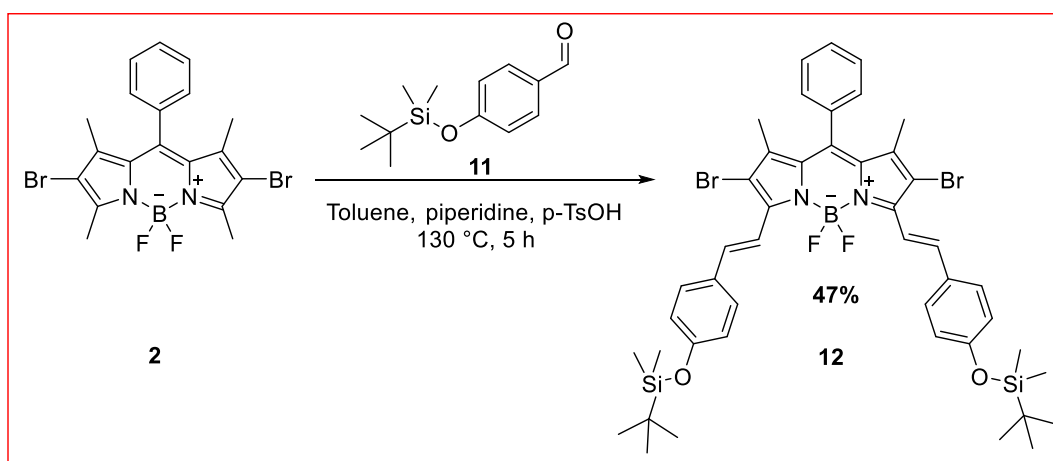


**Scheme 2.10.** Attempted synthetic pathways for compound **10**

Since deprotection of the PMB group proved unsuccessful, we decided introduce a silicon based protection which is in general terms easier to remove compared to PMB. Along these line 4-hydroxybenzaldehyde was protected with TBDMS successfully, and the double condensation with this protected aldehyde also shown to proceed with moderate yield.

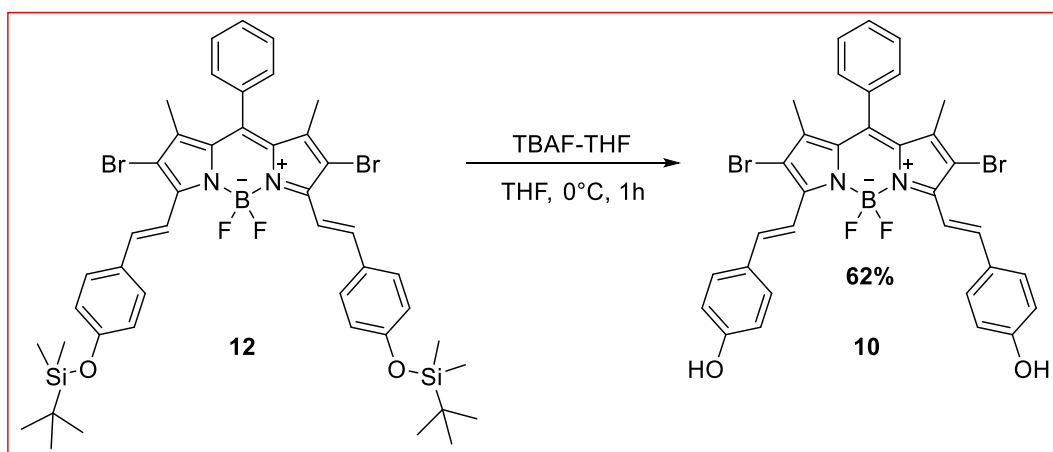


**Scheme 2.11.** Synthetic pathway for compound **11**



**Scheme 2.12.** Synthetic pathway for compound **12**

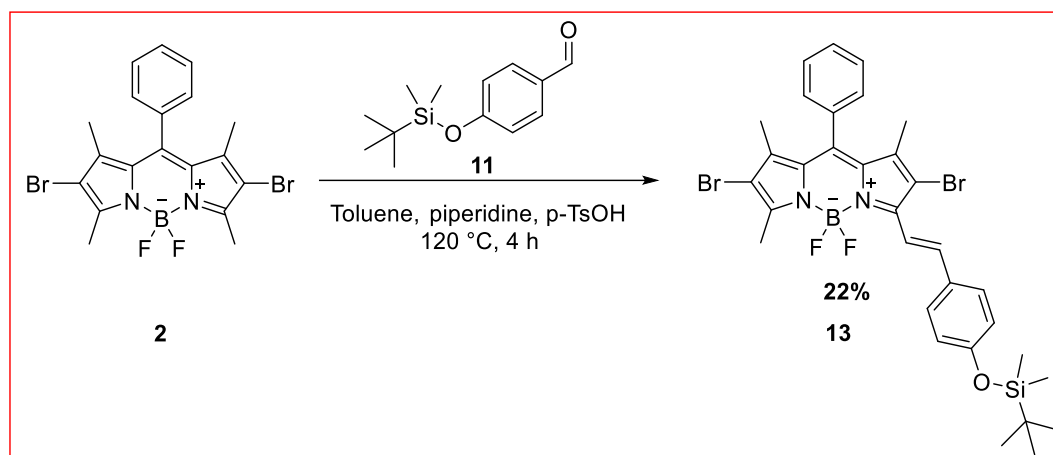
The new model compound **12** was then subjected to deprotection with TBAF and the target compound **10** was attained successfully.



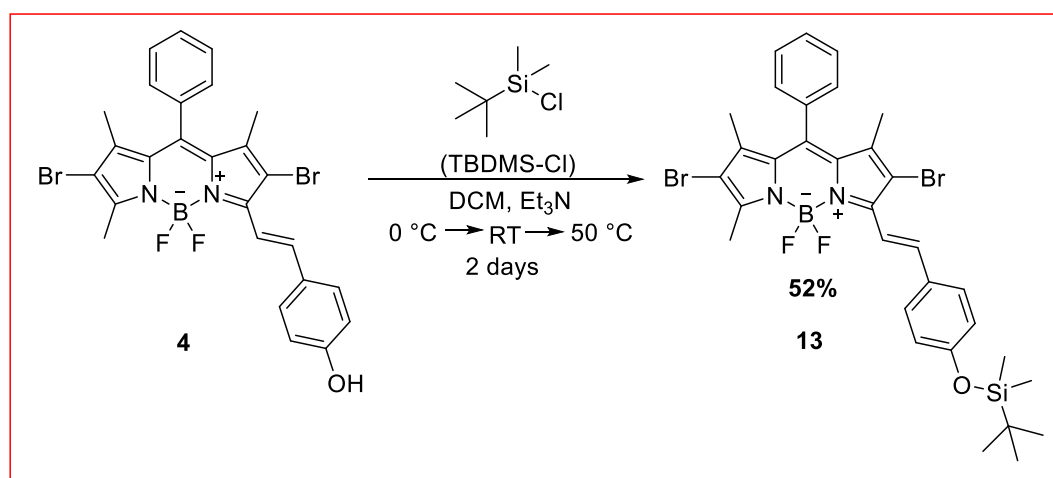
**Scheme 2.13.** Synthetic pathway for compound **10**

With protection/deprotection chemistry decided on model compounds, we moved to the synthesis of target asymmetrically substituted BODIPY. The main motivation here is to insert different functionalities to the main BODIPY core. In the current work, we aimed to introduce methyl pyridinium unit for water solubility and mitochondria targeting, and azido masked unit for realization of H<sub>2</sub>S activated PDT agent. Mono condensation with TBDMS protected aldehyde was performed.

The crude NMR analyses showed the desired product was successfully obtained, but after the column chromatography, low yields were obtained since the protecting group was partially removed.



**Scheme 2.14.** Synthetic pathway for compound **13**

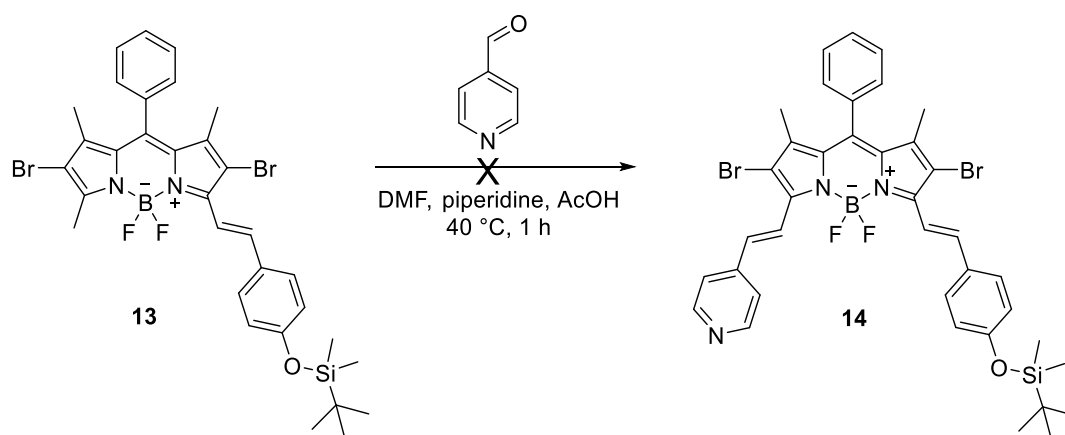


**Scheme 2.15.** Synthetic pathway for compound **13**

With deprotected compound **4** in hand, we decided to introduce the silicon protecting group. The protection was successful and single flash chromatography gave compound **13** in moderate yield.

Next, we onto the introduction of pyridine unit with protected **14** in hand. Unfortunately, the desired condensation reaction could not be achieved even though the phenol unit was protected.

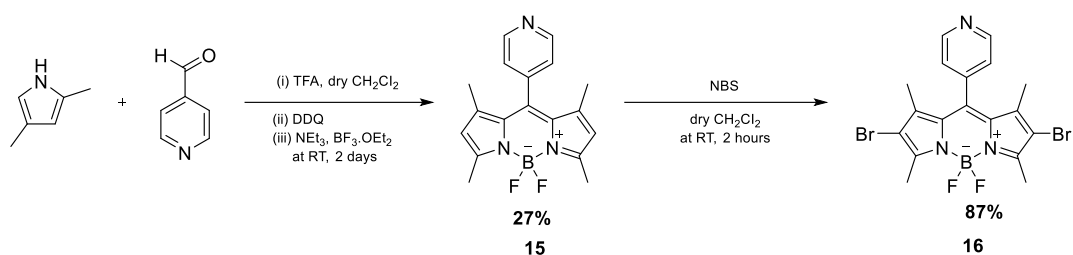
Due to major issues faced in introduction of the pyridine unit through condensation reactions, we decided to change our synthetic approach and introduce pyridine unit to the BODIPY core.



**Scheme 2.16.** Attempted synthetic pathway for compound **14**

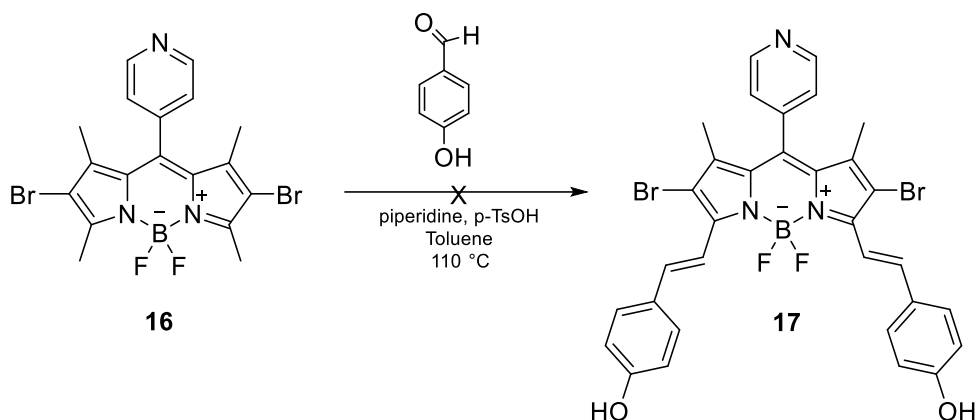
### 2.1.2 Efforts Towards Synthesis of S2-BODMe

The first step towards obtaining our new target was the synthesis of pyridine containing BODIPY core (**15**) from 2,4-dimethyl pyrrole and 4-pyridinecarboxaldehyde as starting materials. The literature reported method (Luo et al., 2014) proved successful and BODIPY **15** was attained. Then, using NBS solution in DCM, the BODIPY core was brominated (**16**) from 2 and 6 positions (Bartelmess et al., 2014)



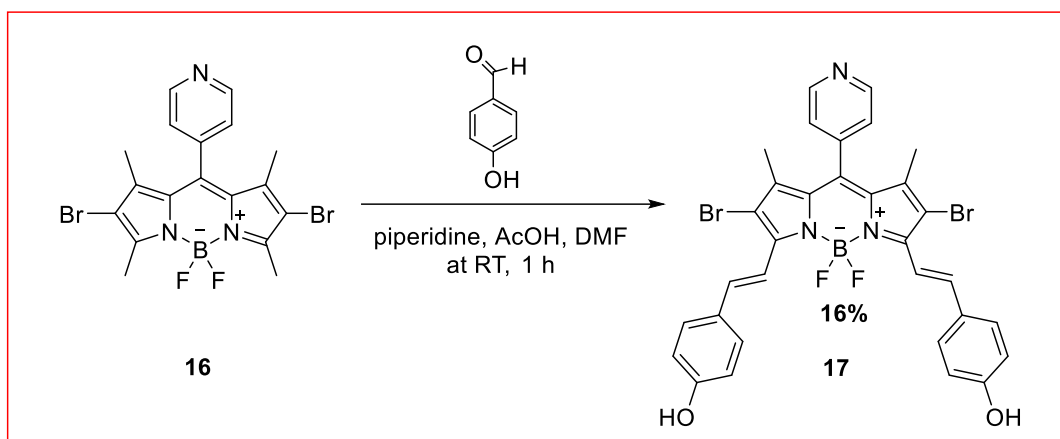
**Scheme 2.17.** Synthesis of compounds **15** and **16**.

As the third step, double Knoevenagel condensation was attempted on brominated-BODIPY core (**3**) with 4-hydroxybenzaldehyde as the aldehyde component. The specified temperature/solvent/acid as a reagent have been reported in the literature for similar reactions however the attempted condensation could not be achieved.



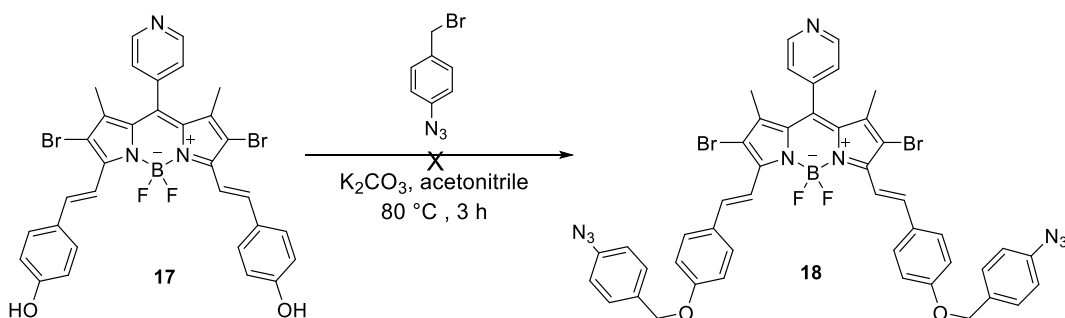
**Scheme 2.18.** Attempted synthetic pathway for compound **17**.

While Knoevenagel reaction in toluene with piperidine/p-TsOH couple was not successful, changing the solvent to DMF, changing the acid to AcOH, and decreasing the temperature to room temperature gave the desired product **17** albeit in low yield.



**Scheme 2.19.** Synthetic pathway for compound **17**

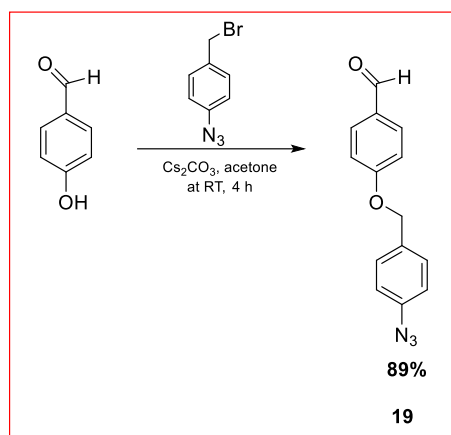
Next, we attempted to introduce masking unit using azide substituted benzyl bromide with  $\text{K}_2\text{CO}_3$  in acetonitrile for attaining the targeted BODIPY **18**. Unfortunately, under these conditions the desired product could not be attained.



**Scheme 2.20.** Attempted synthetic pathway for compound **18**

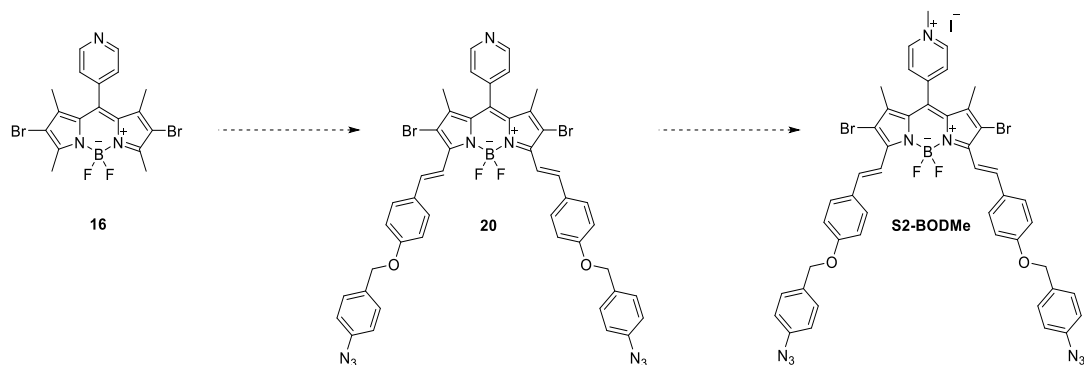
Next, we decided to attach the masking group to the corresponding aldehyde before the condensation reaction. Azido-benzyl masking unit was successfully introduced to the aldehyde under the action of  $\text{Cs}_2\text{CO}_3$  in acetone to give the target the compound **19**.





**Scheme 2.21.** Synthetic pathway for compound **19**.

Our initial attempt for the double condensation looked promising in the crude NMR, albeit with difficulties in removing the excess aldehyde used in the synthesis. As a future work, the purification of **20** will be performed followed by methylation to get the title compound **S2-BODMe**. Then, photophysical measurements and cell studies will be performed in detail.



**Scheme 2.22.** Schematic representation of the final steps towards realizing **S2-BODMe**

## CHAPTER 3

### CONCLUSION

The main aim of this project was to synthesize two different NIR absorbing, water-soluble, mitochondria-targeted and activatable photosensitizers. Two essential alterations on the BODIPY core were pursued. Firstly, methyl pyridinium (MP) substituents are incorporated to the hydrophobic bromine-containing BODIPY core to realize a water-soluble agent. This insertion not only increases the solubility of photosensitizer in water, but also increase localization in the mitochondria, the most oxygen rich organelle in cancerous cells for increased PDT efficiency. In addition, this adjustment also causes a considerable red shift in the photosensitizer's absorption maxima is mainly achieved by increase in extend of conjugation. Secondly, by utilizing an azide containing masking unit that is activated by a cancer cell metabolite, H<sub>2</sub>S, significant activation difference between healthy and cancerous cells is aimed. With the design proposed here we are attempting the first example of a BODIPY based agent utilizing NIR absorption, significant water solubility, mitochondria targeting with activatable nature.

For this purpose, brominated BODIPY core is modified at different positions with pyridinium unit and azido-benzyl masking unit, which is activated with H<sub>2</sub>S, an over-expressed tumor metabolite. In the first photosensitizer (S-BODMe), two consecutive Knoevenagel condensation processes were attempted to introduce pyridinium unit to the 5-position and the corresponding protected aldehyde to the 3-position which would have been deprotected and modified with the masking unit for H<sub>2</sub>S activation. Unfortunately, the target molecule could not be attained due to significant issues arised in achieving consecutive Knoevenagel condensations and protection/deprotection chemistry that has been pursued. In the second approach (S2-BODMe), the pyridine unit was incorporated to the bromo-BODIPY core and the aldehyde with open position for masking group introduction was incorporated

successfully with a double Knoevenagel condensation, however insertion of the azido-based masking unit could not be accomplished. Later, azido-based masking group was successfully attached to the corresponding aldehyde before the Knoevenagel reaction. As a future work, this new aldehyde containing masking unit will be used to modify the bromo-BODIPY core, followed by methylation of the pyridine unit to attain the target molecule.



## CHAPTER 4

### EXPERIMENTAL

#### 4.1 Materials and Methods

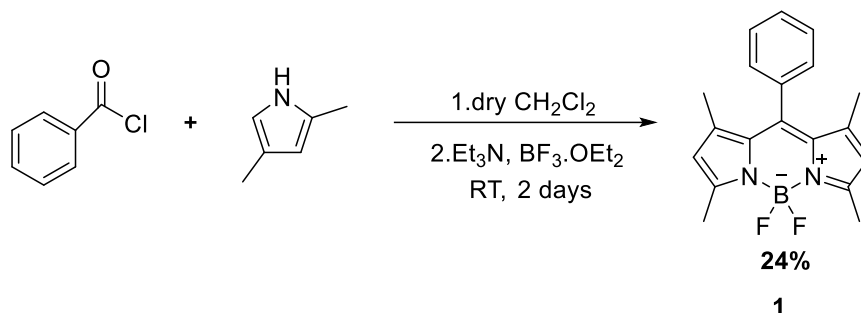
A Bruker Avance III Ultrashield (400 MHz) spectrometer was used to record the  $^1\text{H}$  and  $^{13}\text{C}$ -NMR spectra. The chemical shifts are given in parts per million (ppm) downfield from an internal TMS (trimethylsilane) reference. Coupling constants (J) were expressed in hertz (Hz), and spin multiplicities were given by the symbols: s (singlet), d (doublet), t (triplet), and m (multiplet). MestReNova program was used to process NMR spectrums. Column chromatography was conducted by utilizing thick-walled glass columns and silica Gel 60 (Merck 230-400 mesh). Commercially prepared 0.25 mm silica gel plates were used to perform Thin-layer chromatography (TLC Merck Silica Gel 60 F254) and a UV lamp was used for visualization. In chromatography solvent mixtures, the volume: volume ratio refers to the relative proportions of solvents. All of the reagents were purchased from mostly Sigma-Aldrich and TLC commercially and utilized without further purification. The Mbraun MBSPS5 solvent drying system supplied all dry solvents used in the reactions. Argon gas was used for the inert atmosphere.

#### 4.2 Equipments

The solvents  $\text{CDCl}_3$  and  $\text{d}_6$ -DMSO were used for the  $^1\text{H}$  and  $^{13}\text{C}$ -NMR analyses on Bruker Spectrospin Avance DPX-400 Spectrometer and the internal reference was tetramethylsilane. To determine the exact masses of the synthesized compounds, High resolution mass spectroscopy with Waters Synapt MS System was used.

### 4.3 Experiments Towards Synthesis of S-BODMe

#### 4.3.1 Synthesis of Compound 1

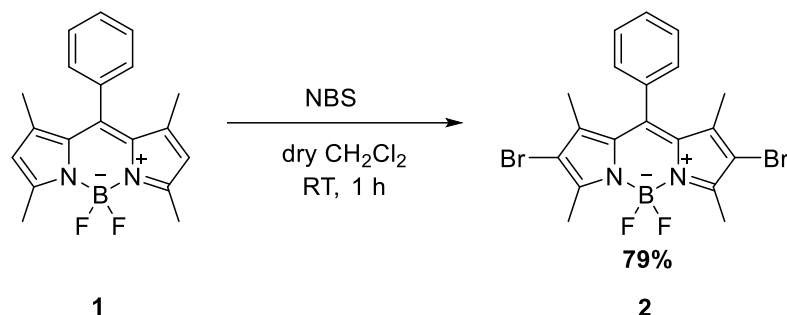


*Scheme 4.1.* Synthetic route of Compound 1

A literature report on a closely related system was utilized with modification (Karaman et al., 2019). Anhydrous CH<sub>2</sub>Cl<sub>2</sub> (95 ml) was introduced in a 250 ml two-neck flask and argon-purged for 1 hour. Then, under argon atmosphere, 2,4-dimethylpyrrole (1.2 g, 12.6 mmol) and benzoyl chloride (0.975 g, 6.94 mmol) were added respectively. The mixture was stirred under argon atmosphere at room temperature (RT) during overnight in the dark until TLC showed that the aldehyde has been completely consumed. Triethylamine (TEA, 6.5 ml, 47 mmol) and BF<sub>3</sub>·Et<sub>2</sub>O (6.5 ml, 47 mmol) were added dropwise at 0 °C respectively into the reaction mixture, and the reaction mixture was continued to stir overnight at room temperature in the dark. Water was added and the reaction mixture was extracted with CH<sub>2</sub>Cl<sub>2</sub>. Then, the organic layers were washed with saturated Na<sub>2</sub>CO<sub>3</sub>. The collected organic layers were combined and dried over anhydrous Na<sub>2</sub>SO<sub>4</sub> and the solvent was evaporated under reduced pressure. The crude product was purified by column chromatography (silica gel, Hexane:EtOAc - 6:1; DCM:Hexane - 2:1) to obtain the desired product (**Compound 1**) as an orange solid (508 mg, 24%).

$^1\text{H}$  NMR (400 MHz,  $\text{CDCl}_3$ )  $\delta$ : 7.44 – 7.38 (m, 3H), 7.24 – 7.17 (m, 2H), 5.90 (s, 2H), 2.48 (s, 6H), 1.30 (s, 6H);  $^{13}\text{C}$  NMR (101 MHz,  $\text{CDCl}_3$ )  $\delta$ : 155.4, 143.2, 141.7, 135.0, 131.4, 129.1, 128.9, 128.0, 121.2, 14.6, 14.3.

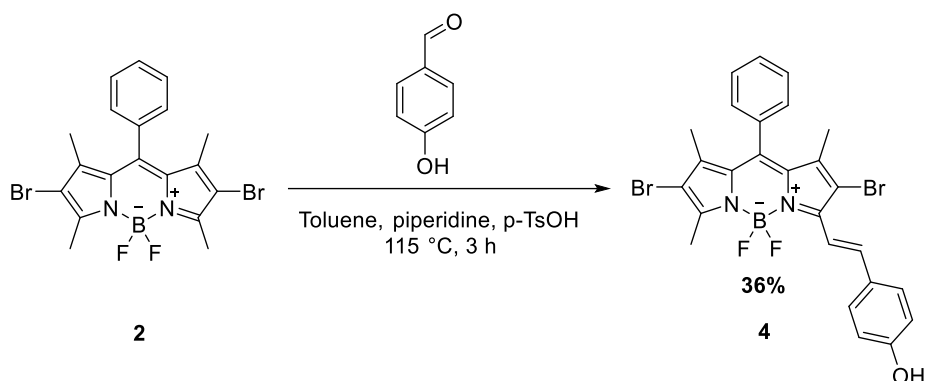
#### 4.3.2 Synthesis of Compound 2



Scheme 4.2. Synthetic route of Compound 2

A literature report on a closely related system was utilized with modification (Karaman et al., 2019). Compound 1 (200 mg, 0.616 mmol) was dissolved in anhydrous DCM (30 ml) and N-bromosuccinimide (NBS, 275 mg, 1.54 mmol) solution was prepared with dry DCM (20 ml) which was added into the solution of compound 1 a dropwise manner. The mixture was stirred at room temperature and the thin layer chromatography (TLC) demonstrated that the reaction was completed after 1 hour stirring. The organic phase washed with water (50 ml), then brine (50 ml). The organic layers were combined and dried over anhydrous  $\text{Na}_2\text{SO}_4$ . The mixture was filtered and the solvent was evaporated under reduced pressure. The crude product was purified by column chromatography (silica gel, DCM:Hexane – 1:1) to obtain the final product (**Compound 2**) as a dark red solid (236 mg, 79%).  $^1\text{H}$  NMR (400 MHz,  $\text{CDCl}_3$ )  $\delta$ : 7.49 – 7.43 (m, 3H), 7.20 – 7.16 (m, 2H), 2.54 (s, 6H), 1.29 (s, 6H);  $^{13}\text{C}$  NMR (101 MHz,  $\text{CDCl}_3$ )  $\delta$ : 152.9, 141.1, 139.6, 133.4, 129.4, 128.5, 128.4, 126.8, 110.7, 12.6

### 4.3.3 Synthesis of Compound 4

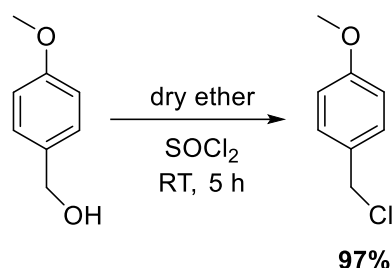


Scheme 4.3. Synthetic route of Compound 4

A literature report on a closely related system was utilized with modification (Bura et al., 2011). In a 50 ml two-neck flask equipped with a Dean-Stark apparatus, compound 2 (100 mg, 0.207 mmol) and toluene (15 ml) were introduced, and the temperature was set as 40 °C. The mixture was stirred at this temperature until compound 2 was totally dissolved. Then, under argon atmosphere, 4-hydroxybenzaldehyde (43.08 mg, 0.353 mmol), piperidine (0.4 ml), and a crystal of p-TsOH were added to a stirred solution of the BODIPY dye. The mixture was heated at its boiling point (115 °C). The thin layer chromatography (TLC) demonstrated that the distortions have begun after 3 hours stirring, so it was ended. The resulting mixture was washed with water and extracted with DCM. The organic layers were combined and dried over MgSO<sub>4</sub>. The mixture was filtered and the solvent was evaporated under reduced pressure. The crude product was purified by column chromatography (silica gel, DCM:MeOH – 100:2) to obtain the final product (**Compound 4**) as violet purple solid (43.7 mg, 36%). <sup>1</sup>H NMR (400 MHz, CDCl<sub>3</sub>) δ: 8.08 (d, *J* = 17.1 Hz, 1H), 7.58 – 7.52 (m, 7H), 7.28 (d, *J* = 3.5 Hz, 1H), 6.86 (d, *J* = 8.7 Hz, 2H), 2.66 (s, 3H), 1.41 (s, 3H), 1.37 (s, 3H).



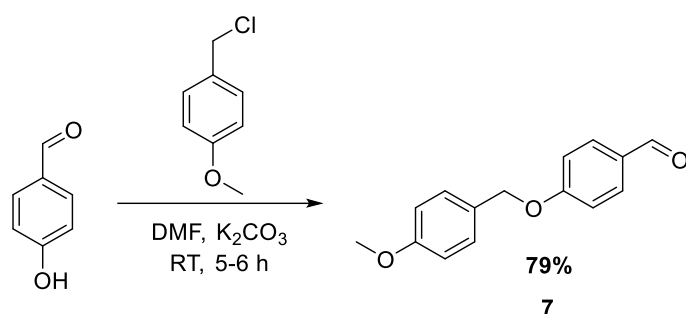
#### 4.3.4 Synthesis of PMB-Cl



*Scheme 4.4.* Synthetic route of PMB-Cl

A literature report on a closely related system was utilized with modification (St. Amant et al., 2016). A solution of 4-methoxybenzyl alcohol (1.38 g, 10 mmol) in Et<sub>2</sub>O (20 ml) was prepared in a 100 ml two-neck flask and thionyl chloride (2.38 g, 20 mmol) was added dropwise. The reaction mixture was stirred at room temperature for 5 hours. Water (20 ml) was added slowly and carefully, and the reaction mixture was stirred for 5 minutes, in the following the mixture was transferred to a separatory funnel. The layers were separated, then the aqueous layer was extracted again with DCM (2 x 20 ml). The organic layers were combined, washed with water (20 ml), then brine (20 ml). The organic layers were dried over MgSO<sub>4</sub>. The mixture was filtered and the solvent was evaporated under reduced pressure. Without purification, 4-methoxybenzyl chloride (1.41 g, 97%) was obtained as pale pink color and clear oil. <sup>1</sup>H NMR (400 MHz, CDCl<sub>3</sub>) δ: 7.20 (d, *J* = 8.7 Hz, 2H), 6.77 (d, *J* = 8.8 Hz, 2H), 4.45 (s, 2H), 3.68 (s, 3H); <sup>13</sup>C NMR (101 MHz, CDCl<sub>3</sub>) δ: 159.7, 130.1, 129.7, 114.2, 55.3, 46.4.

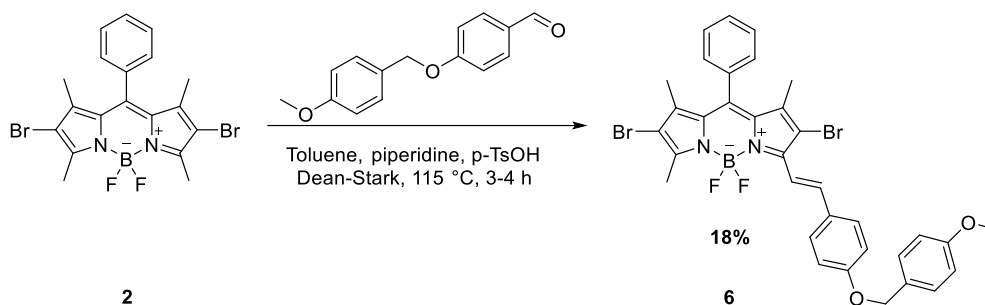
### 4.3.5 Synthesis of Compound 7



Scheme 4.5. Synthetic route of Compound 7

A literature report on a closely related system was utilized with modification (Houze et al., 2012). 4-hydroxybenzaldehyde (100 mg, 0.82 mmol) was dissolved with anhydrous DMF (5 ml) in a 25 ml Schlenk tube. 4-methoxybenzyl chloride (PMB-Cl, 166.8 mg, 1.065 mmol) was added to the mixture, followed by K<sub>2</sub>CO<sub>3</sub> (226.3 mg, 1.638 mmol). The reaction mixture was stirred at room temperature for 5-6 hours. The thin layer chromatography (TLC) showed no further progress in the reaction after 6 hours. The reaction mixture was poured into cold water. Then, the product was collected by filtration and rinsed with water. After drying thoroughly, compound **7** (164 mg, 79%) was obtained as a light-yellow powder. <sup>1</sup>H NMR (400 MHz, CDCl<sub>3</sub>) δ: 9.82 (s, 1H), 7.77 (d, *J* = 8.8 Hz, 2H), 7.30 (d, *J* = 8.8 Hz, 2H), 7.00 (d, *J* = 8.8 Hz, 2H), 6.87 (d, *J* = 8.8 Hz, 2H), 5.01 (s, 2H), 3.76 (s, 3H).

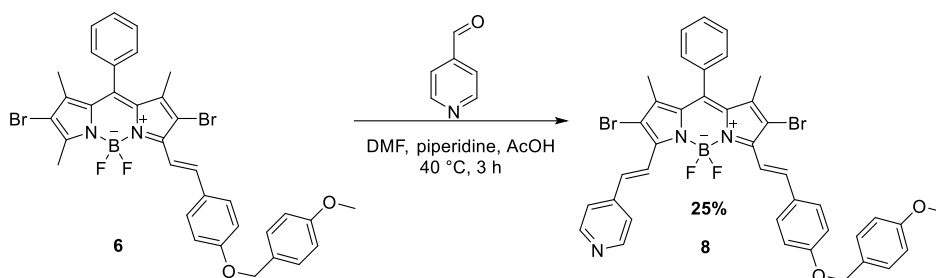
### 4.3.6 Synthesis of Compound 6



Scheme 4.6. Synthetic route of Compound 6

A literature report on a closely related system was utilized with modification (Bura et al., 2011). In a 50 ml two-neck flask equipped with a Dean-Stark apparatus, compound 2 (100 mg, 0.207 mmol) and toluene (15 ml) were introduced, and the temperature was set as 40 °C. The mixture was stirred at this temperature until compound 2 was totally dissolved. Then, under argon atmosphere, 4-hydroxybenzaldehyde (85.5 mg, 0.353 mmol), piperidine (0.4 ml), and a crystal of p-TsOH were added to a stirred solution of the BODIPY dye. The mixture was heated at its boiling point (115 °C). The thin layer chromatography (TLC) demonstrated that the distortions have begun after 3 hours stirring, so it was ended. The resulting mixture was washed with water and extracted with DCM. The organic layers were combined and dried over MgSO<sub>4</sub>. The mixture was filtered and the solvent was evaporated under reduced pressure. The crude product was purified by column chromatography (silica gel, DCM:Hexane – from 2:1 to 4:1 gradually) to obtain the final product (**Compound 6**) as violet purple solid (26 mg, 18%). <sup>1</sup>H NMR (400 MHz, CDCl<sub>3</sub>) δ: 8.03 (d, *J* = 16.8 Hz, 1H), 7.52 (d, *J* = 8.9 Hz, 3H), 7.49 – 7.44 (m, 3H), 7.31 (d, *J* = 8.8 Hz, 2H), 6.92 (d, *J* = 8.9 Hz, 2H), 6.86 (d, *J* = 8.8 Hz, 2H), 4.97 (s, 2H), 3.76 (s, 3H), 2.58 (s, 3H), 1.50 (s, 2H), 1.32 (d, *J* = 13.3 Hz, 6H), 1.18 (s, 1H).

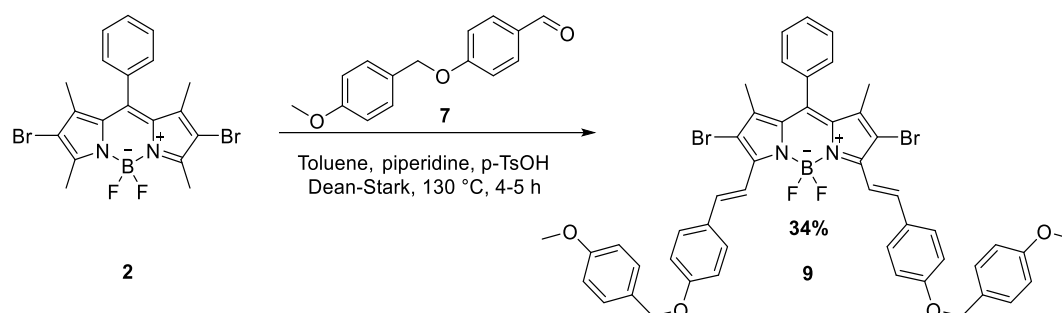
### 4.3.7 Synthesis of Compound 8



Scheme 4.7. Synthetic route of Compound 8

A literature report on a closely related system was utilized with modification (Karaman et al., 2019). Compound 6 (50 mg, 0.0708 mmol) was dissolved with anhydrous DMF (3 ml) in a 10 ml Schlenk tube. Then, 4-pyridinecarboxaldehyde (15 mg, 0.14 mmol) was added to the mixture. To this solution, piperidine (0.15 ml) and acetic acid (0.15 ml) were added dropwise respectively, and the reaction mixture continued to stir at 40 °C. The thin layer chromatography (TLC) demonstrated that the distortions have begun after 3 hours stirring, so it was ended, and it was immediately evaporated with vacuum. Then, the crude product was purified by column chromatography (silica gel, DCM:MeOH – 100:3) to give **Compound 8** as a blackish purple solid (26.8 mg, 25%). <sup>1</sup>H NMR (400 MHz, CDCl<sub>3</sub>) δ: 8.57 (d, *J* = 5.9 Hz, 2H), 8.19 (d, *J* = 16.7 Hz, 1H), 7.89 (s, 2H), 7.57 (d, *J* = 8.9 Hz, 4H), 7.49 (dd, *J* = 5.0, 1.9 Hz, 3H), 7.31 (d, *J* = 8.7 Hz, 2H), 7.25 – 7.21 (m, 2H), 6.97 (d, *J* = 8.8 Hz, 2H), 6.87 (d, *J* = 8.8 Hz, 2H), 5.01 (s, 2H), 3.76 (s, 3H), 1.36 (d, *J* = 15.7 Hz, 6H); <sup>13</sup>C NMR (101 MHz, CDCl<sub>3</sub>) δ: 159.6, 158.6, 150.5, 147.8, 144.7, 143.4, 142.4, 140.4, 138.8, 138.6, 133.5, 132.4, 132.3, 131.0, 128.7, 128.5, 128.4, 128.2, 127.5, 127.2, 122.4, 120.7, 114.7, 114.4, 113.1, 110.7, 109.2, 99.0, 69.0, 54.3, 28.7, 13.0, 12.5.

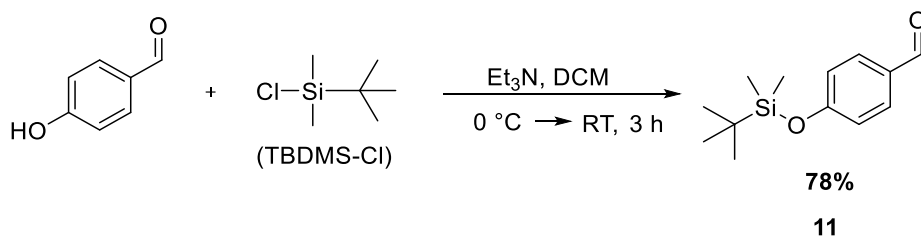
### 4.3.8 Synthesis of Compound 9



Scheme 4.8. Synthetic route of Compound 9

A literature report on a closely related system was utilized with modification (Bura et al., 2011). Compound 2 (100 mg, 0.207 mmol) and toluene (15 ml) were introduced in a 50 ml Schlenk tube, and the temperature was set as 50 °C. The mixture was stirred at this temperature until compound 2 was totally dissolved. Then, under argon atmosphere, 4-hydroxybenzaldehyde (302.4 mg, 1.248 mmol), piperidine (0.34 ml), and a crystal of p-TsOH were added to a stirred solution. The mixture was heated at 130 °C. The thin layer chromatography (TLC) demonstrated that the distortions have begun after 4 hours stirring, so it was ended. The resulting mixture was washed with water and extracted with chloroform. The organic layer was dried over MgSO<sub>4</sub>. The mixture was filtered and the solvent was evaporated under reduced pressure. The crude product was purified by column chromatography (silica gel, DCM:Hexane – from 1.5:1 to 4:1 gradually) to obtain the final product (**Compound 9**) as dark green- blackish solid (101.6 mg, 34%). <sup>1</sup>H NMR (400 MHz, CDCl<sub>3</sub>) δ: 8.04 (d, *J* = 16.6 Hz, 1H), 7.59 – 7.51 (m, 3H), 7.48 – 7.44 (m, 2H), 7.31 (d, *J* = 8.7 Hz, 2H), 7.22 (d, *J* = 3.6 Hz, 1H), 6.95 (d, *J* = 8.8 Hz, 2H), 6.87 (d, *J* = 8.8 Hz, 2H), 4.98 (s, 2H), 3.75 (s, 3H), 1.51 – 1.15 (m, 6H).

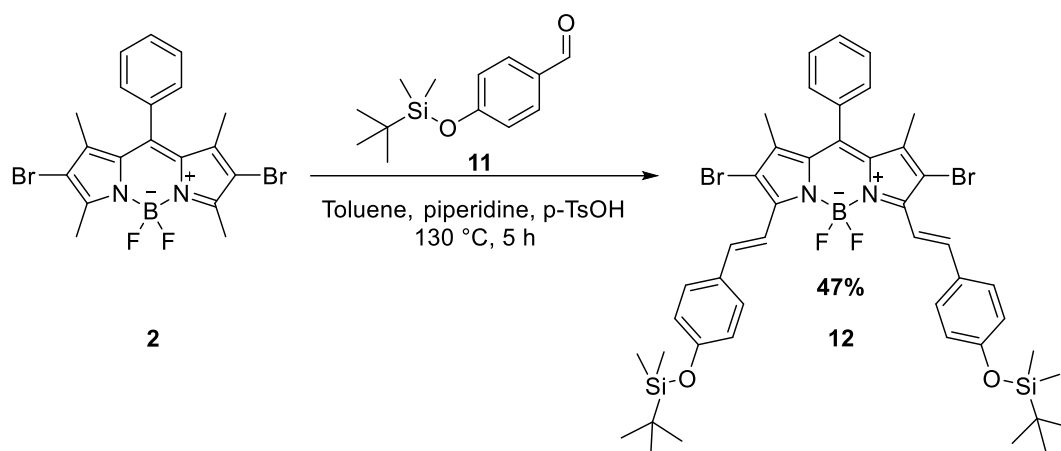
### 4.3.9 Synthesis of Compound 11



*Scheme 4.9.* Synthetic route of Compound 11

A literature report on a closely related system was utilized with modification (Panduawala et al., 2019). Anhydrous DCM (80 ml) was introduced in a 250 ml two-neck flask, then 4-hydroxybenzaldehyde (4 g, 16.4 mmol) and Et<sub>3</sub>N (7 ml, 24.6 mmol) were added, and the flask was placed in ice. A solution of TBDMS-Cl (7.4 g, 24.6 mmol) in DCM (10 ml) was added to the mixture at 0 °C portionwise. The reaction mixture was stirred at room temperature for 3 hours. The thin layer chromatography (TLC) showed no further progress in the reaction, then it was quenched with water (20 ml) and continued to stir for 5 minutes more. The organic layer was separated and the aqueous layer was extracted with DCM. All organic layers were combined and washed with brine, dried over MgSO<sub>4</sub>. Then, it was filtered and the solvent was evaporated under reduced pressure. The crude product was purified by column chromatography (silica gel, EtOAc:petroleum ether – 1:9) to give **Compound 11** as pale yellow oil (7.84 g, 78%). <sup>1</sup>H NMR (400 MHz, CDCl<sub>3</sub>) δ: 9.63 (s, 1H), 7.56 – 7.52 (m, 2H), 6.72 – 6.66 (m, 2H), 0.74 (s, 9H); <sup>13</sup>C NMR (101 MHz, CDCl<sub>3</sub>) δ: 190.9, 171.1, 161.5, 131.9, 130.4, 120.5, 25.7, 25.5, 18.2, -3.6, -4.4.

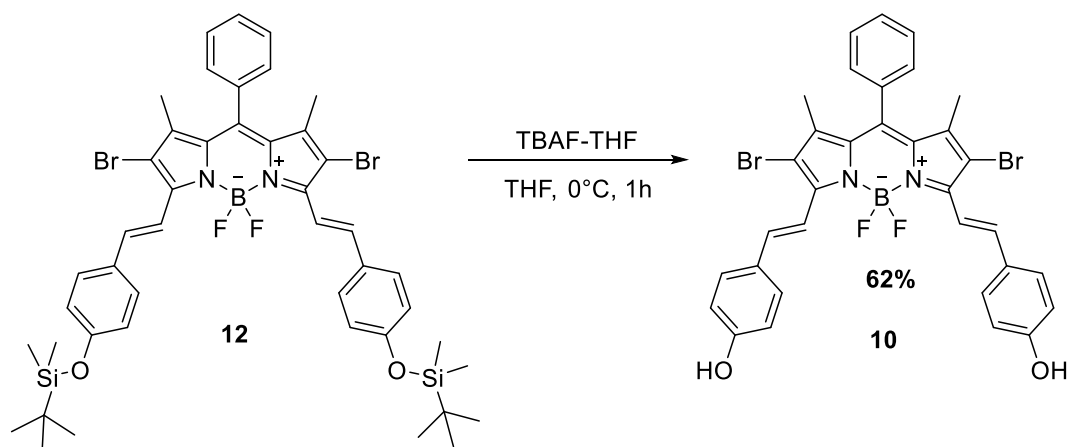
#### 4.3.10 Synthesis of Compound 12



Scheme 4.10. Synthetic route of Compound 12

A literature report on a closely related system was utilized with modification (Bura et al., 2011). Compound 2 (200 mg, 0.415 mmol) and toluene (30 ml) were introduced in a 100 ml Schlenk tube, and the temperature was set to 50 °C. The mixture was stirred at this temperature until compound 2 was completely dissolved. Then, 4-hydroxybenzaldehyde (451.3 mg, 0.955 mmol), piperidine (1.4 ml), and a crystal of p-TsOH were added to a stirred solution. The mixture was heated to 130 °C. The thin layer chromatography (TLC) demonstrated that the distortions have begun after 5 hours stirring, so it was ended. Water was added to the final reaction mixture and extracted with DCM. MgSO<sub>4</sub> was used to dry the organic layer. After the filtration of the mixture, the solvent was evaporated under reduced pressure. The crude product was purified by column chromatography (silica gel, DCM:Hexane – 2:1) to obtain the **Compound 12** as dark green- blackish solid (179 mg, 47%). <sup>1</sup>H NMR (400 MHz, CDCl<sub>3</sub>) δ: 8.03 (d, *J* = 16.7 Hz, 1H), 7.54 – 7.44 (m, 4H), 7.22 (d, *J* = 3.6 Hz, 1H), 6.82 (d, *J* = 8.7 Hz, 2H), 1.33 (s, 3H), 0.94 (s, 9H), 0.17 (s, 6H).

### 4.3.11 Deprotection of TBDMS Protection Group

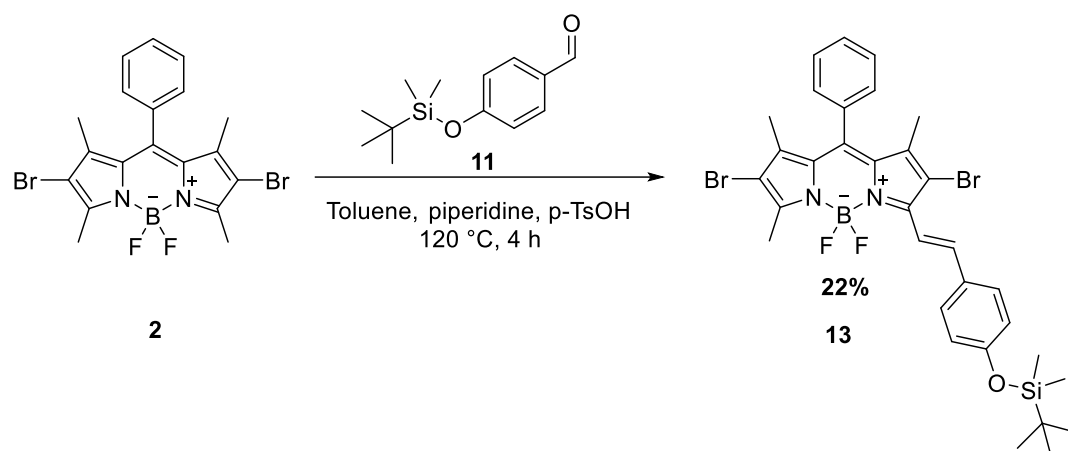


*Scheme 4.11.* Synthetic route of Deprotection of the TBDMS Group

A literature report on a closely related system was utilized with modification (S.J. Kim et al., 2014). In a 25 ml Schlenk tube, compound **12** (50 mg, 0.054 mmol) was dissolved with dry THF (6 ml). After dissolution of starting material, it was placed into the ice-water bath to decrease the temperature to 0 °C. TBAF solution (31.4 mg, 0.12 mmol) was diluted with dry THF (0.3 ml) and added over starting material dropwise. Completion of the reaction after 1 hour, the mixture was extracted with DCM, the collected organic layer was washed with saturated NH<sub>4</sub>Cl solution, then brine is used. Following evaporation of the solvents, the residue was purified by column chromatography (silica gel, DCM:MeOH – 100:3) to obtain the **Compound 10** as dark green solid (23.4 mg, 62%). <sup>1</sup>H NMR (400 MHz, d<sub>6</sub>-DMSO) δ: 8.10 (d, *J* = 16.7 Hz, 2H), 7.70 – 7.66 (m, 3H), 7.57 (d, *J* = 8.8 Hz, 4H), 7.55 – 7.52 (m, 2H), 7.48 (d, *J* = 16.4 Hz, 2H), 6.96 (d, *J* = 8.7 Hz, 4H), 1.43 (s, 6H).



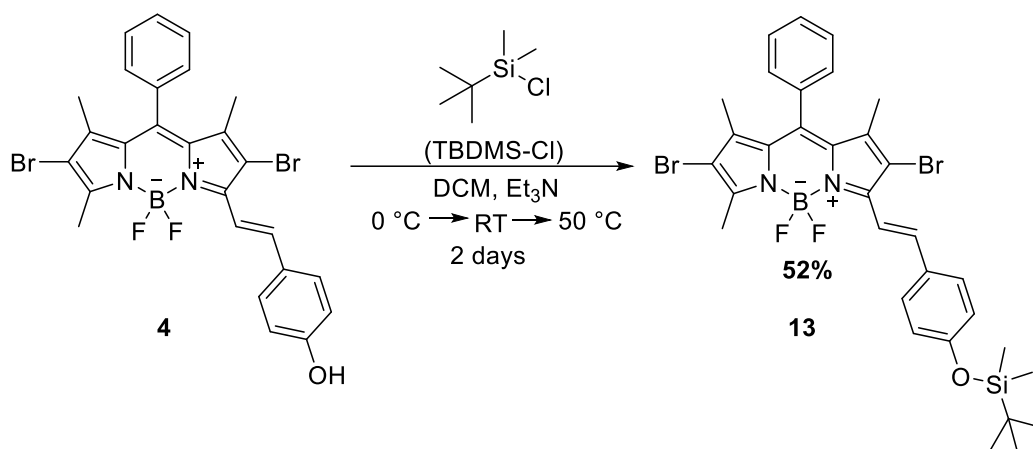
### 4.3.12 Synthesis of Compound 13



Scheme 4.12. Synthetic route of Compound 13

A literature report on a closely related system was utilized with modification (Bura et al., 2011). Compound 2 (200 mg, 0.415 mmol) and toluene (30 ml) were introduced in a 100 ml Schlenk tube, and the temperature was adjusted to 50 °C. Compound 2 was completely dissolved when the mixture was stirred at this temperature. Then, 4-hydroxybenzaldehyde (225.6 mg, 0.955 mmol), piperidine (0.7 ml), and a crystal of p-TsOH were added to a stirred solution. The mixture was heated to 120 °C. The distortions have begun after 5 hours stirring according to the thin layer chromatography (TLC) demonstration, so it was ended. The reaction mixture was washed with water and then extracted with DCM. MgSO<sub>4</sub> was used to dry the organic layer. After the filtration of the mixture, the solvent was evaporated under reduced pressure. The crude product was purified by column chromatography (silica gel, DCM:Hexane – from 1.5:1 to 2.5 gradually) to get the **Compound 13** as purple violet solid (36.7 mg, 22%). <sup>1</sup>H NMR (400 MHz, CDCl<sub>3</sub>) δ: 7.98 (d, *J* = 16.7 Hz, 1H), 7.43 (dd, *J* = 5.9, 2.9 Hz, 4H), 7.18 (d, *J* = 4.0 Hz, 2H), 6.76 (d, *J* = 8.5 Hz, 2H), 2.55 (s, 3H), 0.89 (s, 9H), 0.12 (s, 6H).

### 4.3.13 Synthesis of Compound 13

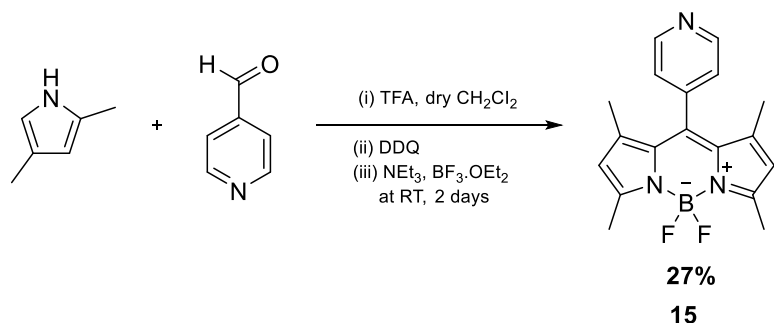


Scheme 4.13. Synthetic route of Compound 13

A literature report on a closely related system was utilized with modification (Panduawala et al., 2019). Compound 4 (100 mg, 0.17 mmol) was introduced in a 25 ml Schlenk tube, and chloroform (12 ml) was added. After the dissolution occurs, Et<sub>3</sub>N (25.8 mg, 0.255 mmol) was diluted in chloroform (0.5 ml) and was added to the solution of compound 4, then the flask was placed in ice-water bath. A solution of TBDMS-Cl (38.4 mg, 0.255 mmol) in chloroform (0.5 ml) was added to the mixture at 0 °C dropwise. When the addition was completed, the ice bath was removed, and the reaction was continued to stir at room temperature for 3 hours, then the temperature was adjusted to 50 °C for 2 days. No further progress in the reaction was observed according to the thin layer chromatography (TLC), then it was quenched with water (20 ml). The organic layer was separated and the aqueous layer was extracted with DCM. All organic layers were combined and washed with brine, dried over MgSO<sub>4</sub>. Then, it was filtered and the solvent was evaporated under reduced pressure. The crude product was purified by column chromatography (silica gel, DCM:MeOH – 100:2) to give **Compound 13** as violet purple (146 mg, 52%). <sup>1</sup>H NMR (400 MHz, CDCl<sub>3</sub>) δ: 7.98 (d, *J* = 16.7 Hz, 1H), 7.43 (dd, *J* = 5.9, 2.9 Hz, 4H), 7.18 (d, *J* = 4.0 Hz, 2H), 6.76 (d, *J* = 8.5 Hz, 2H), 2.55 (s, 3H), 0.89 (s, 9H), 0.12 (s, 6H).

## 4.4 Experiments Towards Synthesis of S2-BODMe

### 4.4.1 Synthesis of Compound 15

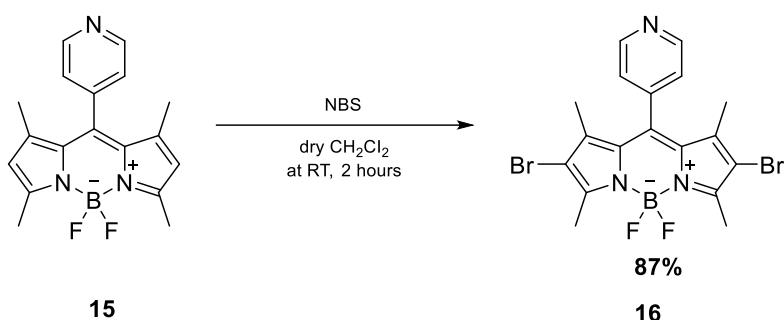


*Scheme 4.14.* Synthetic route of compound 15

A literature report on a closely related system was utilized with modification (Luo et al., 2014). Anhydrous  $\text{CH}_2\text{Cl}_2$  (150 ml) was introduced in a 250 ml two-neck flask and argon-purged for 20 minutes. Then, under a nitrogen atmosphere, 2,4-dimethylpyrrole (0.62 ml, 6 mmol) and 4-pyridinecarboxaldehyde (0.28 ml, 3 mmol) were added respectively. Trifluoroacetic acid (TFA, 0.15 ml, 1.96 mmol) was added to the mixture dropwise. The mixture was stirred overnight at room temperature (RT) in the dark until TLC showed that the aldehyde has been completely consumed. Dichlorodicyanobenzoquinone (DDQ, 681 mg, 3 mmol) was added within 30 minutes portion wise and the mixture was stirred for an additional 2 hours. A large excess of triethylamine (TEA, 9 ml, 64,5 mmol) and  $\text{BF}_3\cdot\text{Et}_2\text{O}$  (9 ml, 72,9 mmol) were added dropwise respectively into the reaction mixture, and the reaction mixture was continued to stir overnight at room temperature in the dark. Water was added the reaction mixture was extracted with  $\text{CH}_2\text{Cl}_2$ . The organic layers were combined and dried over  $\text{MgSO}_4$  and the solvent was evaporated under reduced pressure. The crude product was purified by column chromatography (silica gel, MeOH:DCM - 2:98) to obtain the desired product (**Compound 15**) as a dark orange solid (264 mg, 27%).  $^1\text{H}$  NMR (400 MHz,  $\text{CDCl}_3$ )  $\delta$ : 8.78 (s, 2H), 7.31 (d, 2H,  $J=3.8$  Hz), 6.00 (s,

2H), 2.54 (s, 6H), 1.39 (s, 6H);  $^{13}\text{C}$  NMR (101 MHz,  $\text{CDCl}_3$ )  $\delta$ : 156.6, 150.6, 143.8, 142.7, 137.7, 130.4, 123.5, 121.9, 14.9

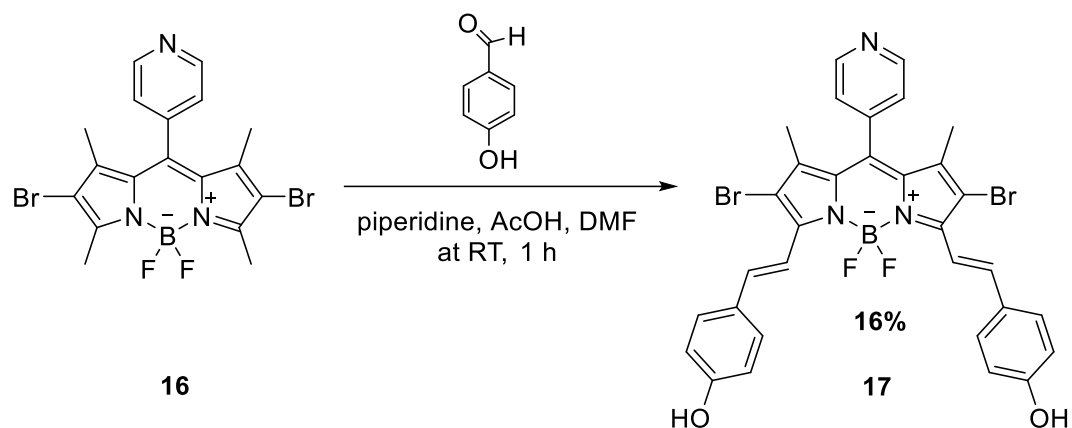
#### 4.4.2 Synthesis of Compound 16



*Scheme 4.15.* Synthetic route of Compound 16

A literature report on a closely related system was utilized with modification (Bartelmess et al., 2014). Compound 15 (211 mg, 0.68 mmol) was dissolved in anhydrous DCM (33 ml) and N-bromosuccinimide (NBS, 302 mg, 1.7 mmol) solution in dry DCM (22 ml) was added in a dropwise manner. The mixture was stirred at room temperature and the thin layer chromatography (TLC) demonstrated that the reaction was completed. The organic phase washed with water (80 ml), followed by brine (80 ml). The organic layers were combined and dried over anhydrous  $\text{Na}_2\text{SO}_4$ . The mixture was filtered, and the solvent was evaporated under reduced pressure. The crude product was purified by column chromatography (silica gel, EtOAc:DCM – 15:100) to obtain the final product (**Compound 16**) as a dark red solid (286 mg, 87%).  $^1\text{H}$  NMR (400 MHz,  $\text{CDCl}_3$ )  $\delta$ : 8.84 (d, 2H,  $J=4.8$  Hz), 7.32 (d, 2H,  $J=4.8$  Hz), 2.60 (s, 6H), 1.39 (s, 6H);  $^{13}\text{C}$  NMR (101 MHz,  $\text{CDCl}_3$ )  $\delta$ : 154.9, 150.3, 143.3, 139.9, 137.4, 129.1, 123.1, 112.3, 13.9 13.7

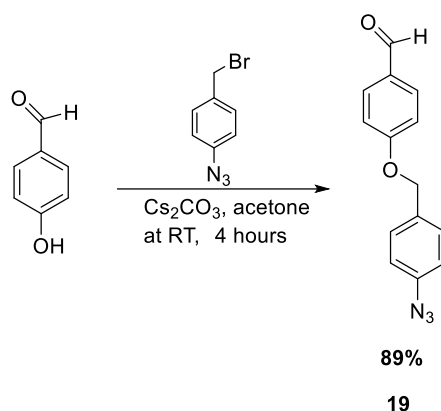
#### 4.4.3 Synthesis of Compound 17



Scheme 4.16. Synthetic route of Compound 17

A literature report on a closely related system was utilized with modification (Karaman et al., 2019). Compound 16 (100 mg, 0.207 mmol) was dissolved with anhydrous DMF (5 ml) in a 25 ml Schlenk tube. Then, 4-hydroxybenzaldehyde (100.14 mg, 0.82 mmol) was added to the mixture. To this solution, piperidine (0.3 ml) and acetic acid (0.3 ml) were added dropwise respectively, and the reaction mixture continued to stir at room temperature. The TLC showed that the reaction was completed after 1 hour, and it was immediately evaporated with vacuum. Then, the crude product was purified by column chromatography (silica gel, MeOH:Chloroform – 3:97) to give **Compound 17** as a dark green solid (22.9 mg, 16%). <sup>1</sup>H NMR (400 MHz, DMSO-d<sub>6</sub>) δ: 10.16 (s, 2H), 8.83 (br. s, 2H), 8.33 (s, 2H), 8.06 (d, 2H, J= 16 Hz), 7.63 (s, 2H), 7.50 (d, 4H, J=7.3 Hz), 7.4 (d, 2H, 16 Hz), 6.90 (d, 4H, J=7.3 Hz), 1.40 (s, 6H).

#### 4.4.4 Synthesis of Compound 19



*Scheme 4.17.* Synthetic route of azide containing masking unit

A literature report on a closely related system was utilized with modification (Patti et al., 2009). 4-hydroxybenzaldehyde (82.3 mg, 0.674 mmol) was dissolved with acetone (5 ml) in a 50 ml Schlenk tube. Then, 1-azido-4-(bromomethyl)benzene (143 mg, 0.674 mmol) and cesium carbonate ( $\text{Cs}_2\text{CO}_3$ , 307.5 mg, 0.944 mmol) were added to the solution. The TLC indicated that the reaction was completed after 6 hours. Then, the reaction mixture was filtered and the solution part of it was taken to dryness under reduced pressure. The desired compound was obtained without purification as colorless oil (151.6 mg, 89%).  $^1\text{H}$  NMR (400 MHz,  $\text{CDCl}_3$ )  $\delta$ : 9.91 (s, 2H), 7.87 (d, 2H,  $J=8.8$  Hz), 7.45 (d, 2H,  $J=8.7$  Hz), 7.09 (d, 4H,  $J=8.7$  Hz), 5.14 (s, 2H).

## REFERENCES

- Ismail, Y. (2017). *Synthesis and Characterization of BODIPY-Derived Singlet Oxygen Sensor* [MSc. Thesis] Bilkent University
- Abrahamse, H., & Hamblin, M. R. (2016). New photosensitizers for photodynamic therapy. *Biochemical Journal*, *473*(4), 347–364.  
<https://doi.org/10.1042/BJ20150942>
- Ackroyd, R., Kelty, C., Brown, N., & Reed, M. (2001). The History of Photodetection and Photodynamic Therapy. *Photochemistry and Photobiology*, *74*(5), 656. [https://doi.org/10.1562/00318655\(2001\)074<0656:THOPAP>2.0.CO;2](https://doi.org/10.1562/00318655(2001)074<0656:THOPAP>2.0.CO;2)
- Agarwal, M. L., Clay, M. E., Harvey, E. J., Evans, H. H., Antunez, A. R., & Oleinick, N. L. (1991). Photodynamic therapy induces rapid cell death by apoptosis in L5178Y mouse lymphoma cells. *Cancer Research*, *51*(21), 5993–5996.
- Agostinis, P., Berg, K., Cengel, K. A., Foster, T. H., Girotti, A. W., Gollnick, S. O., Hahn, S. M., Hamblin, M. R., Juzeniene, A., Kessel, D., Korbelik, M., Moan, J., Mroz, P., Nowis, D., Piette, J., Wilson, B. C., & Golab, J. (2011). Photodynamic therapy of cancer: An update. *CA: A Cancer Journal for Clinicians*, *61*(4), 250–281. <https://doi.org/10.3322/caac.20114>
- Allison, R. R., Downie, G. H., Cuenca, R., Hu, X.-H., Childs, C. J., & Sibata, C. H. (2004). Photosensitizers in clinical PDT. *Photodiagnosis and Photodynamic Therapy*, *1*(1), 27–42. [https://doi.org/10.1016/S1572-1000\(04\)00007-9](https://doi.org/10.1016/S1572-1000(04)00007-9)
- Allison, R. R., & Moghissi, K. (2013). Photodynamic Therapy (PDT): PDT Mechanisms. *Clinical Endoscopy*, *46*(1), 24.  
<https://doi.org/10.5946/ce.2013.46.1.24>

- Allison, R. R., & Sibata, C. H. (2010). Oncologic photodynamic therapy photosensitizers: A clinical review. *Photodiagnosis and Photodynamic Therapy*, 7(2), 61–75. <https://doi.org/10.1016/j.pdpdt.2010.02.001>
- Ascencio, M., Collinet, P., Farine, M. O., & Mordon, S. (2008). Protoporphyrin IX fluorescence photobleaching is a useful tool to predict the response of rat ovarian cancer following hexaminolevulinate photodynamic therapy. *Lasers in Surgery and Medicine*, 40(5), 332–341. <https://doi.org/10.1002/lsm.20629>
- Auler, H., & Banzer, G. (1942). Untersuchungen über die Rolle der Porphyrine bei geschwulstkranken Menschen und Tieren. *Zeitschrift Für Krebsforschung*, 53(2), 65–68. <https://doi.org/10.1007/BF01792783>
- Awuah, S. G., & You, Y. (2012). Boron dipyrromethene (BODIPY)-based photosensitizers for photodynamic therapy. *RSC Advances*, 2(30), 11169. <https://doi.org/10.1039/c2ra21404k>
- Bacellar, I., Tsubone, T., Pavani, C., & Baptista, M. (2015). Photodynamic Efficiency: From Molecular Photochemistry to Cell Death. *International Journal of Molecular Sciences*, 16(9), 20523–20559. <https://doi.org/10.3390/ijms160920523>
- Bachor, R., Shea, C. R., Gillies, R., & Hasan, T. (1991). Photosensitized destruction of human bladder carcinoma cells treated with chlorin e6-conjugated microspheres. *Proceedings of the National Academy of Sciences*, 88(4), 1580–1584. <https://doi.org/10.1073/pnas.88.4.1580>
- Bañuelos, J. (2016). BODIPY Dye, the Most Versatile Fluorophore Ever? *The Chemical Record*, 16(1), 335–348. <https://doi.org/10.1002/tcr.201500238>
- Bartelmess, J., Francis, A. J., el Roz, K. A., Castellano, F. N., Weare, W. W., & Sommer, R. D. (2014). Light-Driven Hydrogen Evolution by BODIPY-Sensitized Cobaloxime Catalysts. *Inorganic Chemistry*, 53(9), 4527–4534. <https://doi.org/10.1021/ic500218q>



- Baskaran, R., Lee, J., & Yang, S.-G. (2018). Clinical development of photodynamic agents and therapeutic applications. *Biomaterials Research*, 22(1), 25. <https://doi.org/10.1186/s40824-018-0140-z>
- Battersby, A. R. (2000). Tetrapyrroles: the pigments of life. *Natural Product Reports*, 17(6), 507–526. <https://doi.org/10.1039/b002635m>
- Benstead, M., Mehl, G. H., & Boyle, R. W. (2011). 4,4'-Difluoro-4-bora-3a,4a-diaza-s-indacenes (BODIPYs) as components of novel light active materials. *Tetrahedron*, 67(20), 3573–3601. <https://doi.org/10.1016/j.tet.2011.03.028>
- Boyle, R. W., & Dolphin, D. (1996). Structure and Biodistribution Relationships of Photodynamic Sensitizers. *Photochemistry and Photobiology*, 64(3), 469–485. <https://doi.org/10.1111/j.1751-1097.1996.tb03093.x>
- Brancaleon, L., & Moseley, H. (2002). Laser and Non-laser Light Sources for Photodynamic Therapy. *Lasers in Medical Science*, 17(3), 173–186. <https://doi.org/10.1007/s101030200027>
- Bura, T., Retailleau, P., Ulrich, G., & Ziessel, R. (2011). Highly Substituted Bodipy Dyes with Spectroscopic Features Sensitive to the Environment. *The Journal of Organic Chemistry*, 76(4), 1109–1117. <https://doi.org/10.1021/jo102203f>
- Buytaert, E., Callewaert, G., Hendrickx, N., Scorrano, L., Hartmann, D., Missiaen, L., Vandenheede, J. R., Heirman, I., Grooten, J., & Agostinis, P. (2006). Role of endoplasmic reticulum depletion and multidomain proapoptotic BAX and BAK proteins in shaping cell death after hypericin-mediated photodynamic therapy. *The FASEB Journal*, 20(6), 756–758. <https://doi.org/10.1096/fj.05-4305fje>
- Buytaert, E., Dewaele, M., & Agostinis, P. (2007). Molecular effectors of multiple cell death pathways initiated by photodynamic therapy. *Biochimica et Biophysica Acta (BBA) - Reviews on Cancer*, 1776(1), 86–107. <https://doi.org/10.1016/j.bbcan.2007.07.001>

- Buyukcakil, O., Bozdemir, O. A., Kolemen, S., Erbas, S., & Akkaya, E. U. (2009). Tetrastyril-Bodipy Dyes: Convenient Synthesis and Characterization of Elusive Near IR Fluorophores. *Organic Letters*, *11*(20), 4644–4647. <https://doi.org/10.1021/ol9019056>
- Calzavara-Pinton, P., Venturini, M., & Sala, R. (2007). Photodynamic therapy: update 2006 Part 1: Photochemistry and photobiology. *Journal of the European Academy of Dermatology and Venereology*, *21*(3), 293–302. <https://doi.org/10.1111/j.1468-3083.2006.01902.x>
- Cantisani, C., Paolino, G., Bottoni, U., & Calvieri, S. (2015). Daylight-Photodynamic Therapy for the Treatment of Actinic Keratosis in Different Seasons. *Journal of Drugs in Dermatology : JDD*, *14*(11), 1349–1353.
- Castano, A. P., Demidova, T. N., & Hamblin, M. R. (2004). Mechanisms in photodynamic therapy: part one—photosensitizers, photochemistry and cellular localization. *Photodiagnosis and Photodynamic Therapy*, *1*(4), 279–293. [https://doi.org/10.1016/S1572-1000\(05\)00007-4](https://doi.org/10.1016/S1572-1000(05)00007-4)
- Castano, A. P., Demidova, T. N., & Hamblin, M. R. (2005). Mechanisms in photodynamic therapy: Part three—Photosensitizer pharmacokinetics, biodistribution, tumor localization and modes of tumor destruction. *Photodiagnosis and Photodynamic Therapy*, *2*(2), 91–106. [https://doi.org/10.1016/S1572-1000\(05\)00060-8](https://doi.org/10.1016/S1572-1000(05)00060-8)
- Castano, A. P., Mroz, P., & Hamblin, M. R. (2006). Photodynamic therapy and anti-tumour immunity. *Nature Reviews Cancer*, *6*(7), 535–545. <https://doi.org/10.1038/nrc1894>
- Chatterjee, D. K., Fong, L. S., & Zhang, Y. (2008). Nanoparticles in photodynamic therapy: An emerging paradigm. *Advanced Drug Delivery Reviews*, *60*(15), 1627–1637. <https://doi.org/10.1016/j.addr.2008.08.003>
- Chen, , Wei R., Zhu, W.-G., Dynlacht, J. R., Liu, H., & Nordquist, R. E. (1999). Long-term tumor resistance induced by laser photo-immunotherapy.

*International Journal of Cancer*, 81(5), 808–812.

[https://doi.org/10.1002/\(SICI\)1097-0215\(19990531\)81:5<808::AID-IJC23>3.0.CO;2-J](https://doi.org/10.1002/(SICI)1097-0215(19990531)81:5<808::AID-IJC23>3.0.CO;2-J)

Chen, B., Pogue, B. W., Luna, J. M., Hardman, R. L., Hoopes, P. J., & Hasan, T.

(2006). Tumor Vascular Permeabilization by Vascular-Targeting Photosensitization: Effects, Mechanism, and Therapeutic Implications.

*Clinical Cancer Research*, 12(3), 917–923. <https://doi.org/10.1158/1078-0432.CCR-05-1673>

Chen, B., Roskams, T., & de Witte, P. A. M. (2002). Antivascular Tumor

Eradication by Hypericin-mediated Photodynamic Therapy. *Photochemistry and Photobiology*, 76(5), 509. [https://doi.org/10.1562/0031-8655\(2002\)076<0509:ATEBHM>2.0.CO;2](https://doi.org/10.1562/0031-8655(2002)076<0509:ATEBHM>2.0.CO;2)

Chen, D., Zheng, H., Huang, Z., Lin, H., Ke, Z., Xie, S., & Li, B. (2012). Light-

Emitting Diode-Based Illumination System for In Vitro Photodynamic Therapy. *International Journal of Photoenergy*, 2012, 1–6.

<https://doi.org/10.1155/2012/920671>

Correia, J. H., Rodrigues, J. A., Pimenta, S., Dong, T., & Yang, Z. (2021).

Photodynamic Therapy Review: Principles, Photosensitizers, Applications, and Future Directions. *Pharmaceutics*, 13(9), 1332.

<https://doi.org/10.3390/pharmaceutics13091332>

Coutier, S., Bezdetnaya, L., Marchal, S., Melnikova, V., Belitchenko, I., Merlin, J.

L., & Guillemin, F. (1999). Foscan® (mTHPC) photosensitized macrophage activation: enhancement of phagocytosis, nitric oxide release and tumour

necrosis factor- $\alpha$ -mediated cytolytic activity. *British Journal of Cancer*, 81(1), 37–42. <https://doi.org/10.1038/sj.bjc.6690648>

Dąbrowski, J. M. (2017). *Reactive Oxygen Species in Photodynamic Therapy:*

*Mechanisms of Their Generation and Potentiation* (pp. 343–394).

<https://doi.org/10.1016/bs.adioch.2017.03.002>

- Dang, J., He, H., Chen, D., & Yin, L. (2017). Manipulating tumor hypoxia toward enhanced photodynamic therapy (PDT). *Biomaterials Science*, 5(8), 1500–1511. <https://doi.org/10.1039/C7BM00392G>
- de Rosa, F. S., & Bentley, M. v. (2000). Photodynamic therapy of skin cancers: sensitizers, clinical studies and future directives. *Pharmaceutical Research*, 17(12), 1447–1455. <https://doi.org/10.1023/a:1007612905378>
- Detty, M. R., Gibson, S. L., & Wagner, S. J. (2004). Current Clinical and Preclinical Photosensitizers for Use in Photodynamic Therapy. *Journal of Medicinal Chemistry*, 47(16), 3897–3915. <https://doi.org/10.1021/jm040074b>
- Diamond, I., Mcdonagh, A. F., Wilson, C. B., Granelli, S. G., Nielsen, S., & Jaenicke, R. (1972). Photodynamic Therapy of Malignant Tumours. *The Lancet*, 300(7788), 1175–1177. [https://doi.org/10.1016/S0140-6736\(72\)92596-2](https://doi.org/10.1016/S0140-6736(72)92596-2)
- Dolmans, D. E. J. G. J., Fukumura, D., & Jain, R. K. (2003). Photodynamic therapy for cancer. *Nature Reviews Cancer*, 3(5), 380–387. <https://doi.org/10.1038/nrc1071>
- Dolmans, D. E. J. G. J., Kadambi, A., Hill, J. S., Flores, K. R., Gerber, J. N., Walker, J. P., Borel Rinkes, I. H. M., Jain, R. K., & Fukumura, D. (2002). Targeting tumor vasculature and cancer cells in orthotopic breast tumor by fractionated photosensitizer dosing photodynamic therapy. *Cancer Research*, 62(15), 4289–4294.
- Dolmans, D. E. J. G. J., Kadambi, A., Hill, J. S., Waters, C. A., Robinson, B. C., Walker, J. P., Fukumura, D., & Jain, R. K. (2002). Vascular accumulation of a novel photosensitizer, MV6401, causes selective thrombosis in tumor vessels after photodynamic therapy. *Cancer Research*, 62(7), 2151–2156.
- Dougherty, T. J., Gomer, C. J., Henderson, B. W., Jori, G., Kessel, D., Korblik, M., Moan, J., & Peng, Q. (1998). Photodynamic Therapy. *JNCI Journal of the*

*National Cancer Institute*, 90(12), 889–905.

<https://doi.org/10.1093/jnci/90.12.889>

Dougherty, T. J., Grindey, G. B., Fiel, R., Weishaupt, K. R., & Boyle, D. G. (1975). Photoradiation Therapy. II. Cure of Animal Tumors With Hematoporphyrin and Light. *JNCI: Journal of the National Cancer Institute*, 55(1), 115–121. <https://doi.org/10.1093/jnci/55.1.115>

Drucker, B. J. (2005). Renal cell carcinoma: Current status and future prospects. *Cancer Treatment Reviews*, 31(7), 536–545. <https://doi.org/10.1016/j.ctrv.2005.07.009>

Dummin, H., Cernay, Th., & Zimmermann, H. W. (1997). Selective photosensitization of mitochondria in HeLa cells by cationic Zn(II)phthalocyanines with lipophilic side-chains. *Journal of Photochemistry and Photobiology B: Biology*, 37(3), 219–229. [https://doi.org/10.1016/S1011-1344\(96\)07416-7](https://doi.org/10.1016/S1011-1344(96)07416-7)

Duska, L. R., Hamblin, M. R., Miller, J. L., & Hasan, T. (1999). Combination Photoimmunotherapy and Cisplatin: Effects on Human Ovarian Cancer Ex Vivo. *JNCI Journal of the National Cancer Institute*, 91(18), 1557–1563. <https://doi.org/10.1093/jnci/91.18.1557>

Figge, F. H. J., Weiland, G. S., & Manganiello, L. O. J. (1948). Cancer Detection and Therapy. Affinity of Neoplastic, Embryonic, and Traumatized Tissues for Porphyrins and Metalloporphyrins. *Experimental Biology and Medicine*, 68(3), 640–641. <https://doi.org/10.3181/00379727-68-16580>

Finsen, N. R. (1901). *Phototherapy*. London: Edward Arnold.

Fitzgerald, F. (Ed.). (2017). *Photodynamic Therapy (PDT): Principles, Mechanisms and Applications*. Nova Science Publishers, Inc.

Foote, C. S. (1968). Mechanisms of Photosensitized Oxidation. *Science*, 162(3857), 963–970. <https://doi.org/10.1126/science.162.3857.963>

- Gler, M. T., Skripconoka, V., Sanchez-Garavito, E., Xiao, H., Cabrera-Rivero, J. L., Vargas-Vasquez, D. E., Gao, M., Awad, M., Park, S.-K., Shim, T. S., Suh, G. Y., Danilovits, M., Ogata, H., Kurve, A., Chang, J., Suzuki, K., Tupasi, T., Koh, W.-J., Seaworth, B., ... Wells, C. D. (2012). Delamanid for Multidrug-Resistant Pulmonary Tuberculosis. *New England Journal of Medicine*, 366(23), 2151–2160. <https://doi.org/10.1056/NEJMoa1112433>
- Gollnick, S. O., & Brackett, C. M. (2010). Enhancement of anti-tumor immunity by photodynamic therapy. *Immunologic Research*, 46(1–3), 216–226. <https://doi.org/10.1007/s12026-009-8119-4>
- Gollnick, S. O., Evans, S. S., Baumann, H., Owczarczak, B., Maier, P., Vaughan, L., Wang, W. C., Unger, E., & Henderson, B. W. (2003). Role of cytokines in photodynamic therapy-induced local and systemic inflammation. *British Journal of Cancer*, 88(11), 1772–1779. <https://doi.org/10.1038/sj.bjc.6600864>
- Gollnick, S. O., Liu, X., Owczarczak, B., Musser, D. A., & Henderson, B. W. (1997). Altered expression of interleukin 6 and interleukin 10 as a result of photodynamic therapy in vivo. *Cancer Research*, 57(18), 3904–3909.
- Guliyev, R., Coskun, A., & Akkaya, E. U. (2009). Design Strategies for Ratiometric Chemosensors: Modulation of Excitation Energy Transfer at the Energy Donor Site. *Journal of the American Chemical Society*, 131(25), 9007–9013. <https://doi.org/10.1021/ja902584a>
- Gunaydin, G., Gedik, M. E., & Ayan, S. (2021a). Photodynamic Therapy—Current Limitations and Novel Approaches. *Frontiers in Chemistry*, 9. <https://doi.org/10.3389/fchem.2021.691697>
- Gunaydin, G., Gedik, M. E., & Ayan, S. (2021b). Photodynamic Therapy for the Treatment and Diagnosis of Cancer—A Review of the Current Clinical Status. *Frontiers in Chemistry*, 9. <https://doi.org/10.3389/fchem.2021.686303>
- Hamblin, M. R., & Huang, Y. (Eds.). (2017). *Imaging in Photodynamic Therapy*. Taylor & Francis Group: Boca Raton.

- Hammerer, F., Poyer, F., Fourmois, L., Chen, S., Garcia, G., Teulade-Fichou, M.-P., Maillard, P., & Mahuteau-Betzer, F. (2018). Mitochondria-targeted cationic porphyrin-triphenylamine hybrids for enhanced two-photon photodynamic therapy. *Bioorganic & Medicinal Chemistry*, 26(1), 107–118. <https://doi.org/10.1016/j.bmc.2017.11.024>
- Hausmann, W. (1911). Die sensibilisierende Wirkung des Hematoporphyrins. *Biochem. Zeitung*, 30, 276–316.
- Henderson, B. W., & Dougherty, T. J. (1992). How does Photodynamic Therapy work? *Photochemistry and Photobiology*, 55(1), 145–157. <https://doi.org/10.1111/j.1751-1097.1992.tb04222.x>
- Hinkeldey, B., Schmitt, A., & Jung, G. (2008). Comparative Photostability Studies of BODIPY and Fluorescein Dyes by Using Fluorescence Correlation Spectroscopy. *ChemPhysChem*, 9(14), 2019–2027. <https://doi.org/10.1002/cphc.200800299>
- Hoppe-Seyler, F. (1871). Med. Chem. Untersuchungen. *Eberhard-Karls-Universität, Berlin*.
- Houze, J. B., Zhu, L., Sun, Y., Akerman, M., Qiu, W., Zhang, A. J., Sharma, R., Schmitt, M., Wang, Y., Liu, J., Liu, J., Medina, J. C., Reagan, J. D., Luo, J., Tonn, G., Zhang, J., Lu, J. Y.-L., Chen, M., Lopez, E., ... Lin, D. C.-H. (2012). AMG 837: A potent, orally bioavailable GPR40 agonist. *Bioorganic & Medicinal Chemistry Letters*, 22(2), 1267–1270. <https://doi.org/10.1016/j.bmcl.2011.10.118>
- The Chemogenesis Web Book - Collecting It All Together: The Five Reaction Chemistries [https://www.meta-synthesis.com/webbook/11\\_five/five.php](https://www.meta-synthesis.com/webbook/11_five/five.php). (n.d.).
- Huang, Z., Xu, H., Meyers, A. D., Musani, A. I., Wang, L., Tagg, R., Barqawi, A. B., & Chen, Y. K. (2008). Photodynamic Therapy for Treatment of Solid Tumors — Potential and Technical Challenges. *Technology in Cancer*

- Research & Treatment*, 7(4), 309–320.  
<https://doi.org/10.1177/153303460800700405>
- Igney, F. H., & Krammer, P. H. (2002). Death and anti-death: tumour resistance to apoptosis. *Nature Reviews Cancer*, 2(4), 277–288.  
<https://doi.org/10.1038/nrc776>
- Josefsen, L. B., & Boyle, R. W. (2008). Photodynamic therapy: novel third-generation photosensitizers one step closer? *British Journal of Pharmacology*, 154(1), 1–3. <https://doi.org/10.1038/bjp.2008.98>
- Jovanović, S., Marković, Z., & Todorović Marković, B. (2017). Carbon-Based Nanomaterials as agents for Photodynamic Therapy. In F. Fitzgerald (Ed.), *Photodynamic Therapy: Principles, Mechanisms and Applications*. Nova Biomedical.
- Juarranz, Á., Jaén, P., Sanz-Rodríguez, F., Cuevas, J., & González, S. (2008). Photodynamic therapy of cancer. Basic principles and applications. *Clinical and Translational Oncology*, 10(3), 148–154. <https://doi.org/10.1007/s12094-008-0172-2>
- Juzeniene, A., & Moan, J. (2007). The history of PDT in Norway. *Photodiagnosis and Photodynamic Therapy*, 4(1), 3–11.  
<https://doi.org/10.1016/j.pdpdt.2006.11.002>
- Kabingu, E., Vaughan, L., Owczarczak, B., Ramsey, K. D., & Gollnick, S. O. (2007). CD8+ T cell-mediated control of distant tumours following local photodynamic therapy is independent of CD4+ T cells and dependent on natural killer cells. *British Journal of Cancer*, 96(12), 1839–1848.  
<https://doi.org/10.1038/sj.bjc.6603792>
- Kalyanasundaram, K. (1992). *Photochemistry of polypyridine and porphyrin complexes*. London; San Diego : Academic Press



- Kamkaew, A., Lim, S. H., Lee, H. B., Kiew, L. V., Chung, L. Y., & Burgess, K. (2013). BODIPY dyes in photodynamic therapy. *Chem. Soc. Rev.*, *42*(1), 77–88. <https://doi.org/10.1039/C2CS35216H>
- Karaman, O., Almammadov, T., Emre Gedik, M., Gunaydin, G., Kolemen, S., & Gunbas, G. (2019). Mitochondria-Targeting Selenophene-Modified BODIPY-Based Photosensitizers for the Treatment of Hypoxic Cancer Cells. *ChemMedChem*, *14*(22). <https://doi.org/10.1002/cmdc.201900380>
- Kelly, J. F., & Snell, M. E. (1976). Hematoporphyrin Derivative: A Possible Aid in the Diagnosis and Therapy of Carcinoma of the Bladder. *Journal of Urology*, *115*(2), 150–151. [https://doi.org/10.1016/S0022-5347\(17\)59108-9](https://doi.org/10.1016/S0022-5347(17)59108-9)
- Kelly, J. F., Snell, M. E., & Berenbaum, M. C. (1975). Photodynamic destruction of human bladder carcinoma. *British Journal of Cancer*, *31*(2), 237–244. <https://doi.org/10.1038/bjc.1975.30>
- Kennedy, J. C., Pottier, R. H., & Pross, D. C. (1990). Photodynamic therapy with endogenous protoporphyrin. *Journal of Photochemistry and Photobiology B: Biology*, *6*(1–2), 143–148. [https://doi.org/10.1016/1011-1344\(90\)85083-9](https://doi.org/10.1016/1011-1344(90)85083-9)
- Kessel, D., Luo, Y., Deng, Y., & Chang, C. K. (1997). The Role of Subcellular Localization in Initiation of Apoptosis by Photodynamic Therapy. *Photochemistry and Photobiology*, *65*(3), 422–426. <https://doi.org/10.1111/j.1751-1097.1997.tb08581.x>
- Kessel, D., & Oleinick, N. L. (2009). *Chapter 1 Initiation of Autophagy by Photodynamic Therapy* (pp. 1–16). [https://doi.org/10.1016/S0076-6879\(08\)04001-9](https://doi.org/10.1016/S0076-6879(08)04001-9)
- Kessel, D., & Reiners, J. J. (2007). Apoptosis and Autophagy After Mitochondrial or Endoplasmic Reticulum Photodamage. *Photochemistry and Photobiology*, *83*(5), 1024–1028. <https://doi.org/10.1111/j.1751-1097.2007.00088.x>

- Kessel, D., Vicente, M. G. H., & Reiners, J. J. (2006). Initiation of apoptosis and autophagy by photodynamic therapy. *Lasers in Surgery and Medicine*, 38(5), 482–488. <https://doi.org/10.1002/lsm.20334>
- Kim, M. M., & Darafsheh, A. (2020). Light Sources and Dosimetry Techniques for Photodynamic Therapy. *Photochemistry and Photobiology*, 96(2), 280–294. <https://doi.org/10.1111/php.13219>
- Kim, S.-J., Vassão, D. G., Moinuddin, S. G. A., Bedgar, D. L., Davin, L. B., & Lewis, N. G. (2014). Allyl/propenyl phenol synthases from the creosote bush and engineering production of specialty/commodity chemicals, eugenol/isoeugenol, in *Escherichia coli*. *Archives of Biochemistry and Biophysics*, 541, 37–46. <https://doi.org/10.1016/j.abb.2013.10.019>
- Klonisch, T., Wiehac, E., Hombach-Klonisch, S., Ande, S. R., Wesselborg, S., Schulze-Osthoff, K., & Los, M. (2008). Cancer stem cell markers in common cancers – therapeutic implications. *Trends in Molecular Medicine*, 14(10), 450–460. <https://doi.org/10.1016/j.molmed.2008.08.003>
- Konan, Y. N., Gurny, R., & Allemann, E. (2002). State of the art in the delivery of photosensitizers for photodynamic therapy. *Journal of Photochemistry and Photobiology B: Biology*, 66(2), 89–106. [https://doi.org/10.1016/S1011-1344\(01\)00267-6](https://doi.org/10.1016/S1011-1344(01)00267-6)
- Korbelik, M. (2010). *Photodynamic Therapy-Generated Cancer Vaccines* (pp. 147–153). [https://doi.org/10.1007/978-1-60761-697-9\\_11](https://doi.org/10.1007/978-1-60761-697-9_11)
- Kübler, A. C. (2005). Photodynamic therapy. *Medical Laser Application*, 20(1), 37–45. <https://doi.org/10.1016/j.mla.2005.02.001>
- Kwiatkowski, S., Knap, B., Przystupski, D., Saczko, J., Kędzierska, E., Knap-Czop, K., Kotlińska, J., Michel, O., Kotowski, K., & Kulbacka, J. (2018). Photodynamic therapy – mechanisms, photosensitizers and combinations. *Biomedicine & Pharmacotherapy*, 106, 1098–1107. <https://doi.org/10.1016/j.biopha.2018.07.049>

- Lacour, J.-P., Ulrich, C., Gilaberte, Y., von Felbert, V., Basset-Seguin, N., Dreno, B., Girard, C., Redondo, P., Serra-Guillen, C., Synnerstad, I., Tarstedt, M., Tsianakas, A., Venema, A. W., Kelleners-Smeets, N., Adamski, H., Perez-Garcia, B., Gerritsen, M. J., Leclerc, S., Kerrouche, N., & Szeimies, R.-M. (2015). Daylight photodynamic therapy with methyl aminolevulinate cream is effective and nearly painless in treating actinic keratoses: a randomised, investigator-blinded, controlled, phase III study throughout Europe. *Journal of the European Academy of Dermatology and Venereology*, *29*(12), 2342–2348. <https://doi.org/10.1111/jdv.13228>
- Lavie, G., Kaplinsky, C., Toren, A., Aizman, I., Meruelo, D., Mazur, Y., & Mandel, M. (1999). A photodynamic pathway to apoptosis and necrosis induced by dimethyl tetrahydroxyhelianthone and hypericin in leukaemic cells: possible relevance to photodynamic therapy. *British Journal of Cancer*, *79*(3–4), 423–432. <https://doi.org/10.1038/sj.bjc.6690066>
- Lee, C. N., Hsu, R., Chen, H., & Wong, T. W. (2020). Daylight Photodynamic Therapy: An Update. *Molecules*, *25*(21), 5195. <https://doi.org/10.3390/molecules25215195>
- Lee, H. Y., Bae, D. R., Park, J. C., Song, H., Han, W. S., & Jung, J. H. (2009). A Selective Fluoroionophore Based on BODIPY-functionalized Magnetic Silica Nanoparticles: Removal of Pb<sup>2+</sup> from Human Blood. *Angewandte Chemie International Edition*, *48*(7), 1239–1243. <https://doi.org/10.1002/anie.200804714>
- Levine, B., & Klionsky, D. J. (2004). Development by Self-Digestion. *Developmental Cell*, *6*(4), 463–477. [https://doi.org/10.1016/S1534-5807\(04\)00099-1](https://doi.org/10.1016/S1534-5807(04)00099-1)
- Lipson, R. L., & Baldes, E. J. (1960). The Photodynamic Properties of a Particular Hematoporphyrin Derivative. *Archives of Dermatology*, *82*(4), 508. <https://doi.org/10.1001/archderm.1960.01580040026005>

- Lipson, R. L., Baldes, E. J., & Olsen, A. M. (1961a). The use of a derivative of hematoporphyrin in tumor detection. *Journal of the National Cancer Institute*, 26, 1–11.
- Lipson, R. L., Baldes, E. J., & Olsen, A. M. (1961b). Hematoporphyrin derivative: a new aid for endoscopic detection of malignant disease. *The Journal of Thoracic and Cardiovascular Surgery*, 42, 623–629.
- Loudet, A., & Burgess, K. (2007). BODIPY Dyes and Their Derivatives: Syntheses and Spectroscopic Properties. *Chemical Reviews*, 107(11), 4891–4932. <https://doi.org/10.1021/cr078381n>
- Luksiene, Z. (2003). Photodynamic therapy: mechanism of action and ways to improve the efficiency of treatment. *Medicina (Kaunas, Lithuania)*, 39(12), 1137–1150.
- Luo, G. G., Fang, K., Wu, J. H., Dai, J. C., & Zhao, Q. H. (2014). Noble-metal-free BODIPY–cobaloxime photocatalysts for visible-light-driven hydrogen production. *Phys. Chem. Chem. Phys.*, 16(43), 23884–23894. <https://doi.org/10.1039/C4CP03343D>
- Luo, Y., & Kessel, D. (1997). Initiation of Apoptosis versus Necrosis by Photodynamic Therapy with Chloroaluminum Phthalocyanine. *Photochemistry and Photobiology*, 66(4), 479–483. <https://doi.org/10.1111/j.1751-1097.1997.tb03176.x>
- Meyer–Betz, F. (1913). Untersuchungen über die biologische photodynamische Wirkung des Hematoporphyrins und anderer Derivative des Blut und Galenafarbstoffs. *Dtsch. Arch. Klin.*, 112, 476–503.
- Moan, J., & Berg, K. (1991). The Photodegradation of Porphyrins in cells can be used to estimate the lifetime of singlet oxygen. *Photochemistry and Photobiology*, 53(4), 549–553. <https://doi.org/10.1111/j.1751-1097.1991.tb03669.x>

- Moan, J., & Berg, K. (1992). Photochemotherapy of Cancer: Experimental Research *Photochemistry and Photobiology*, 55(6), 931–948.  
<https://doi.org/10.1111/j.1751-1097.1992.tb08541.x>
- Moan, J., & Wold, E. (1979). Detection of singlet oxygen production by ESR. *Nature*, 279(5712), 450–451. <https://doi.org/10.1038/279450a0>
- Moriwaki, K., Sawada, T., Akiyama, M., Ikeda, A., Kikuchi, J., Matsumura, T., Yano, S., Kataoka, H., Inoue, M., & Akashi, H. (2018). Synthesis and Photophysical Properties of *S*-Mannosylated Chlorins and Their Effect on Photocytotoxicity in HeLa Cells. *Bulletin of the Chemical Society of Japan*, 91(2), 230–236. <https://doi.org/10.1246/bcsj.20170271>
- Morton, C. (2002). The emerging role of 5-ALA-PDT in dermatology: is PDT superior to standard treatments? *Journal of Dermatological Treatment*, 13(sup1), s25–s29. <https://doi.org/10.1080/095466302317414672>
- Morton, C. A., McKenna, K. E., & Rhodes, L. E. (2008). Guidelines for topical photodynamic therapy: update. *British Journal of Dermatology*, 159(6), 1245–1266. <https://doi.org/10.1111/j.1365-2133.2008.08882.x>
- Mroz, P., Szokalska, A., Wu, M. X., & Hamblin, M. R. (2010). Photodynamic Therapy of Tumors Can Lead to Development of Systemic Antigen-Specific Immune Response. *PLoS ONE*, 5(12), e15194.  
<https://doi.org/10.1371/journal.pone.0015194>
- Nagata, S., Obana, A., Gohto, Y., & Nakajima, S. (2003). Necrotic and apoptotic cell death of human malignant melanoma cells following photodynamic therapy using an amphiphilic photosensitizer, ATX-S10(Na). *Lasers in Surgery and Medicine*, 33(1), 64–70. <https://doi.org/10.1002/lsm.10190>
- Nelius, T., de Riese, W. T. W., & Filleur, S. (2004). *Photodynamic therapy: a promising alternative in oncology* (K. E. Bartels, L. S. Bass, W. T. W. de Riese, K. W. Gregory, H. Hirschberg, A. Katzir, N. Kollias, S. J. Madsen, R. S. Malek, K. M. McNally-Heintzelman, K. D. Paulsen, D. S. Robinson, L. P.

- Tate, Jr., E. A. Trowers, & B. J. Wong, Eds.; p. 234).  
<https://doi.org/10.1117/12.530311>
- Nowak-Stepniowska, A., Pergoń, P., & Padzik-Graczyk, A. (2013). Photodynamic method of cancer diagnosis and therapy--mechanisms and applications. *Postepy Biochemii*, 59(1), 53–63. PMID:23821943
- Ochsner, M. (1997). Photophysical and photobiological processes in the photodynamic therapy of tumours. *Journal of Photochemistry and Photobiology B: Biology*, 39(1), 1–18. [https://doi.org/10.1016/S1011-1344\(96\)07428-3](https://doi.org/10.1016/S1011-1344(96)07428-3)
- O'Connor, A. E., Gallagher, W. M., & Byrne, A. T. (2009). Porphyrin and Nonporphyrin Photosensitizers in Oncology: Preclinical and Clinical Advances in Photodynamic Therapy. *Photochemistry and Photobiology*, 85(5), 1053–1074. <https://doi.org/10.1111/j.1751-1097.2009.00585.x>
- Ormond, A., & Freeman, H. (2013). Dye Sensitizers for Photodynamic Therapy. *Materials*, 6(3), 817–840. <https://doi.org/10.3390/ma6030817>
- Panduwawala, T. D., Iqbal, S., Thompson, A. L., Genov, M., Pretsch, A., Pretsch, D., Liu, S., Ebright, R. H., Howells, A., Maxwell, A., & Moloney, M. G. (2019). Functionalised bicyclic tetramates derived from cysteine as antibacterial agents. *Organic & Biomolecular Chemistry*, 17(22), 5615–5632. <https://doi.org/10.1039/C9OB01076A>
- Pavani, C., Uchoa, A. F., Oliveira, C. S., Yamamoto, Y., & Baptista, M. S. (2009). Effect of zinc insertion and hydrophobicity on the membrane interactions and PDT activity of porphyrin photosensitizers. *Photochem. Photobiol. Sci.*, 8(2), 233–240. <https://doi.org/10.1039/B810313E>
- Peng, Q., Moan, J., & Nesland, J. M. (1996). Correlation of Subcellular and Intratumoral Photosensitizer Localization with Ultrastructural Features After Photodynamic Therapy. *Ultrastructural Pathology*, 20(2), 109–129. <https://doi.org/10.3109/01913129609016306>

- Policard, A. (1924). Etude sur les aspects offerts par des tumeurs experimentales examinées a la lumière de wood. *C. R. Soc. Biol*, 91, 1423–1428.
- Prime, J. (1900). Les accidentes toxiques par l'eosinate de sodium. (*Jouve & Boyer, Ed.*), Paris.
- Qi, X., Kim, S. K., Han, S. J., Xu, L., Jee, A. Y., Kim, H. N., Lee, C., Kim, Y., Lee, M., Kim, S.-J., & Yoon, J. (2008). New BODIPY–triazine based tripod fluorescent systems. *Tetrahedron Letters*, 49(2), 261–264.  
<https://doi.org/10.1016/j.tetlet.2007.11.063>
- Raab, O. (1900). Uber die Wirkung fluoreszierender Stoffe auf Infusorien. *Zeitung Biol.*, 39, 524–526.
- Rancan, F., Wiehe, A., Nöbel, M., Senge, M. O., Omari, S. al, Böhm, F., John, M., & Röder, B. (2005). Influence of substitutions on asymmetric dihydroxychlorins with regard to intracellular uptake, subcellular localization and photosensitization of Jurkat cells. *Journal of Photochemistry and Photobiology B: Biology*, 78(1), 17–28.  
<https://doi.org/10.1016/j.jphotobiol.2004.08.010>
- Rihn, S., Retailleau, P., de Nicola, A., Ulrich, G., & Ziessel, R. (2012). Synthetic Routes to Fluorescent Dyes Exhibiting Large Stokes Shifts. *The Journal of Organic Chemistry*, 77(20), 8851–8863. <https://doi.org/10.1021/jo301059u>
- Robertson, C. A., Evans, D. H., & Abrahamse, H. (2009). Photodynamic therapy (PDT): A short review on cellular mechanisms and cancer research applications for PDT. *Journal of Photochemistry and Photobiology B: Biology*, 96(1), 1–8. <https://doi.org/10.1016/j.jphotobiol.2009.04.001>
- Rocha, L. G. B. (2015). *Development of a Novel Photosensitizer for Photodynamic Therapy of Cancer*. [Ph.D. Thesis]. University of Coimbra.

- Rother, K. I., & Harlan, D. M. (2004). Challenges facing islet transplantation for the treatment of type 1 diabetes mellitus. *Journal of Clinical Investigation*, *114*(7), 877–883. <https://doi.org/10.1172/JCI23235>
- Ruoslahti, E. (2002). Specialization of tumour vasculature. *Nature Reviews Cancer*, *2*(2), 83–90. <https://doi.org/10.1038/nrc724>
- Rurack, K., Kollmannsberger, M., & Daub, J. (2001). A highly efficient sensor molecule emitting in the near infrared (NIR): 3,5-distyryl-8-(p-dimethylaminophenyl)difluoroboradiaza-s-indacene. *New Journal of Chemistry*, *25*(2), 289–292. <https://doi.org/10.1039/b007379m>
- Sakamoto, K., Kato, T., Kawaguchi, T., Ohno-Okumura, E., Urano, T., Yamaoka, T., Suzuki, S., & Cook, M. J. (2002). Photosensitizer efficacy of non-peripheral substituted alkylbenzopyridoporphyrazines for photodynamic therapy of cancer. *Journal of Photochemistry and Photobiology A: Chemistry*, *153*(1–3), 245–253. [https://doi.org/10.1016/S1010-6030\(02\)00292-7](https://doi.org/10.1016/S1010-6030(02)00292-7)
- Saleh, B. E. A., & Teich, M. C. (Eds.). (2007). *Fundamentals of Photonics, 2nd edn*. John Wiley & Sons.
- Scherer, H. (1841). Chemisch-physiologische untersuchungen. *Ann. Chem. Pharm.*, *40*, 1.
- Schwartz, S., Absolon, K., & Vermund, H. (1955). Some relationships of porphyrins, X-rays and tumors. *Univ. Minn. Med. Bull*, *27*, 7–8.
- Simões, J. C. S., Sarpaki, S., Papadimitroulas, P., Therrien, B., & Loudos, G. (2020). Conjugated Photosensitizers for Imaging and PDT in Cancer Research. *Journal of Medicinal Chemistry*, *63*(23), 14119–14150. <https://doi.org/10.1021/acs.jmedchem.0c00047>
- Sola-Llano, R., & Bañuelos, J. (2019). Introductory Chapter: BODIPY Dye, an All-in-One Molecular Scaffold for (Bio)Photonics. In *BODIPY Dyes - A*



*Privilege Molecular Scaffold with Tunable Properties*. IntechOpen.

<https://doi.org/10.5772/intechopen.82682>

st. Amant, A. H., Frazier, C. P., Newmeyer, B., Fruehauf, K. R., & Read de Alaniz, J. (2016). Direct synthesis of anilines and nitrosobenzenes from phenols.

*Organic & Biomolecular Chemistry*, 14(24), 5520–5524.

<https://doi.org/10.1039/C6OB00073H>

Stone, M. J., Aronoff, B. E., Evans, W. P., Fay, J. W., Lieberman, Z. H., Matthews, C. M., Race, G. J., Scruggs, R. P., & Stringer, C. A. (2003). History of the Baylor Charles A. Sammons Cancer Center. *Baylor University Medical Center Proceedings*, 16(1), 30–58.

<https://doi.org/10.1080/08998280.2003.11927886>

Thudichum, J. L. (1867). Tenth Report of the Medical Officer of the Privy Council. *H. M. Stationary Office, London*.

Tong, R., & Kohane, D. S. (2012). Shedding light on nanomedicine. *Wiley Interdisciplinary Reviews: Nanomedicine and Nanobiotechnology*, 4(6), 638–662. <https://doi.org/10.1002/wnan.1188>

Triesscheijn, M., Baas, P., Schellens, J. H. M., & Stewart, F. A. (2006). Photodynamic Therapy in Oncology. *The Oncologist*, 11(9), 1034–1044. <https://doi.org/10.1634/theoncologist.11-9-1034>

Tromberg, B. J., Orenstein, A., Kimel, S., Barker, S. J., Hyatt, J., Nelson, J. S., & Berns, M. W. (1990). In vivo tumor oxygen tension measurements for the evaluation of the efficiency of Photodynamic Therapy. *Photochemistry and Photobiology*, 52(2), 375–385. <https://doi.org/10.1111/j.1751-1097.1990.tb04193.x>

van Straten, D., Mashayekhi, V., de Bruijn, H., Oliveira, S., & Robinson, D. (2017). Oncologic Photodynamic Therapy: Basic Principles, Current Clinical Status and Future Directions. *Cancers*, 9(12), 19. <https://doi.org/10.3390/cancers9020019>

- Vaupel, P., Thews, O., & Hoekel, M. (2001). Treatment Resistance of Solid Tumors. *Medical Oncology*, 18(4), 243–260.  
<https://doi.org/10.1385/MO:18:4:243>
- von Tappeiner, H. (1900). Über die Wirkung fluoreszierender Stoffe auf Infusorien nach Versuchen von O. Raab. *Münchener Medizinische Wochenschrift*, 47, 5.
- von Tappeiner, H., & Jesionek, A. (1903). Herapeutische versuche mit fluoreszierenden stoffen. *Munch Med Wochenschr.*, 47, 2042–2044.
- von Tappeiner, H., & Jodlbauer, A. (1907). Die sensibilisierende Wirkung fluorescierender Substanzen : Gesammelte Untersuchungen über die photodynamische Erscheinung. *FCW Vogel, Leipzig*.
- Wallace, D. C. (2012). Mitochondria and cancer. *Nature Reviews Cancer*, 12(10), 685–698. <https://doi.org/10.1038/nrc3365>
- Wang, X., Peralta, S., & Moraes, C. T. (2013). Mitochondrial Alterations During Carcinogenesis: A Review of Metabolic Transformation and Targets for Anticancer Treatments. *Advances in Cancer Research*, Volume 119 (pp. 127–160). <https://doi.org/10.1016/B978-0-12-407190-2.00004-6>
- Weishaupt, K. R., Gomer, C. J., & Dougherty, T. J. (1976). Identification of singlet oxygen as the cytotoxic agent in photoinactivation of a murine tumor. *Cancer Research*, 36(7 PT 1), 2326–2329.
- Woodburn, K. W., Vardaxis, N. J., Hill, J. S., Kaye, A. H., & Phillips, D. R. (1991). Subcellular localization of porphyrins using confocal laser scanning microscopy *Photochemistry and Photobiology*, 54(5), 725–732.  
<https://doi.org/10.1111/j.1751-1097.1991.tb02081.x>
- Woodhams, J. H., MacRobert, A. J., & Bown, S. G. (2007). The role of oxygen monitoring during photodynamic therapy and its potential for treatment dosimetry. *Photochemical & Photobiological Sciences*, 6(12), 1246.  
<https://doi.org/10.1039/b709644e>

- Xue, L., Chiu, S., Azizuddin, K., Joseph, S., & Oleinick, N. L. (2007). The Death of Human Cancer Cells Following Photodynamic Therapy: Apoptosis Competence is Necessary for Bcl-2 Protection but not for Induction of Autophagy. *Photochemistry and Photobiology*, *83*(5), 1016–1023. <https://doi.org/10.1111/j.1751-1097.2007.00159.x>
- Yanovsky, R. L., Bartenstein, D. W., Rogers, G. S., Isakoff, S. J., & Chen, S. T. (2019). Photodynamic therapy for solid tumors: A review of the literature. *Photodermatology, Photoimmunology & Photomedicine*, *35*(5), 295–303. <https://doi.org/10.1111/phpp.12489>
- Yogo, T., Urano, Y., Ishitsuka, Y., Maniwa, F., & Nagano, T. (2005). Highly Efficient and Photostable Photosensitizer Based on BODIPY Chromophore. *Journal of the American Chemical Society*, *127*(35), 12162–12163. <https://doi.org/10.1021/ja0528533>
- Yoon, I., Li, J. Z., & Shim, Y. K. (2013). Advance in Photosensitizers and Light Delivery for Photodynamic Therapy. *Clinical Endoscopy*, *46*(1), 7. <https://doi.org/10.5946/ce.2013.46.1.7>
- Yu, F., Han, X., & Chen, L. (2014). Fluorescent probes for hydrogen sulfide detection and bioimaging. *Chem. Commun.*, *50*(82), 12234–12249. <https://doi.org/10.1039/C4CC03312D>
- Zhang, J., Jiang, C., Figueiró Longo, J. P., Azevedo, R. B., Zhang, H., & Muehlmann, L. A. (2018). An updated overview on the development of new photosensitizers for anticancer photodynamic therapy. *Acta Pharmaceutica Sinica B*, *8*(2), 137–146. <https://doi.org/10.1016/j.apsb.2017.09.003>

## APPENDICES

## **A. NMR Spectra**

### **A.1 Compounds Towards Synthesis of S-BODMe**

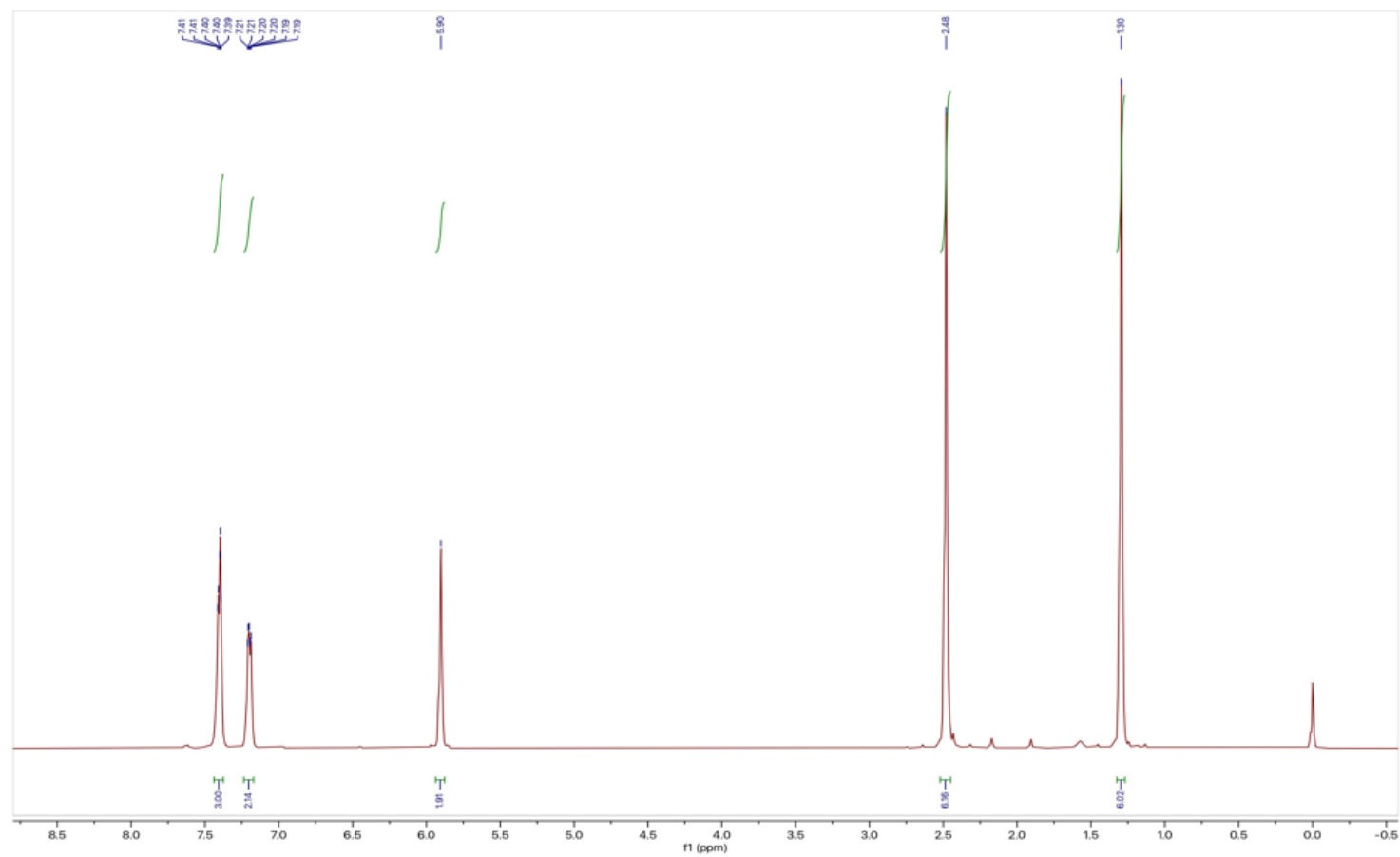
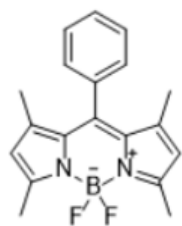


Figure A.1.  $^1\text{H}$  NMR spectrum of compound 1 in  $\text{CDCl}_3$

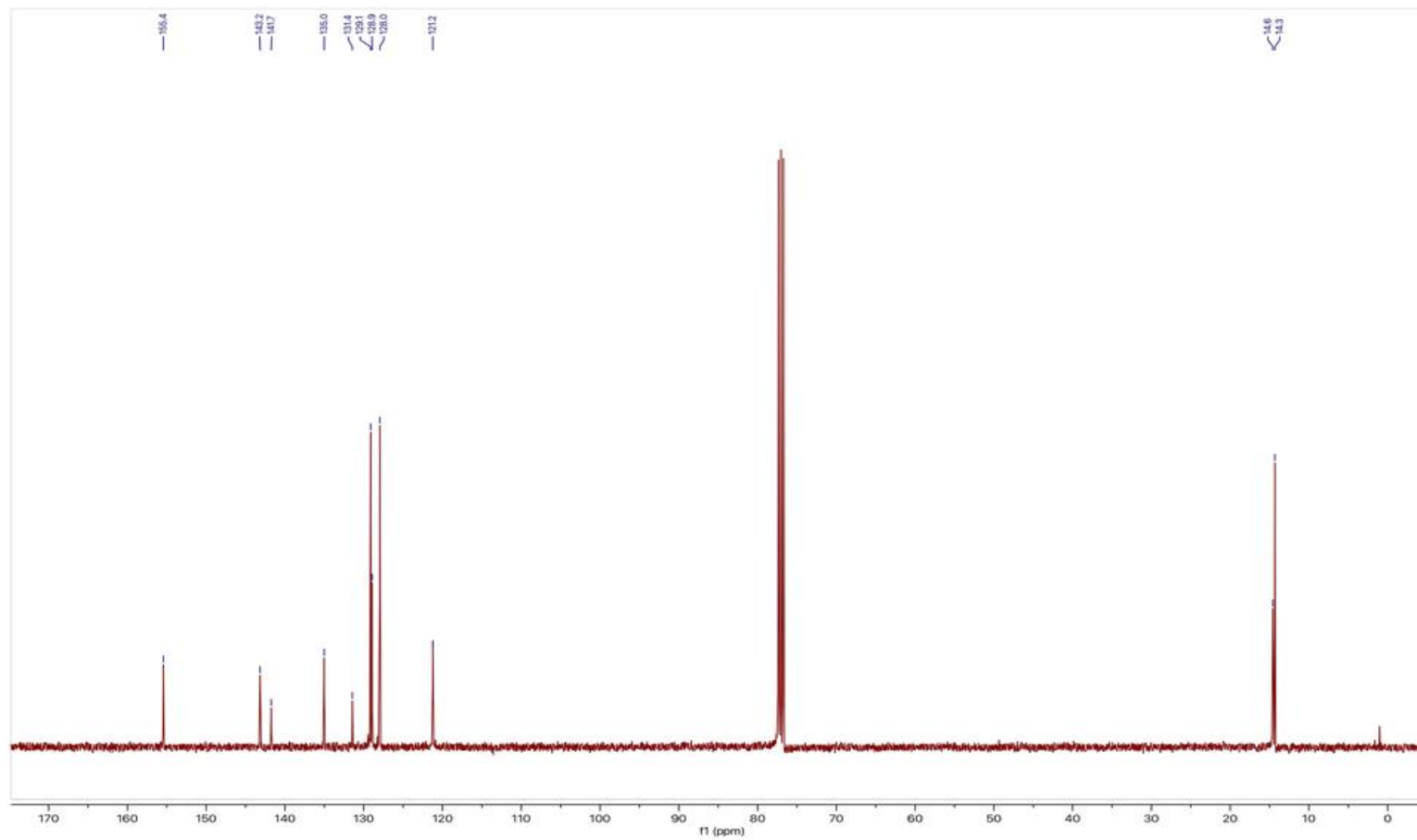
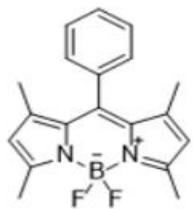
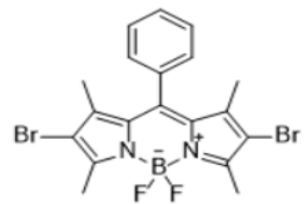


Figure A.2.  $^{13}\text{C}$  NMR spectrum of compound 1 in  $\text{CDCl}_3$



96

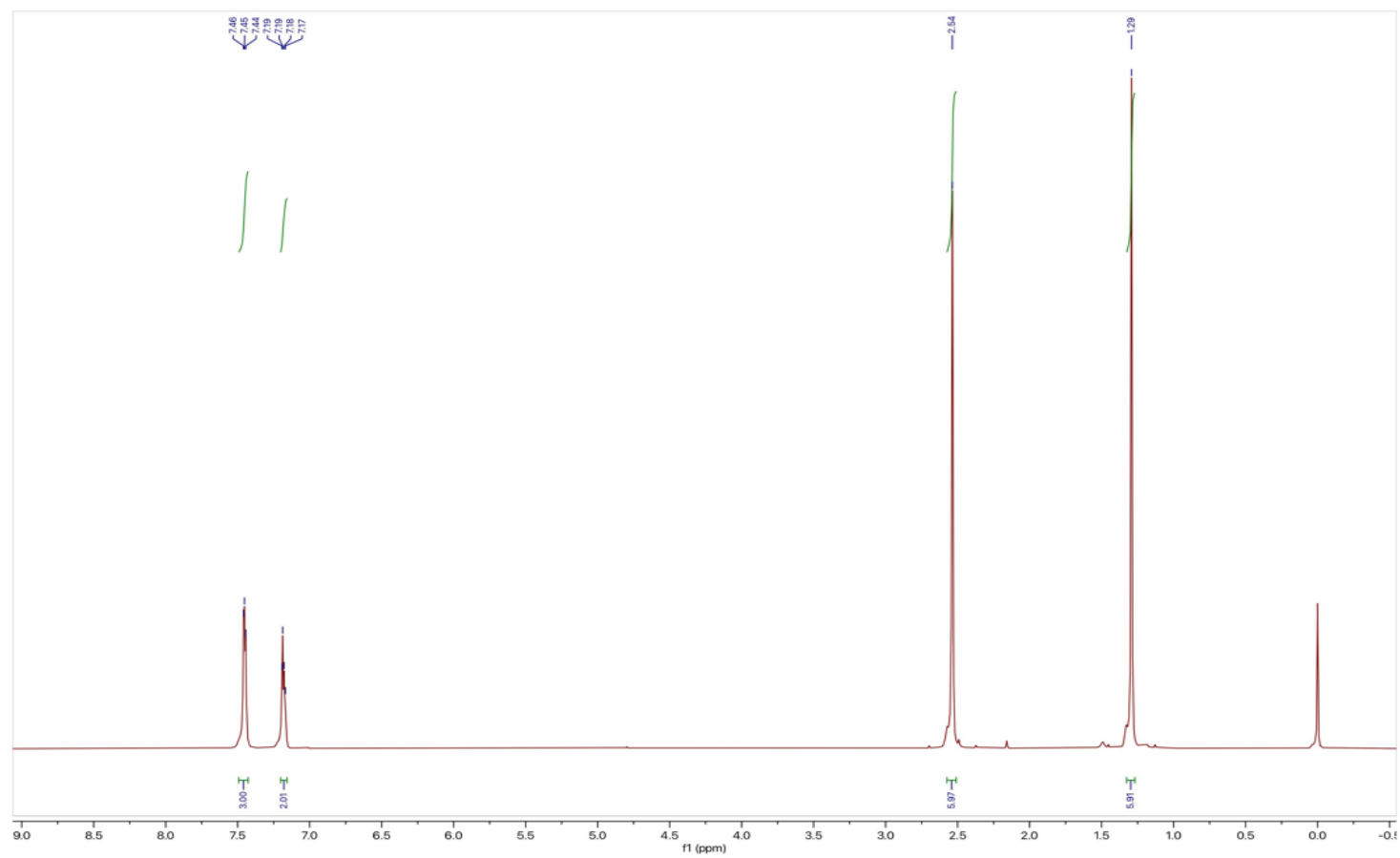


Figure A.3.  $^1\text{H}$  NMR spectrum of compound 2 in  $\text{CDCl}_3$



L6

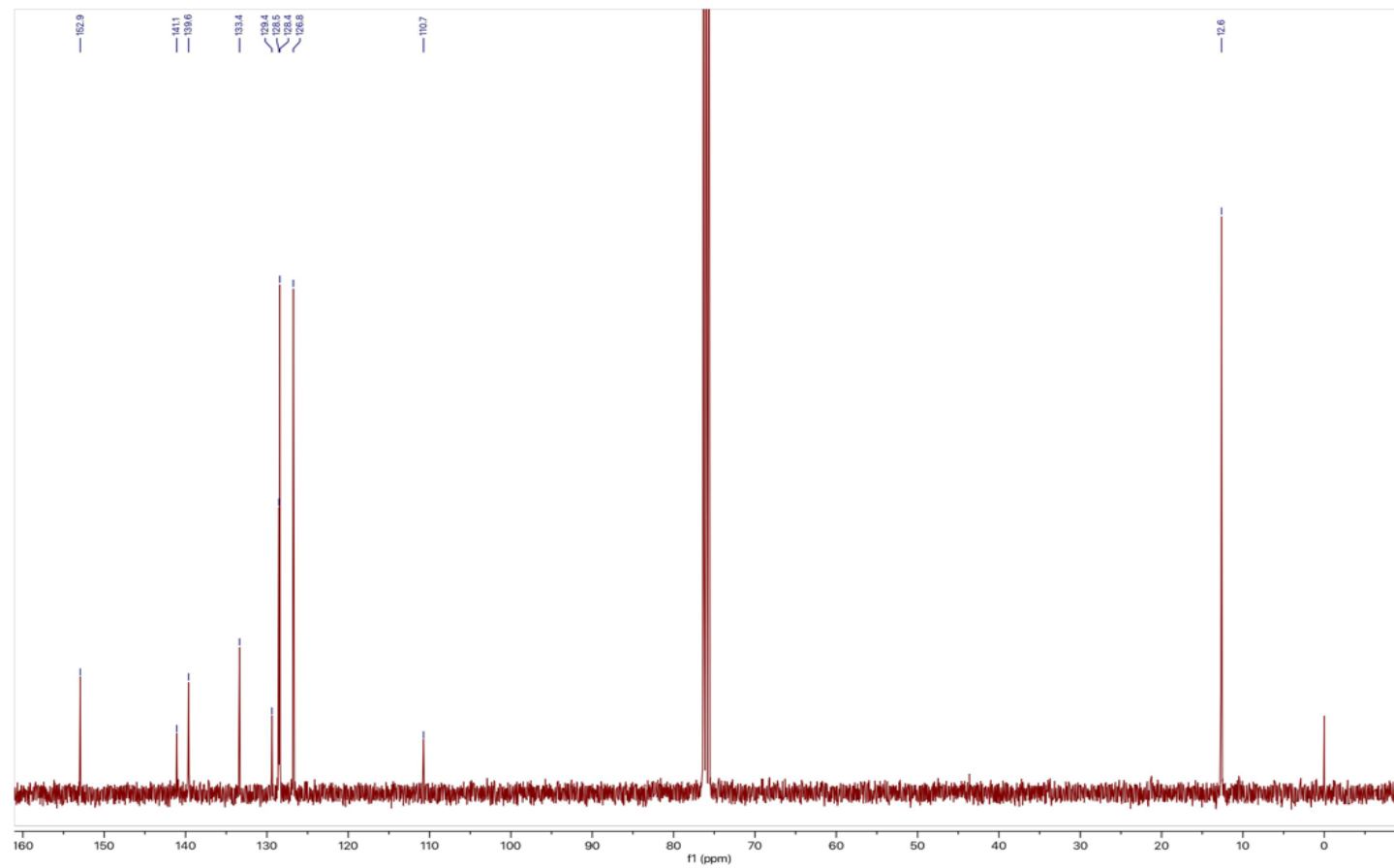
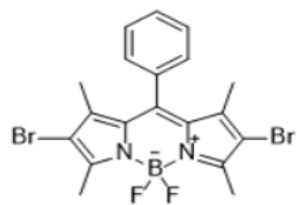


Figure A.4.  $^{13}\text{C}$  NMR spectrum of compound 2 in  $\text{CDCl}_3$

86

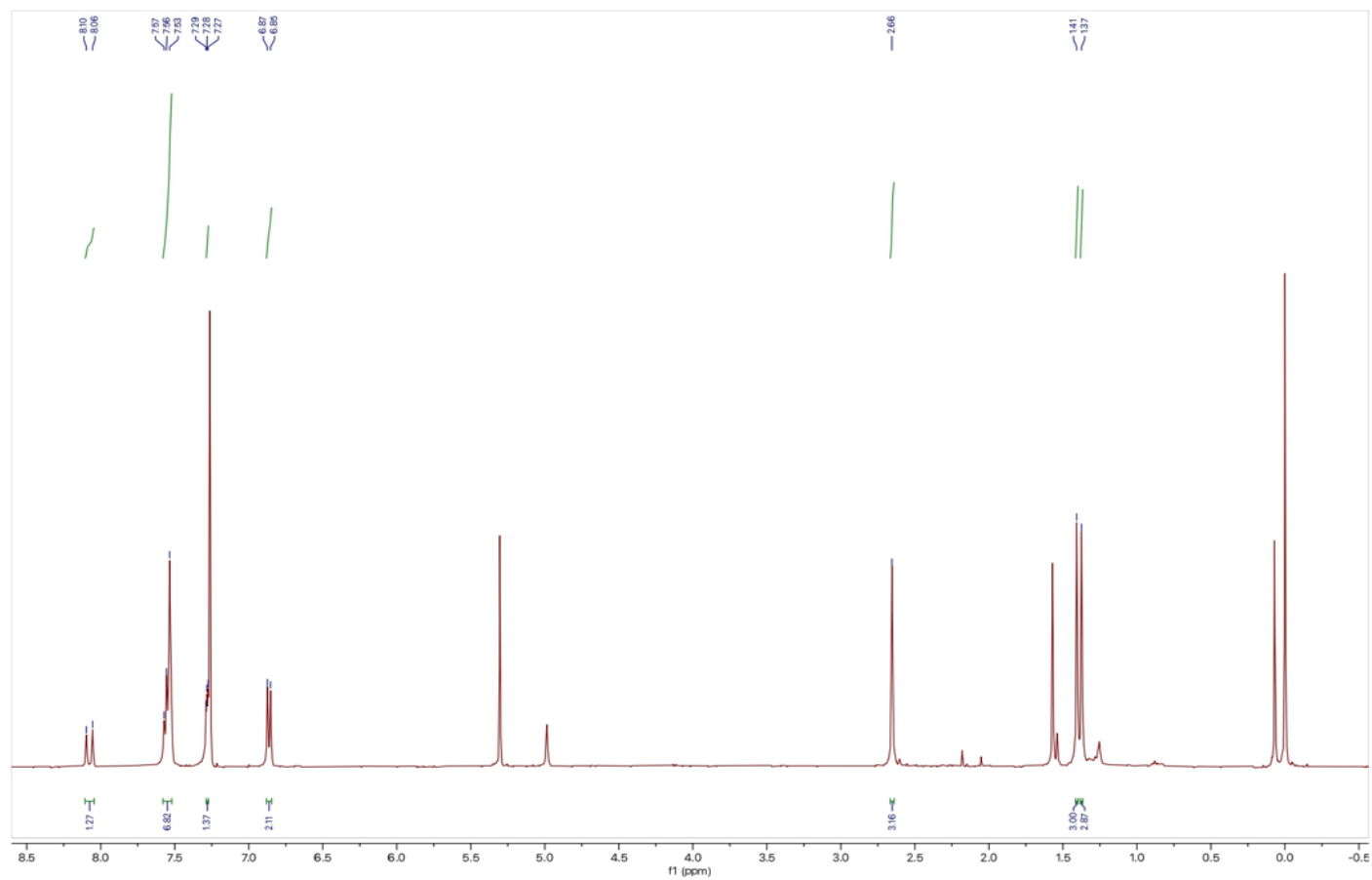
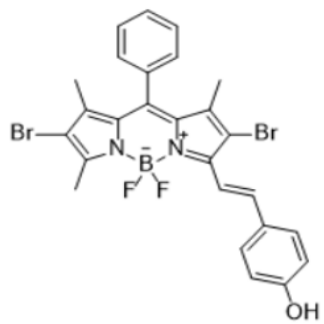


Figure A.5. <sup>1</sup>H NMR spectrum of compound 4 in CDCl<sub>3</sub>

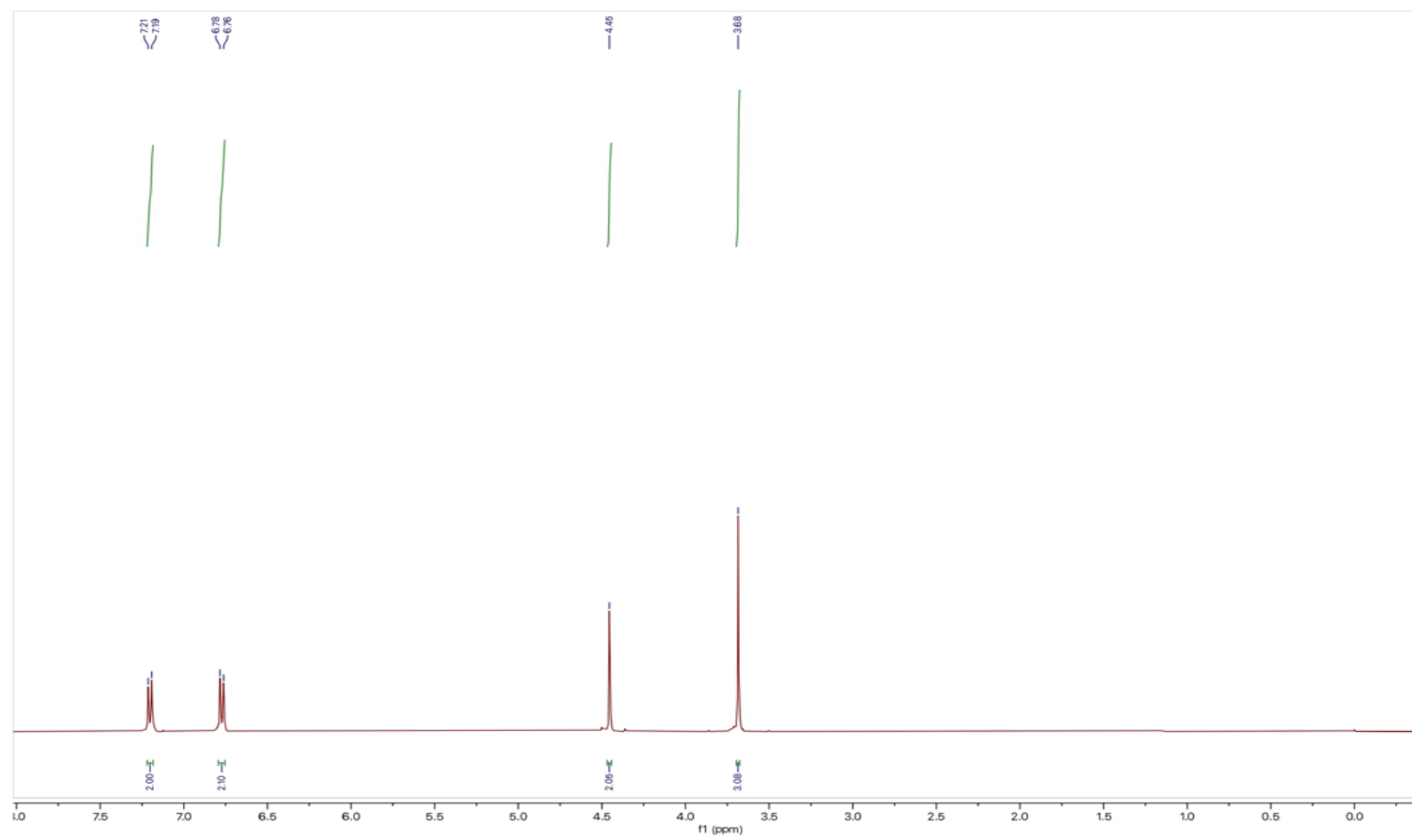
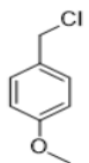


Figure A.6.  $^1\text{H}$  NMR spectrum of PMB-Cl in  $\text{CDCl}_3$

001

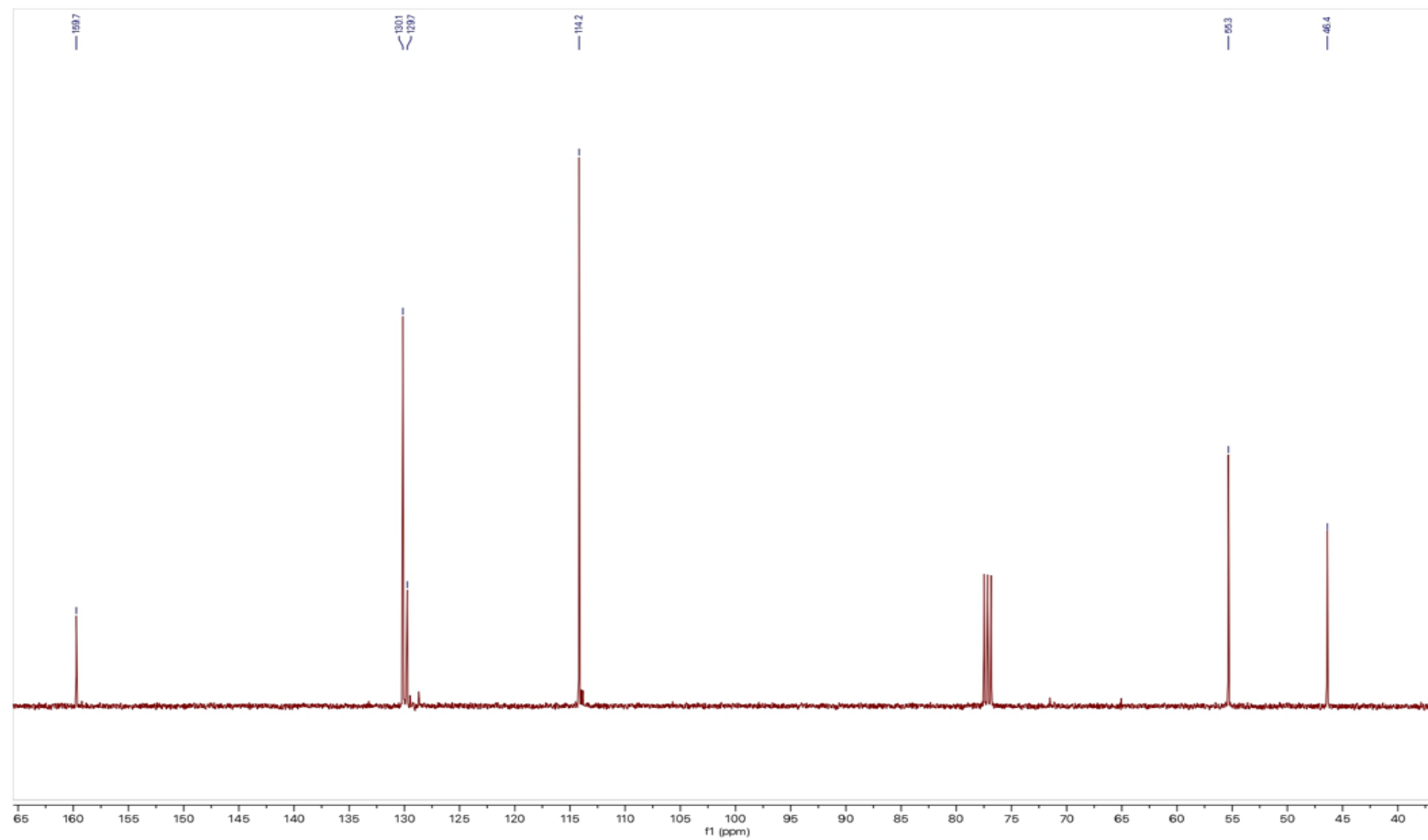
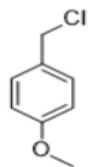
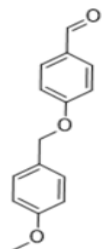


Figure A.7.  $^{13}\text{C}$  NMR spectrum of PMB-Cl in  $\text{CDCl}_3$



101

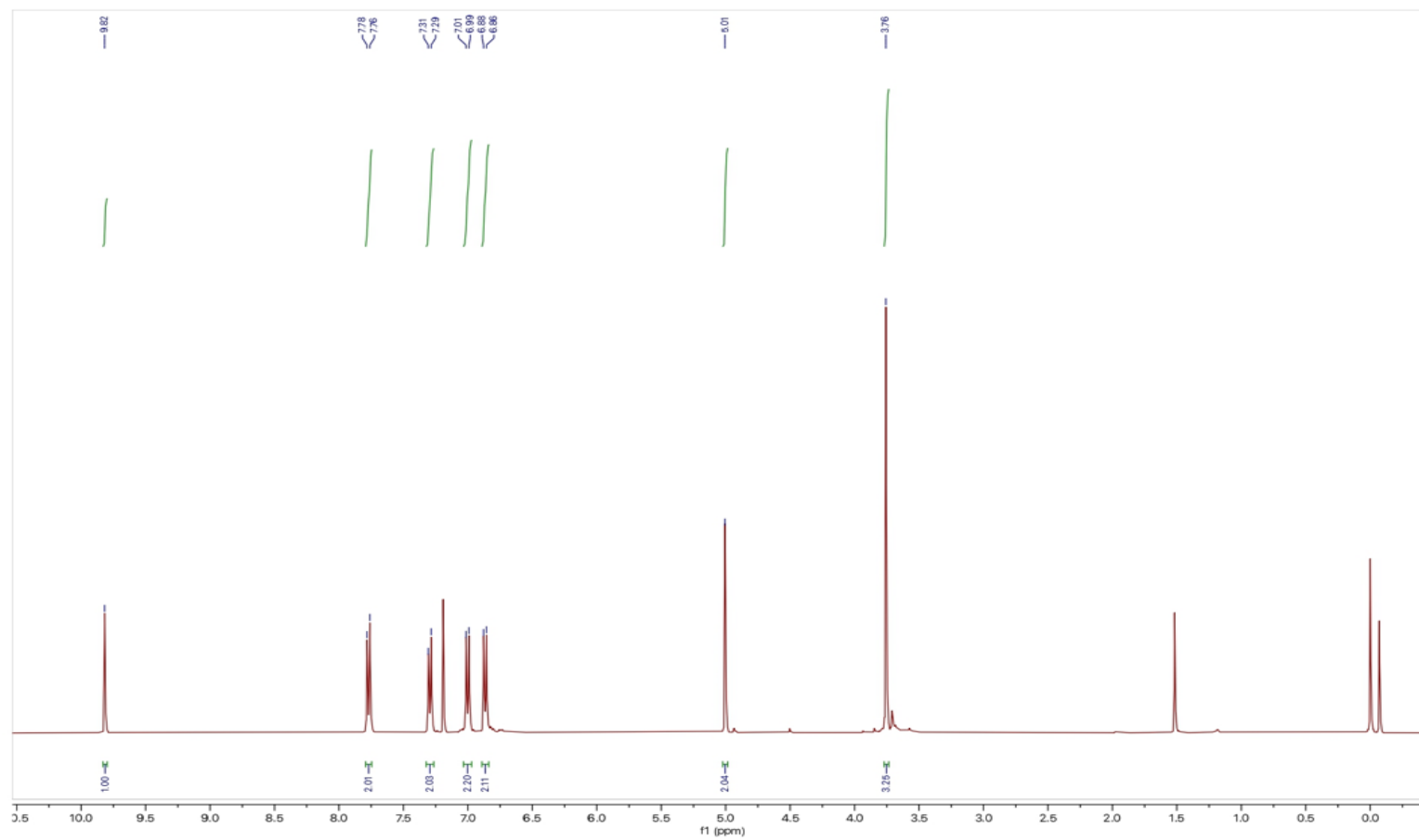


Figure A.8.  $^1\text{H}$  NMR spectrum of compound 7 in  $\text{CDCl}_3$

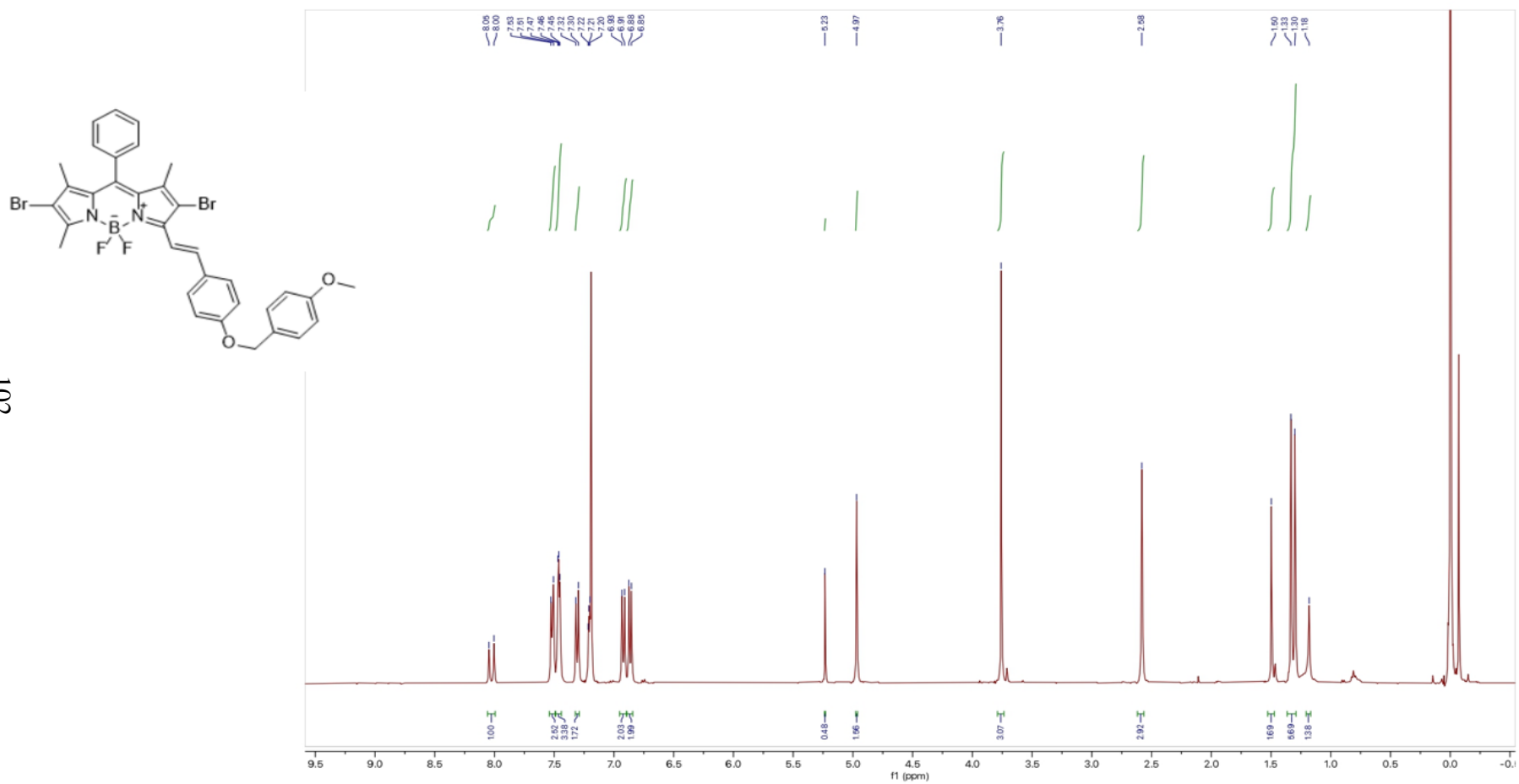


Figure A.9.  $^1\text{H}$  NMR spectrum of compound 6 in  $\text{CDCl}_3$

103

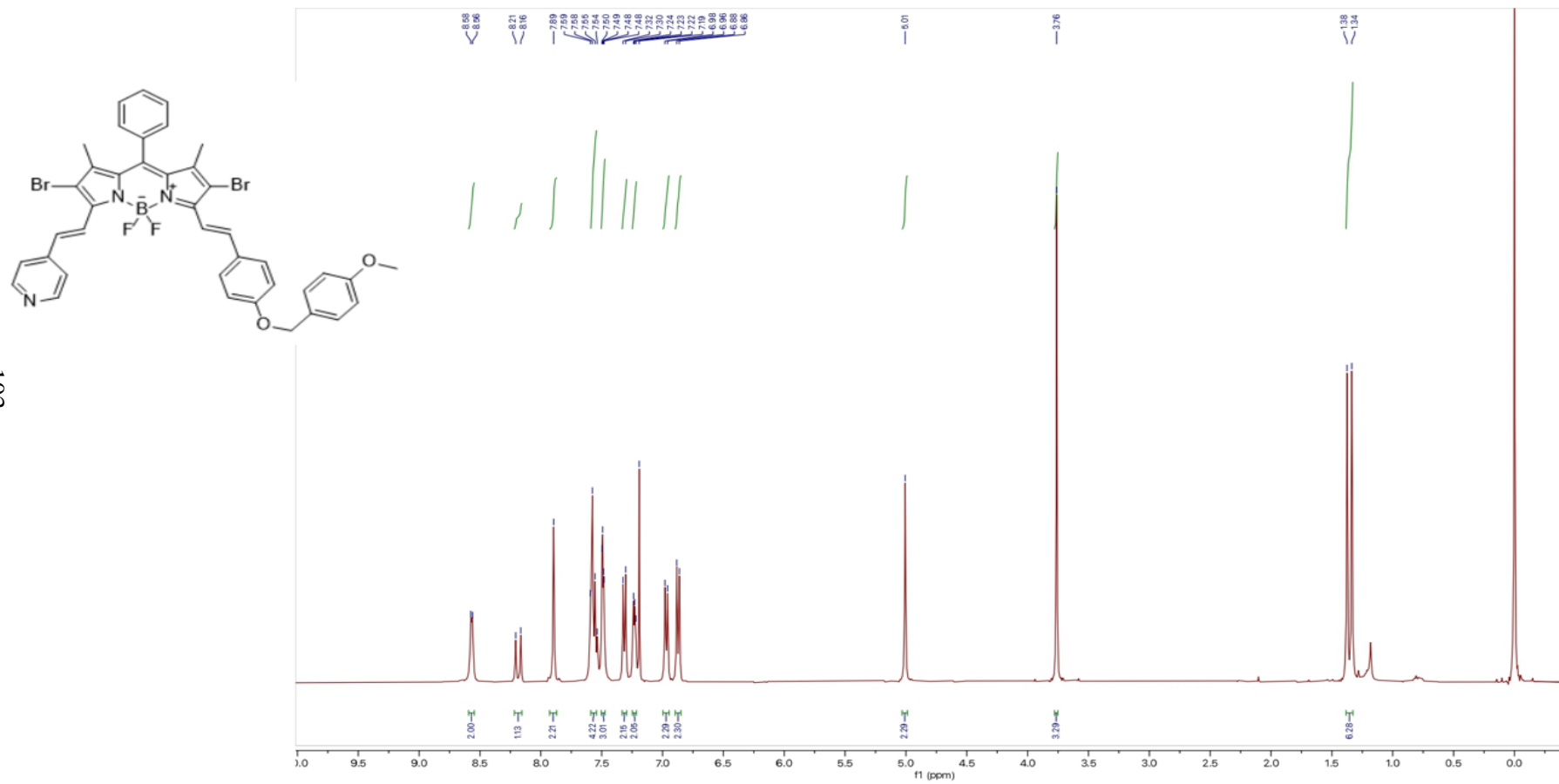


Figure A.10.  $^1\text{H}$  NMR spectrum of compound 8 in  $\text{CDCl}_3$

104

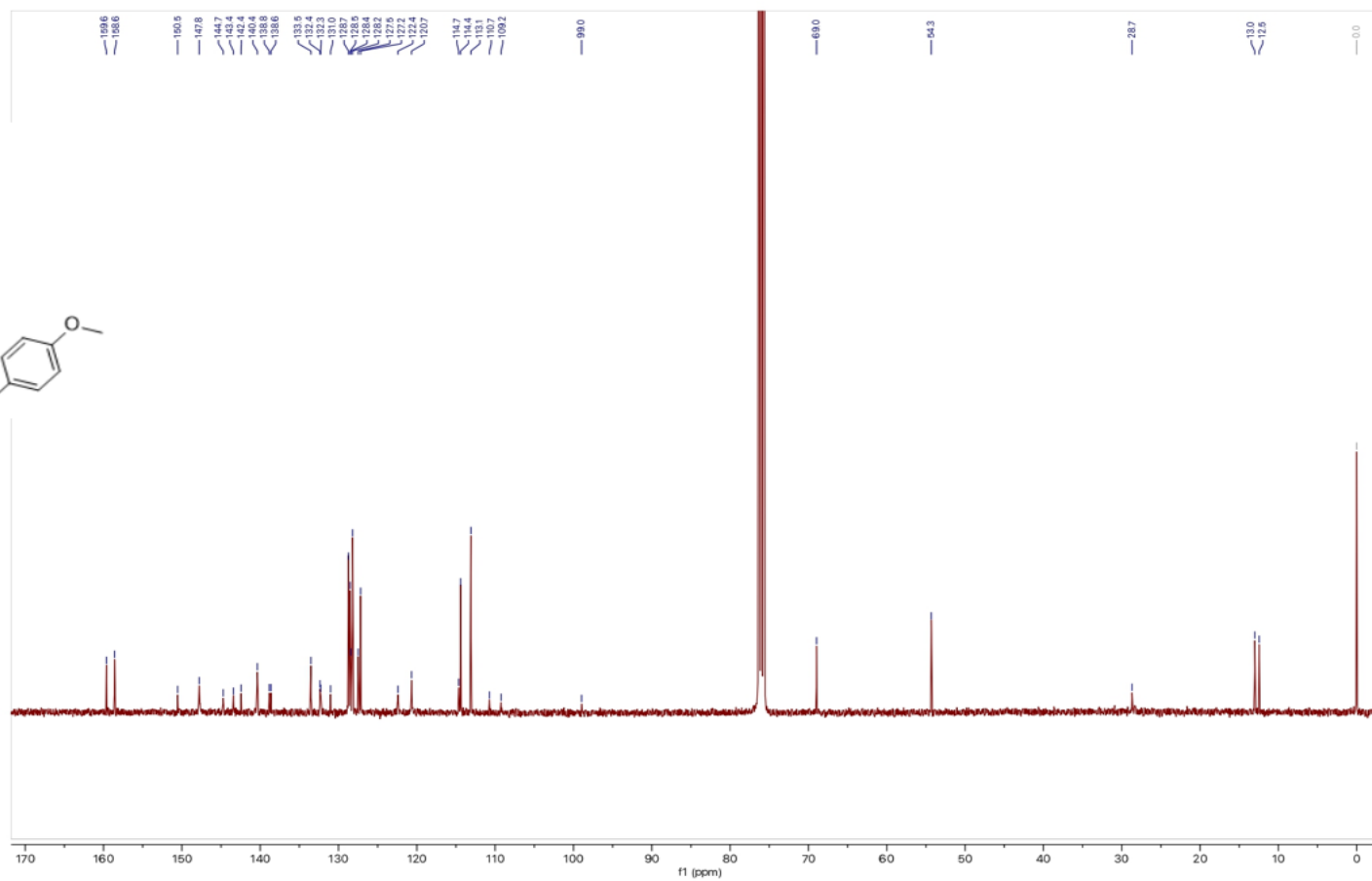
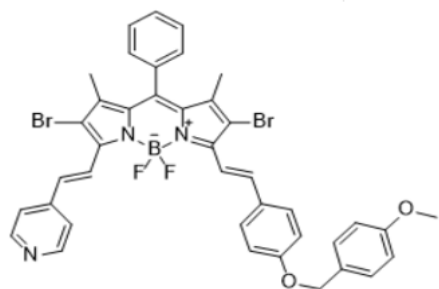


Figure A.11.  $^{13}\text{C}$  NMR spectrum of compound 8 in  $\text{CDCl}_3$



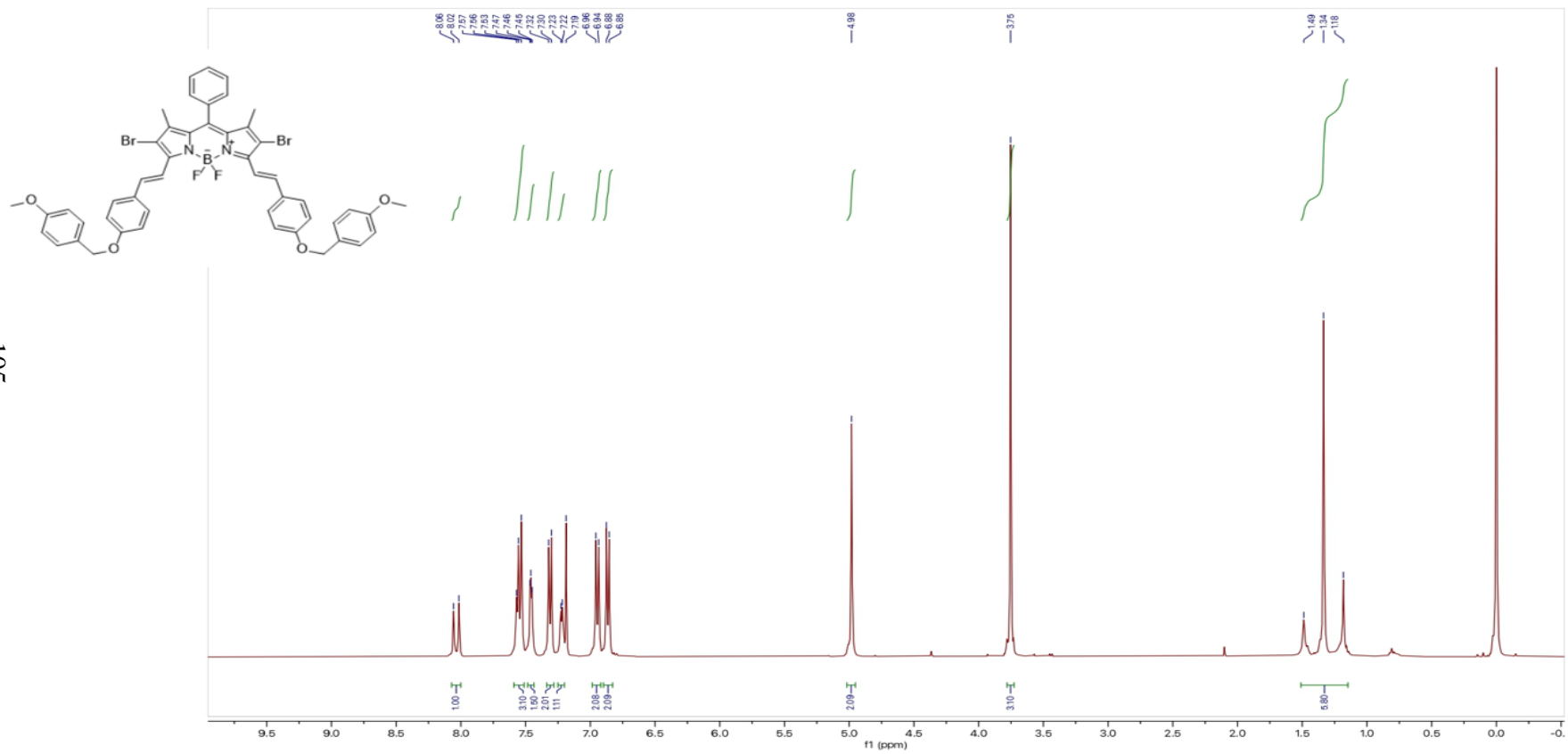


Figure A.12.  $^1\text{H}$  NMR spectrum of compound 9 in  $\text{CDCl}_3$

106

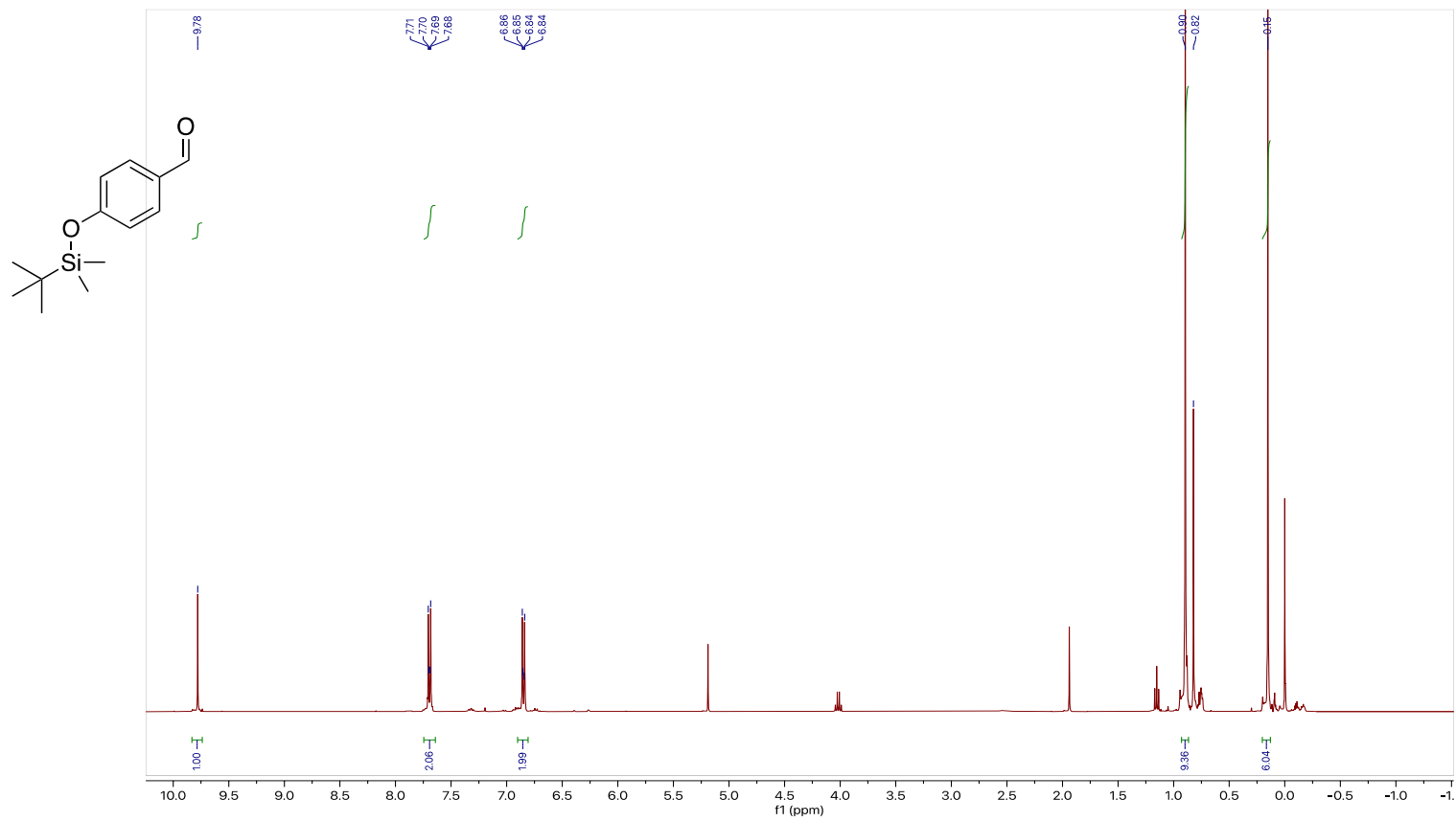


Figure A.13. <sup>1</sup>H NMR spectrum of compound 11 in CDCl<sub>3</sub>

107

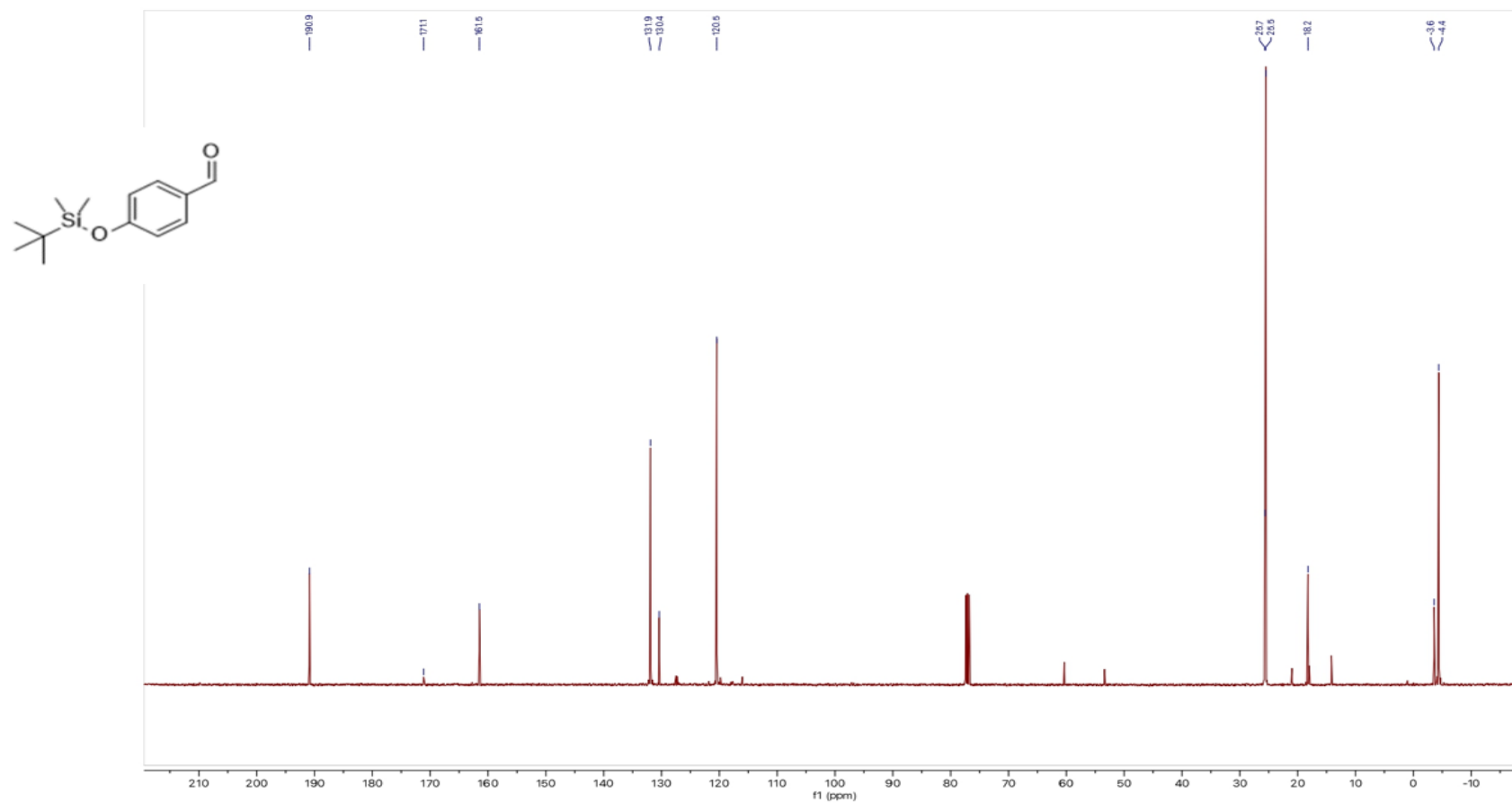


Figure A.14.  $^{13}\text{C}$  NMR spectrum of compound 11 in  $\text{CDCl}_3$

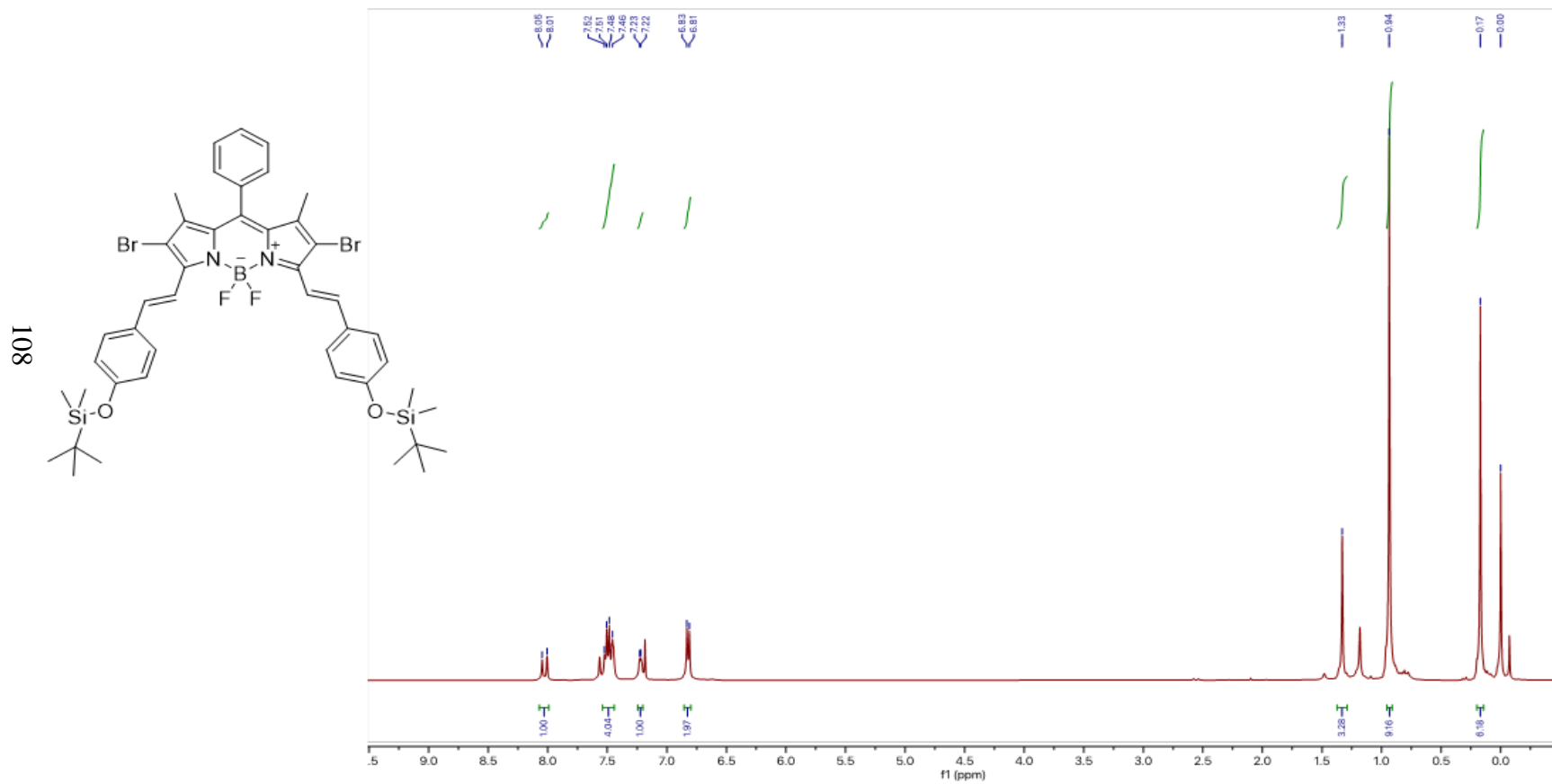


Figure A.15.  $^1\text{H}$  NMR spectrum of compound 12 in CDCl<sub>3</sub>

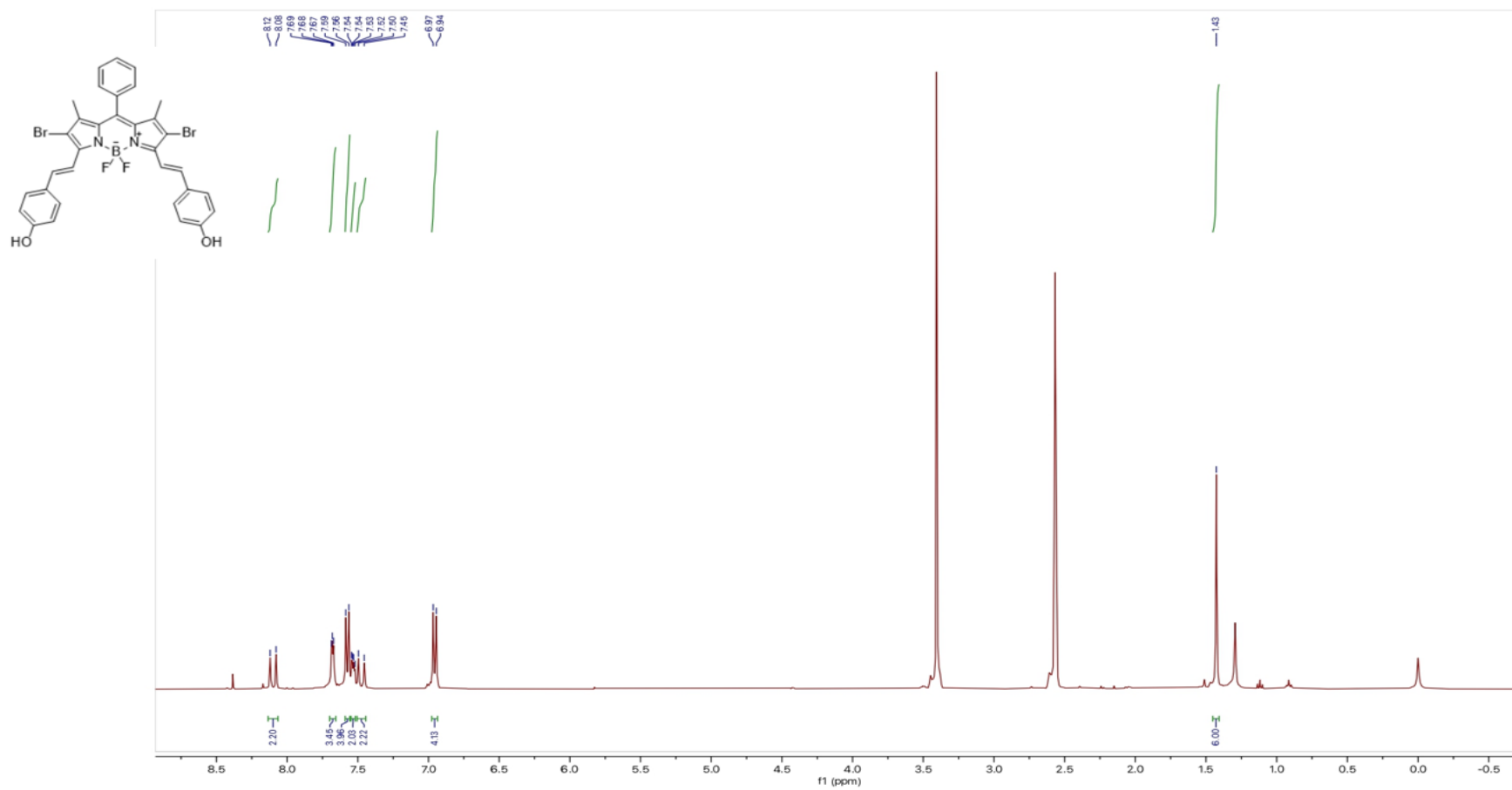


Figure A.16.  $^1\text{H}$  NMR spectrum of compound 10 in  $\text{d}_6\text{-DMSO}$

110

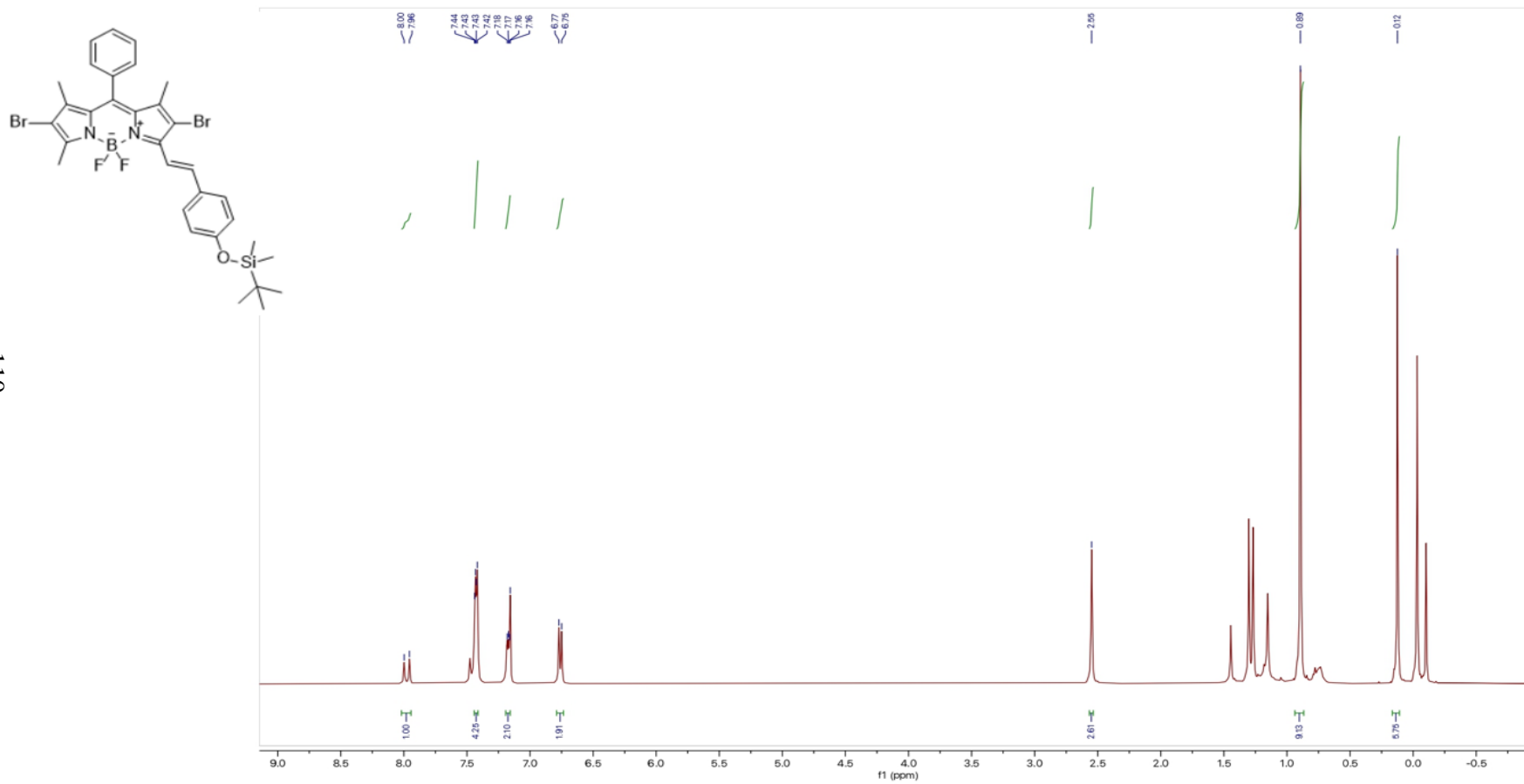


Figure A.17. <sup>1</sup>H NMR spectrum of compound 13 in CDCl<sub>3</sub>

## **A.2 Compounds Towards Synthesis of S2-BODMe**

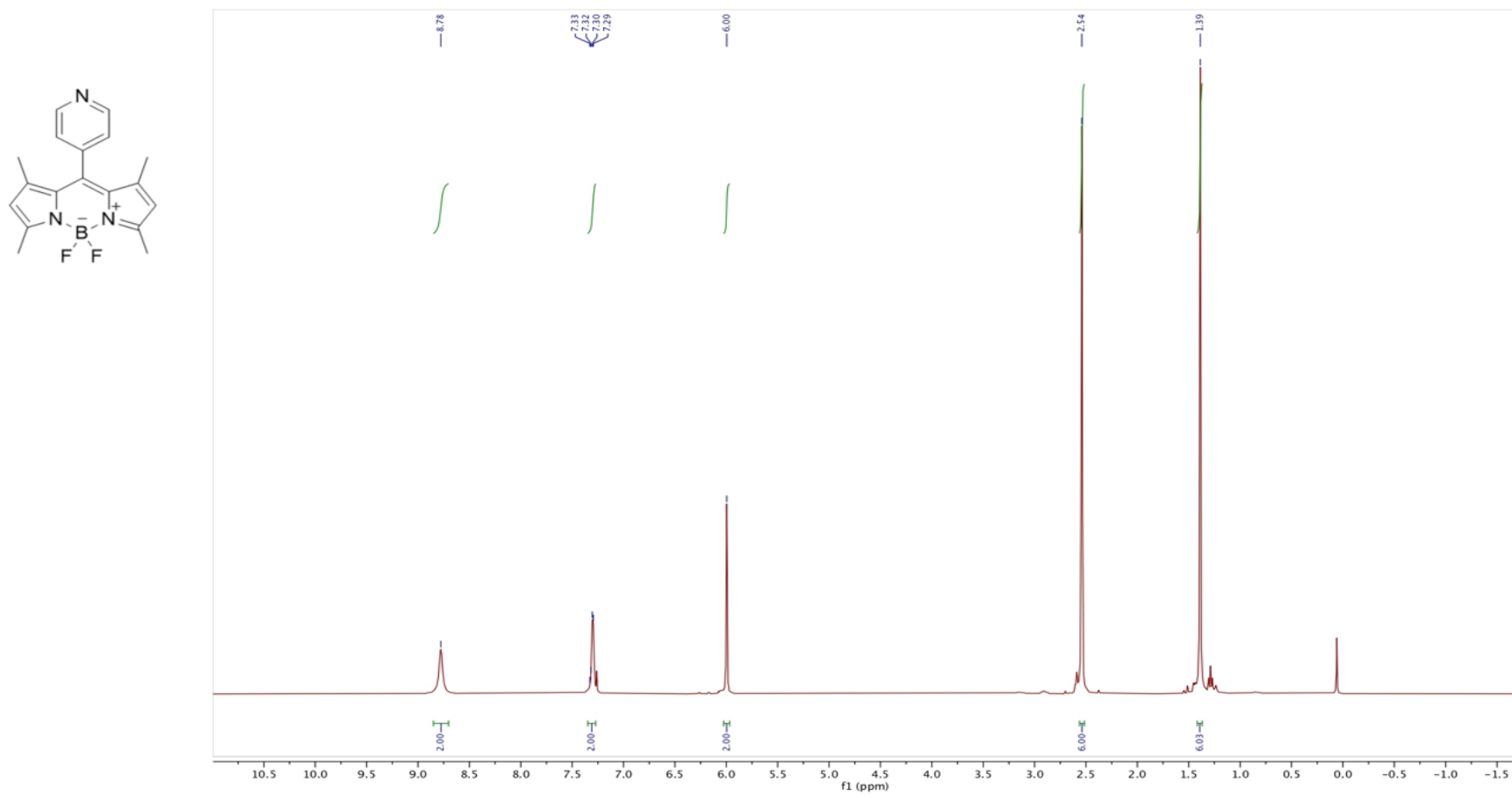


Figure A.18.  $^1\text{H}$  NMR spectrum of compound 15 in  $\text{CDCl}_3$



113

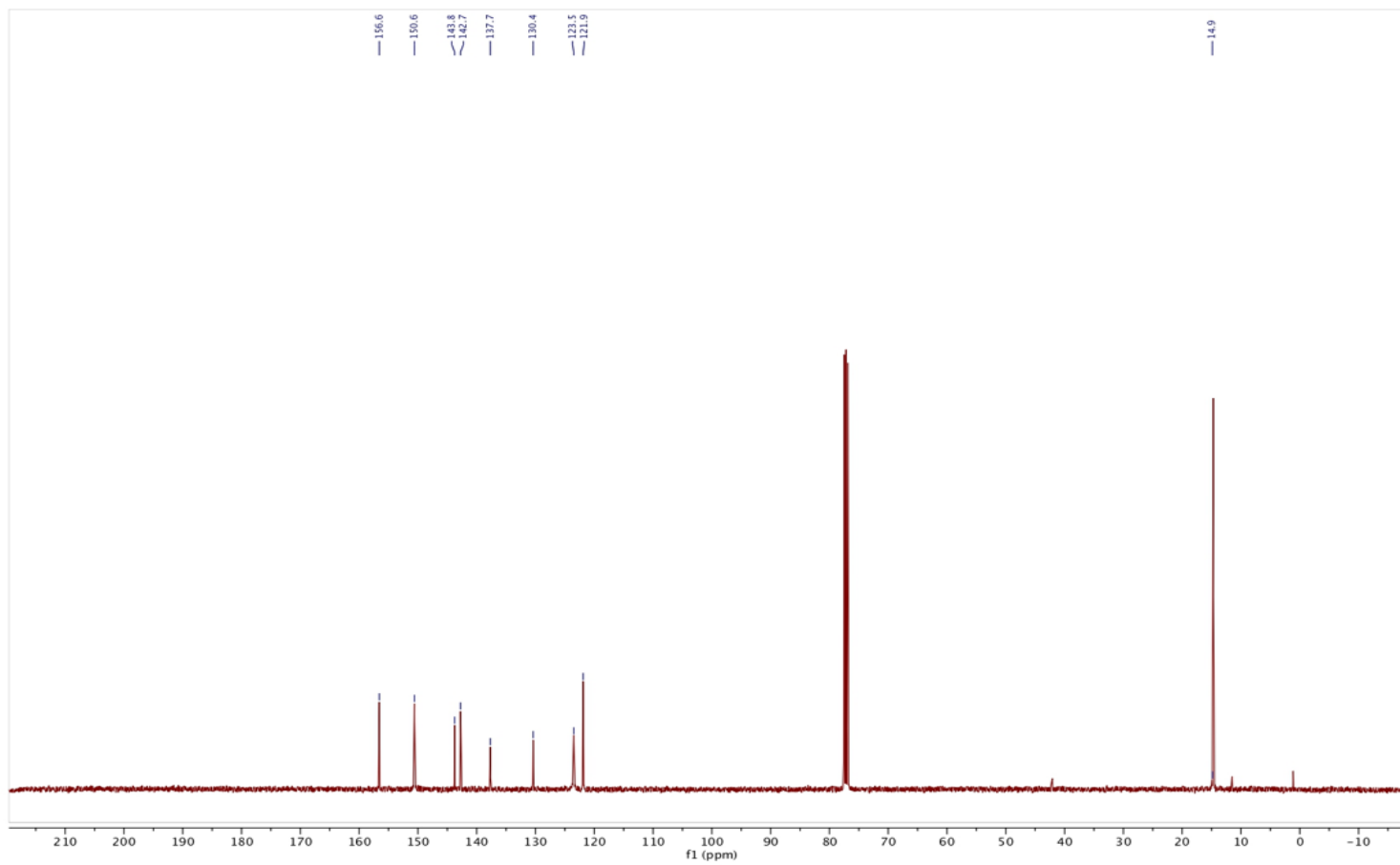
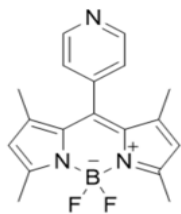


Figure A.19.  $^{13}\text{C}$  NMR spectrum of compound 15 in  $\text{CDCl}_3$

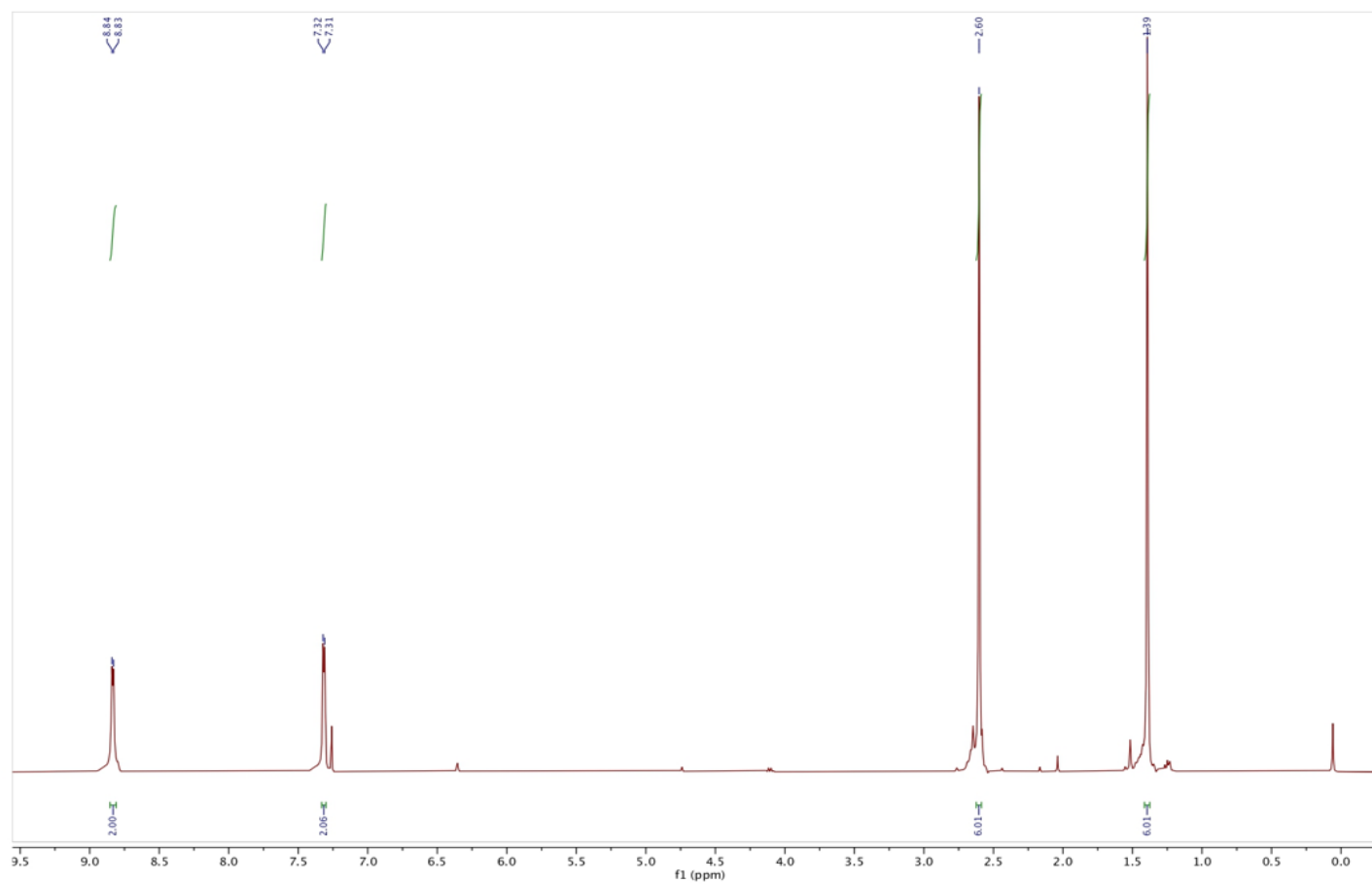
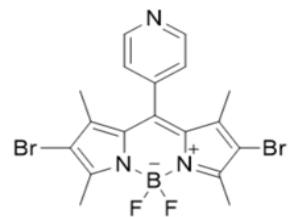


Figure A.20.  $^1\text{H}$  NMR spectrum of compound 16 in  $\text{CDCl}_3$

115

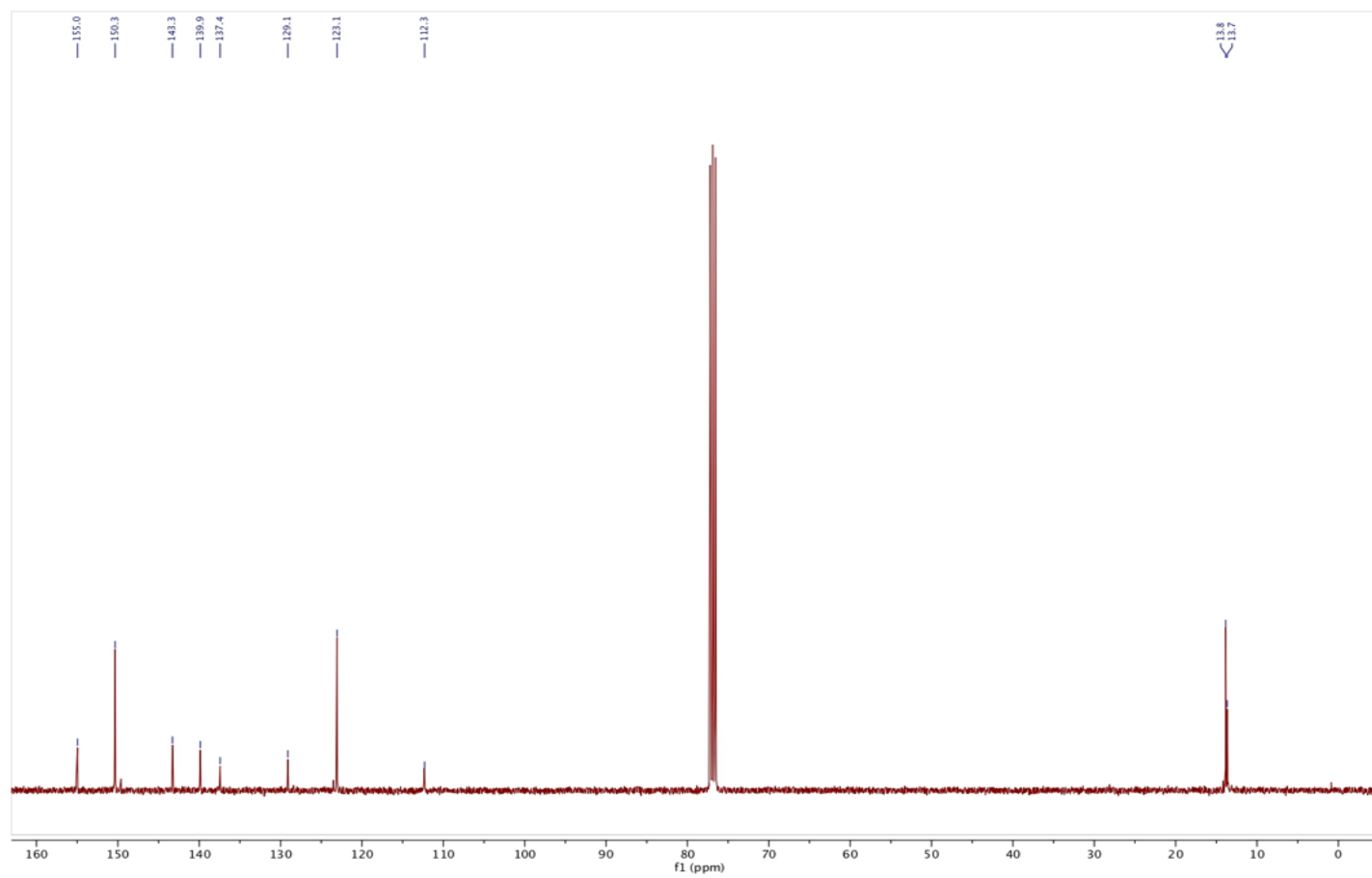
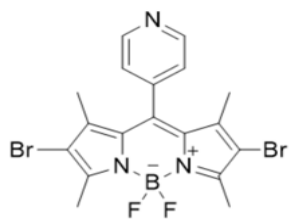


Figure A.21.  $^{13}\text{C}$  NMR spectrum of compound 16 in  $\text{CDCl}_3$

116

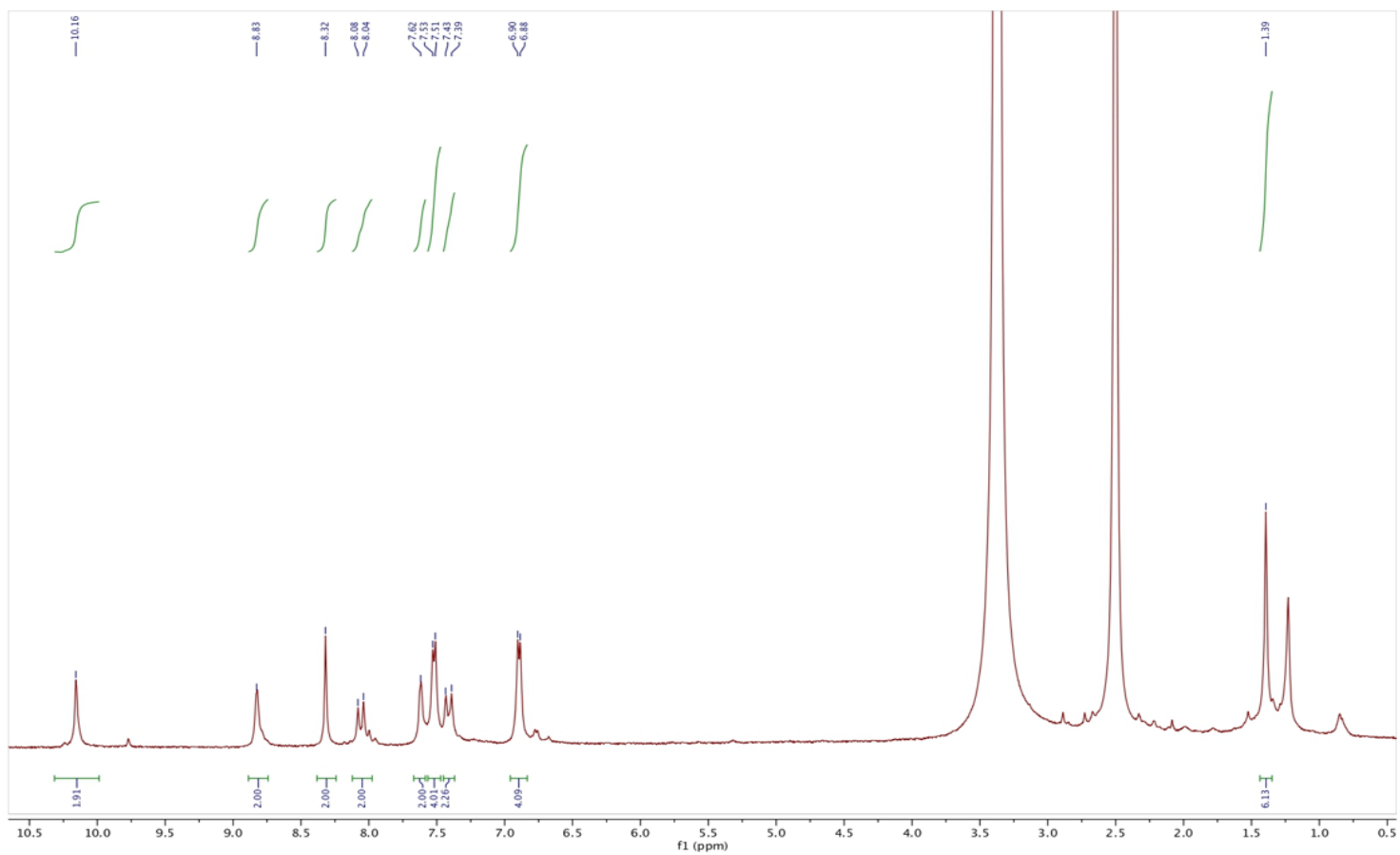
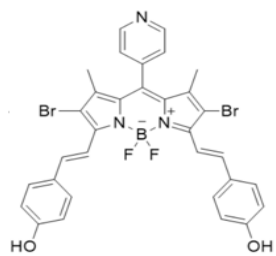
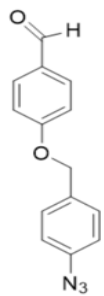


Figure A.22. <sup>1</sup>H NMR spectrum of compound 17 in d<sub>6</sub>-DMSO



117

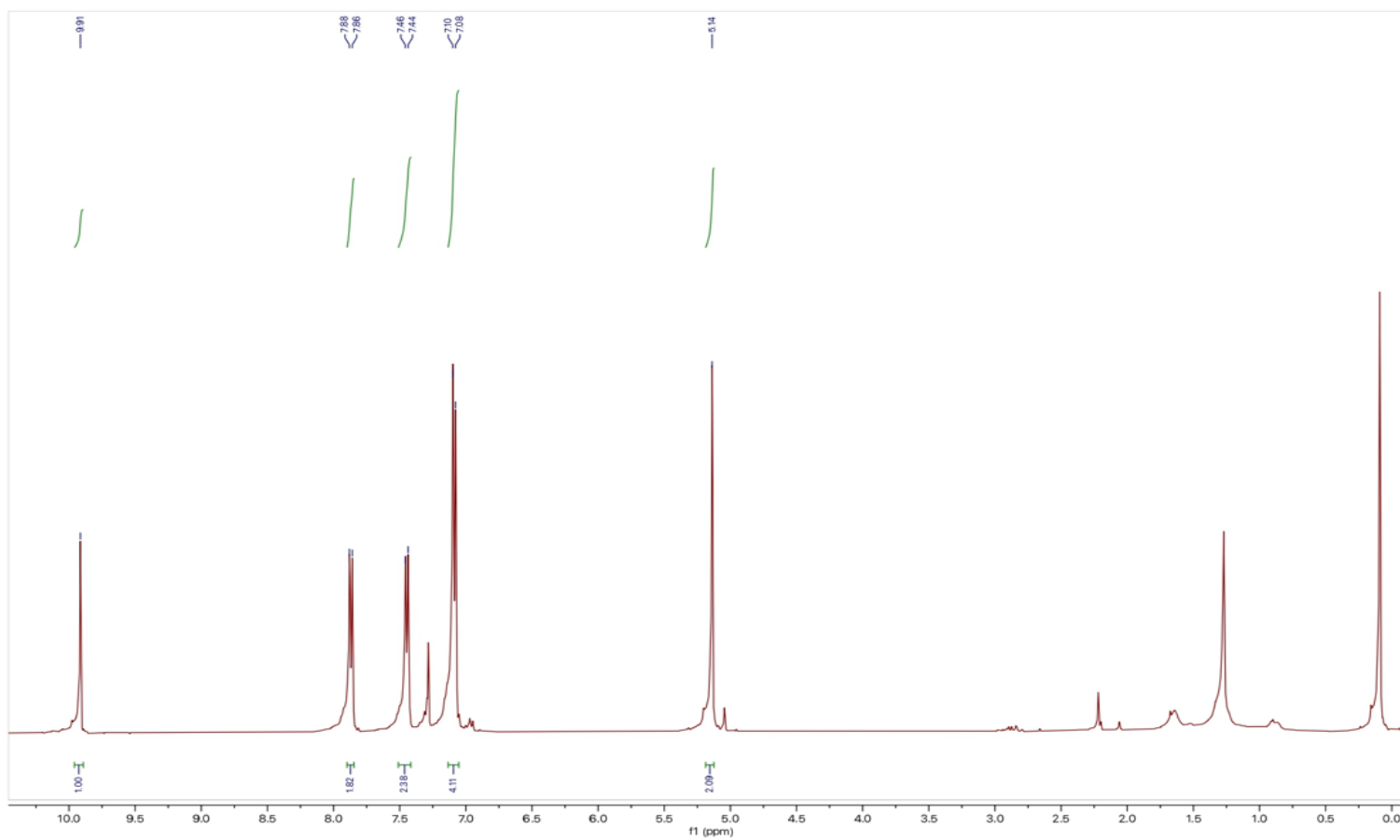


Figure A.23. <sup>1</sup>H NMR spectrum of Azide Containing Masking Unit in CDCl<sub>3</sub>